Chapter 9

New Methods for Kinematic Synthesis

Results that describe new methods for kniematic synthesis presented at various conferences and in archival journals are reprinted in slightly modified form in the following sections. The material presented in the first paper was disseminated in the *Proceedings of the International Federation of Machines and Mechanisms (IFToMM) Tenth World Congress on the Theory of Machines and Mechanisms*, in Oulu, Finland in a paper entitled "The Effect of Data-set Cardinality on the Design and Structural Errors of Four-bar Function-generators" [1]. This paper presents the initial observation that as the input-output (IO) data-set cardinality increases the Euclidean norms of the design and structural errors converge. The important implication is that the minimisation of the Euclidean norm of the structural error can be accomplished indirectly via the minimisation of the corresponding norm of the design error provided that a suitably large number of input-output pairs is prescribed.

The second paper, entitled "Continuous Approximate Synthesis of Planar Function-generators Minimising the Design Error" [2], first appeared in the archival journal *Mechanism and Machine Theory* in June 2016. In this paper the synthesis equations are integrated in the range between minimum and maximum input values, thereby reposing the discrete approximate synthesis problem as a continuous one. Moreover, it is proved that a lower bound of the Euclidean norm, and indeed of any p-norm, of the design error for planar RRRR function-generating linkages exists and is attained with continuous approximate synthesis.

The third paper, "Solving the Burmester Problem Using Kinematic Mapping" [3], initially appeared in the *Proceedings of the American Society of Mechanical Engineers (ASME) Design Engineering Technical Conferences: Mechanisms Conference*, and was presented in Montréal, QC, Canada in September 2002. In this paper a method to solve the five-pose Burmester problem for rigid body guidance using the planar kinematic mapping of Grünwald [4] and Blashke [5] introduced simultaneously, but independently in 1911, is presented. This procedure was generalised to all possible planar four-bar mechanisms in [6].

A new approach for approximate synthesis of planar four-bar mechanisms that solve the rigid body guidance problem is presented in the fourth paper, entitled "Quadric Surface Fitting Applications to Approximate Dimensional Synthesis" [7]. This paper appeared in the *Proceedings of the International Federation of Machines and Mechanisms (IFToMM) Thirteenth World Congress on the Theory of Machines and Mechanisms*, and was presented in Guanajuato, Mexico in June 2011. In this paper an approximate synthesis method is presented that takes a given set of n desired poses of the coupler of a four-bar planar mechanism and finds the "best" mechanism that can achieve them. This is accomplished by solving an equivalent unconstrained non-linear minimisation problem. The hyperboloids of one sheet or hyperbolic paraboloids that minimise the distance between the given n poses in the kinematic mapping image space of Grünwald and Blashke and n corresponding points that belong to the quadric surfaces, represent the "best" mechanism that can achieve the desired poses.

The fifth paper presents work intended to integrate type and dimensional synthesis solving the five-position Burmester problem and is entitled "Towards Integrated Type and Dimensional Synthesis of Mechanisms for Rigid Body Guidance" [8]. In this paper kinematic mapping is used to take the first steps towards development of a general algorithm combining both type and dimensional synthesis of planar mechanisms for rigid body guidance. In this work an algorithm is presented that can size link lengths, locate joint axes, and, using heuristics, decide between RR- and PR-dyads that, when combined, can guide a rigid body exactly through five specified positions and orientations, i.e., the five-position Burmester problem. The paper was presented at the 2004 *Canadian Society for Mechanical Engineering Forum* in London, ON, in June 2004, and appears in the associated Proceedings.

The sixth paper in this chapter, entitled "Integrated Type And Dimensional Synthesis of Planar Four-Bar Mechanisms" [9], appears in a book containing

the proceedings of the eleventh in the series of *Advances in Robot Kinematics Conference*, and was presented in June 2012 in Innsbruck, Austria. In the paper a novel approach to integrated type and approximate dimensional synthesis of general planar four-bar mechanisms (i.e. linkages comprised of any two of RR, PR, RP, and PP dyads) for rigid-body guidance is proposed. The essence is to correlate coordinates of the coupler attachment points in two different coordinate frames, thereby reducing the number of independent variables defining a suitable dyad for the desired rigid-body motion from five to two. After applying these geometric constraints, numerical methods are used to size link lengths, locate joint axes, and decide between RR, PR, RP and PP dyads that, when combined, guide a rigid body through the best approximation, in a least-squares sense, of n specified positions and orientations, where $n > 5$. No initial guesses of type or dimension are required.

The seventh and eighth papers both investigate the derivation and geometry of an algebraic version of the IO equation of planar $4R$ mechanisms. The seventh, entitled "Input-output Equation for Planar Four-bar Linkages" [10], appears in a book containing the proceedings of the sixteenth in the series of Advances in Robot Kinematics Conference, and was presented in July 2018 in Bologna, Italy. While the eighth is entitled "An Algebraic Version of the Input-output Equation of Planar Four-bar Mechanisms" [11], and appears in a book containing the proceedings of the eighteenth in the series of conferences called International Conference on Geometry and Graphics, and was presented in August 2018 in Milan, Italy.

The algebraic IO equation for planar RRRP and PRRP linkages is derived in the same way as in [10] in the ninth paper, entitled "An Algebraic Input-Output Equation for Planar RRRP and PRRP Linkages" [12], first presented at, and appearing in the proceedings of the 10^{th} CCToMM Symposium on Mechanisms, Machines, and Mechatronics, École de technologie supérieure, Montréal, QC, Canada. In this paper it is shown that the IO equations for any planar 4R linkage is precisely the same as those for any planar four-bar linkage containing as many as two P-pairs. However, the inputs and outputs are different parameters.

Given that the IO equations for planar four-bar linkages are the same regardless of the number of P-pairs, provided the maximum is two, the next phase of this research was to develop a generalised approach to deriving the IO equations for planar, spherical, and spatial four-bar linkages of arbitrary kinematic architecture. The first step towards this goal is presented in the tenth paper, entitled "A General Method for Determining Algebraic Input-output Equations for Planar and Spherical 4R Linkages" [13], which has been accepted for pub-

lication in a book containing the proceedings of the seventeenth in the series of *Advances in Robot Kinematics Conference* in Lubljana, Slovenia, originally scheduled between June 28 - July 2, 2020. Given the COVID-19 pandemic, we'll see how that goes.

The results presented in the final three papers in this chapter [14, 15, 16] detail the design parameter spaces of planar and spherical 4R linkages. The first of the three, entitled "Design Parameter Space of Planar Four-bar Linkages" [14], was presented at, and appears in the proceedings of the *15^{th} IFToMM World Congress, 2019*, Krakow, Poland, June 30 - July 04, 2019. The main result of the paper is that the eight linear factors in four of the coefficients of IO equation define a regular double tetrahedron in the parameter space of the link lengths. Each linear factor defines a plane which intersects three other planes in the set in an equilateral triangle, for a total of eight. The two tetrahedra in the regular double tetrahedron belong to the only uniform polyhedral compound, called the stellated octahedron, which has order 48 octahedral symmetry. This double tetrahedron has a regular octahedron at its core and shares its eight vertices with the cube. The eight equilateral triangles bound the faces of this octahedron. Distinct points in this design parameter space represent distinct function generators and the locations of the points relative to the eight planes containing the faces of the double tetrahedron completely determines the mobility of the input and output links.

The last two papers in this set, entitled "Design Parameter Space of Spherical Four-bar Linkages" [15], and "Mobility Classification in the Design Parameter Space of Spherical 4R Linkages" [16], describe a related design parameter space for spherical 4R linkages. Perhaps the most interesting result is that the coefficient factors define eight singular cubic surfaces. Each of the eight cubics possess six real lines each, three on the plane at infinity and three finite ones. The three lines at infinity are common to all eight cubics, while the three finite lines on each surface are equilateral triangles which can be considered the edges of the double tetrahedron for planar 4R linkages! In this way, the design parameter spaces of planar and spherical 4R linkages intersect in the edges of the only uniform polyhedral compound comprising a regular double tetrahedron that intersects itself in a regular octahedron. This is the only uniform polyhedral compound in the entire universe of polyhedra!

TENTH WORLD CONGRESS ON THE THEORY OF
MACHINES AND MECHANISMS
Oulu, Finland, June 20–24, 1999

THE EFFECT OF DATA-SET CARDINALITY ON THE DESIGN AND STRUCTURAL ERRORS OF FOUR-BAR FUNCTION-GENERATORS

M.J.D. Hayes, K. Parsa, J. Angeles
McGill University, Department of Mechanical Engineering and Centre for Intelligent Machines,
817 Sherbrooke W., Montreal, Quebec, H3A 2K6 Canada.
email: *johnh@cim.mcgill.ca, kourosh@cim.mcgill.ca, angeles@cim.mcgill.ca*

Keywords: approximate kinematic synthesis, design, structural error, function-generators.

1 Introduction

Design and structural errors are important performance indicators in the assessment and optimisation of function-generating linkages arising by means of approximate synthesis. The design error indicates the error residual incurred by a specific linkage regarding the verification of the synthesis equations. The structural error, in turn, is the difference between the prescribed linkage output and the actual generated output for a given input value [Tinubu and Gupta 1984]. From a design point of view it may be successfully argued that the structural error is the one that really matters, for it is directly related to the performance of the linkage.

The main goal of this paper is to demonstrate that, as the data-set cardinality increases, the Euclidean norms of the design and structural errors converge. The important implication is that the minimisation of the Euclidean norm of the structural error can be accomplished indirectly via the minimisation of the corresponding norm of the design error, provided that a suitably large number of input-output (I/O) pairs is prescribed. Note that the minimisation of the Euclidean norm of the design error leads to a linear least-square problem whose solution can be obtained directly [Wilde 1982], while the minimisation of the same norm of the structural error leads to a nonlinear least-squares problem, and hence, calls for an iterative solution [Tinubu and Gupta 1984].

2 Procedure

The synthesis problem of four-bar function-generators consists of determining all relevant design parameters such that the mechanism can produce a prescribed set of m input-output (I/O) pairs, $\{\psi_i, \phi_i\}_1^m$, where ψ_i and ϕ_i represent the i^{th} input and output variables, respectively, and m is the cardinality of the data-set.

Let n be the number of independent design parameters required to characterise the mechanism. For planar $RRRR$ linkages, $n = 3$ [Freudenstein 1955], while for spherical $RRRR$ linkages $n = 4$ [Hartenberg and Denavit 1964]. For spatial $RCCC$ function-generators, the issue is not as straightforward. The output of this type of linkage consists of both angular and translational displacements, although they are coupled. If we only consider the angular output, which is necessary if comparisons are to be made with the other two for generating identical functions, then $n = 4$ [Liu 1993].

Approximate synthesis problems involve sets of I/O equations such that $m > n$. If $m = n$, the problem is termed *exact synthesis* and may be considered a special case of the former [Liu and Angles 1992]. The optimisation problem of four-bar function-generators usually involves the approximate solution of an overdetermined linear system of equations with the minimum error. The I/O equations can be written in the form

$$\mathbf{Sk} = \mathbf{b}, \tag{1}$$

where $\mathbf{S}$ is the $m \times n$ *synthesis matrix*, $\mathbf{b}$ is an m-dimensional vector, whereas $\mathbf{k}$ is the n-dimensional vector of design variables, usually called the *Freudenstein parameters* as they were first introduced in [Freudenstein 1955] for the synthesis of planar four-bar linkages. Moreover, the i^{th} row of $\mathbf{S}$, $\mathbf{s}_i^T$, and the i^{th} component of $\mathbf{b}$, b_i, are functions of ψ_i and ϕ_i only. For the planar $RRRR$ mechanism:

$$\mathbf{s}_i^T = [\ 1 \quad \cos\phi_i \quad -\cos\psi_i\ ], \quad i = 1, ..., m, \tag{2}$$

$$b_i = [\ \cos(\psi_i - \phi_i)\ ], \quad i = 1, ..., m, \tag{3}$$

$$\mathbf{k} = [\ k_1 \quad k_2 \quad k_3\ ]^T. \tag{4}$$

For the spherical $RRRR$ mechanism:

$$\mathbf{s}_i^T = [\ 1 \quad -\cos\phi_i \quad \cos\psi_i \quad \cos\phi_i\cos\psi_i\ ], \quad i = 1, ..., m, \tag{5}$$

$$b_i = [\ -\sin\psi_i \sin\phi_i\ ], \quad i = 1, ..., m, \tag{6}$$

$$\mathbf{k} = [\ k_1 \quad k_2 \quad k_3 \quad k_4\ ]^T. \tag{7}$$

For the spatial $RCCC$ mechanism:

$$\mathbf{s}_i^T = [\ 1 \quad \sin\phi_i \quad \sin\psi_i \quad \sin\phi_i\sin\psi_i\ ], \quad i = 1, ..., m, \tag{8}$$

$$b_i = [\ \cos\psi_i\cos\phi_i\ ], \quad i = 1, ..., m, \tag{9}$$

$$\mathbf{k} = [\ k_1 \quad k_2 \quad k_3 \quad k_4\ ]^T. \tag{10}$$

These synthesis equations are linear in the components of $\mathbf{k}$. This matrix form has obvious representational advantages, but more importantly, it allows us to determine values of the I/O dial zeros, α and β, that will best condition the synthesis matrix, $\mathbf{S}$ [Liu and Angeles 1993]. Here, we regard the I/O pairs as a set of incremental angular changes, $\{\Delta\psi_i\ \Delta\phi_i\}_1^m$. The I/O data set is then

$$\psi_i = \alpha + \Delta\psi_i, \quad \phi_i = \beta + \Delta\phi_i \quad i = 1, \ldots, m. \tag{11}$$

The Nelder-Mead *downhill simplex algorithm in multi-dimensions* [Liu and Angeles 1993] is employed to estimate the optimal values for α and β. It should be mentioned that, while changing the dial zeros of the I/O angles improves the condition number, κ, of planar $RRRR$, spherical $RRRR$ and spatial $RCCC$ linkages, this method does not always work for spatial $RSSR$ linkages [Liu and Angeles 1993].

When $m > n$ there is, in general, no $\mathbf{k}$ which will exactly satisfy all the equations. There are two well established indicators to assess the approximation error, namely the design and structural errors. We define the design error vector $\mathbf{d}$ as

$$\mathbf{d} \equiv \mathbf{Sk} - \mathbf{b}. \tag{12}$$

The Freudenstein parameters, $\mathbf{k}$, may be optimised by minimising the Euclidean norm of $\mathbf{d}$. The scalar objective function is

$$z \equiv \frac{1}{2}(\mathbf{d}^T\mathbf{W}\mathbf{d}), \tag{13}$$

which must be minimised over $\mathbf{k}$. The scalar quantity $\mathbf{d}^T\mathbf{W}\mathbf{d}$ is the weighted Euclidean norm of $\mathbf{d}$. The matrix $\mathbf{W}$ is a diagonal matrix of positive weighting factors, which can be used to make some of the data points affect the minimisation more, or less, than others, depending on their relative importance to the design. For the sake of simplicity $\mathbf{W}$ will be set equal to the identity matrix in this article, $\mathbf{d}^T\mathbf{W}\mathbf{d}$ being indicated by $\|\mathbf{d}\|_2$.

The quantity $\|\mathbf{d}\|_2$ can be minimised, in a least squares sense, very efficiently by transforming $\mathbf{S}$ using Householder reflections [Golub and Van Loan 1989], the Moore-Penrose generalised inverse thus not being explicitly computed. Design error minimisation is therefore a linear problem; a desirable trait, indeed. Unfortunately, as a performance indicator, the design error is not directly related to the I/O performance of the function-generator.

Alternatively we may approach the optimisation problem by minimising the same norm of the structural error. Since this error is defined as the difference between the generated and prescribed outputs for a given input, it is directly related to function-generator performance. Let the structural error vector $\mathbf{s}$ be defined as

$$\mathbf{s} \equiv \begin{bmatrix} \varphi_1 - \phi_1 \\ \vdots \\ \varphi_m - \phi_m \end{bmatrix}, \tag{14}$$

where φ_i is the generated value of the output ϕ attained at $\psi = \psi_i$, and ϕ_i is, as defined earlier, the prescribed value of the output angle at $\psi = \psi_i$. It can be shown that the structural and design errors are related by

$$\mathbf{d} = \mathbf{d}(\mathbf{s}) \equiv \mathbf{S}\mathbf{k} - \mathbf{b}, \tag{15}$$

where $\mathbf{d}$ is a nonlinear function of $\mathbf{s}$ [Tinubu and Gupta 1984]. Hence, it is evident that minimising $\|\mathbf{d}\|_2$ is not equivalent to minimising the Euclidean norm of the structural error, $\|\mathbf{s}\|_2$.

To minimise the Euclidean norm of this error, the iterative Gauss-Newton procedure is employed. The conditions under which the procedure converges in the neighbourhood of a minimum are discussed in [Dahlquist and Björck 1969]. In this case, the scalar objective function to be minimised over $\mathbf{k}$ is

$$\zeta \equiv \frac{1}{2}(\mathbf{s}^T\mathbf{W}\mathbf{s}). \tag{16}$$

Here, again, $\mathbf{W}$ is set equal to the identity matrix, the weighted Euclidean norm being indicated by $\|\mathbf{s}\|_2$.

We start with an initial guess for the Freudenstein parameters that minimise the Euclidean norm of the design error, and modify the guess until the normality condition,

$$\frac{\partial \zeta}{\partial \mathbf{k}} = \mathbf{0}, \tag{17}$$

is satisfied to a specified tolerance, ϵ, such that

$$\frac{\partial \zeta}{\partial \mathbf{k}} < \epsilon, \quad \text{for } \epsilon > 0. \tag{18}$$

We do not actually evaluate the normal equations, since they are typically ill-conditioned. Rather, we proceed in the following way: the i^{th} I/O equation is a function of ψ_i, ϕ_i and the Freudenstein parameters, $\mathbf{k}$, and may be written as

$$f_i(\psi_i, \phi_i; \mathbf{k}) = 0. \tag{19}$$

The Jacobian of $\mathbf{f}$ with respect to the vector of output values, $\boldsymbol{\phi}$, is the following diagonal matrix:

$$\frac{\partial \mathbf{f}}{\partial \boldsymbol{\phi}} \;=\; \mathrm{diag}\left(\frac{\partial f_1}{\partial \phi_1}, \ldots, \frac{\partial f_m}{\partial \phi_m}\right) \;\equiv\; \mathbf{D}. \tag{20}$$

If we regard Eq. (19) as a function of only ϕ_i we can write

$$\boldsymbol{\phi}(\mathbf{k}) \;=\; \boldsymbol{\phi}. \tag{21}$$

However, we want

$$\boldsymbol{\phi}(\mathbf{k}) \;=\; \boldsymbol{\varphi}. \tag{22}$$

Assume we have an approximation to $\mathbf{k}_{\mathrm{opt}}$, which we call $\mathbf{k}^{\nu}$, obtained from the ν^{th} iteration. We now require a correction vector, $\Delta\mathbf{k}$, so that

$$\boldsymbol{\phi}(\mathbf{k}^{\nu} + \Delta\mathbf{k}) \;=\; \boldsymbol{\varphi}. \tag{23}$$

It can be shown [Dahlquist and Björck 1969], after expanding the left-hand side of Eq. (23) in series, and ignoring higher order terms, that

$$\boldsymbol{\phi}(\mathbf{k}^{\nu}) - \boldsymbol{\varphi} \;=\; \mathbf{D}^{-1}\mathbf{S}\Delta\mathbf{k}, \tag{24}$$

the left-hand side of Eq. (24) being $-\mathbf{s}^{\nu}$. Now we find $\Delta\mathbf{k}$ as the least-square approximation of Eq. (24). It can be proven that $\Delta\mathbf{k} \approx \mathbf{0}$ implies $\partial\zeta/\partial\mathbf{k} \approx \mathbf{0}$, which means that we can satisfy the normality condition without evaluating it explicitly.

We show with one example below that, as the cardinality m of the data points increases, the design and structural errors converge.

3 Example

We synthesise here a planar $RRRR$, a spherical $RRRR$ and a spatial $RCCC$ four-bar mechanism to generate a quadratic function for an input range of $0^{\circ} \leq \Delta\psi \leq 60^{\circ}$, namely,

$$\Delta\phi_i \;=\; \frac{9\Delta\psi_i^2}{8\pi}. \tag{25}$$

For each mechanism the I/O dial zeros (α, β) are selected to minimise the condition number κ of $\mathbf{S}$ for each data-set [Liu and Angeles 1993]. Then both the design and structural errors are determined for the linkages that minimise the respective Euclidean norms for data-sets with cardinalities of $m = \{10, 40, 70, \text{ and } 100\}$. These results are listed in Tables 1–4. Finally the structural errors, corresponding to $m = 40$, of the linkages that minimise the Euclidean norms of the design and structural errors are graphically displayed in Fig. 1.

Table 1: Results for $m = 10$.

	Planar $RRRR$	Spherical $RRRR$	Spatial $RCCC$
α_{opt} (deg.)	123.8668	43.3182	-46.6817
β_{opt} (deg.)	91.7157	89.5221	-0.4781
κ_{opt}	33.2974	200.5262	200.5262
$\|\mathbf{d}\|_2$	7.273×10^{-3}	7.60×10^{-4}	7.60×10^{-4}
$\|\mathbf{s}\|_2$	5.965×10^{-3}	4.17×10^{-4}	4.17×10^{-4}

Table 2: Results for $m = 40$.

	Planar $RRRR$	Spherical $RRRR$	Spatial $RCCC$
α_{opt} (deg.)	117.4593	42.7696	-47.2301
β_{opt} (deg.)	89.4020	88.8964	-1.1037
κ_{opt}	32.5549	203.0317	203.0317
$\|\mathbf{d}\|_2$	1.571×10^{-2}	1.887×10^{-3}	1.887×10^{-3}
$\|\mathbf{s}\|_2$	1.502×10^{-2}	1.057×10^{-3}	1.057×10^{-3}

Table 3: Results for $m = 70$.

	Planar $RRRR$	Spherical $RRRR$	Spatial $RCCC$
α_{opt} (deg.)	116.4699	42.7014	-47.2987
β_{opt} (deg.)	89.0488	88.8045	-1.1956
κ_{opt}	32.5242	204.7696	204.7696
$\|\mathbf{d}\|_2$	2.088×10^{-2}	2.536×10^{-3}	2.536×10^{-3}
$\|\mathbf{s}\|_2$	2.040×10^{-2}	1.423×10^{-3}	1.423×10^{-3}

Table 4: Results for $m = 100$.

	Planar $RRRR$	Spherical $RRRR$	Spatial $RCCC$
α_{opt} (deg.)	116.0679	42.6740	-47.3261
β_{opt} (deg.)	88.9057	88.7674	-1.2326
κ_{opt}	32.5170	205.5603	205.5603
$\|\mathbf{d}\|_2$	2.499×10^{-2}	3.047×10^{-3}	3.047×10^{-3}
$\|\mathbf{s}\|_2$	2.464×10^{-2}	1.712×10^{-3}	1.712×10^{-3}

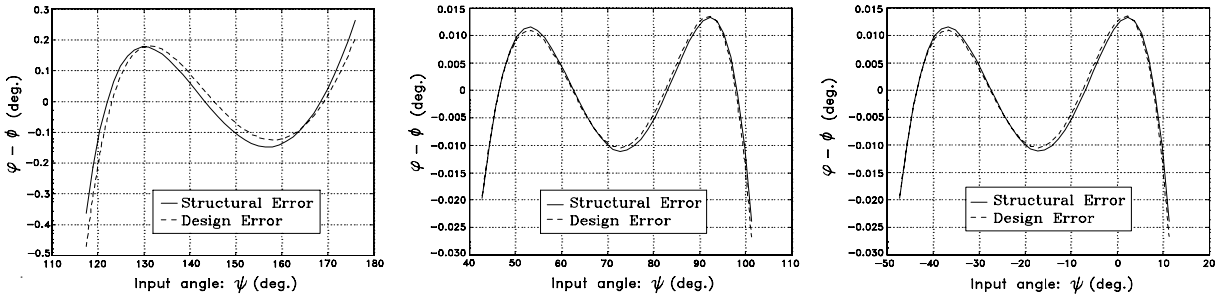

Figure 1. Structural error comparison for *(i)* planar, *(ii)* spherical $RRRR$ and *(iii)* spatial $RCCC$ mechanisms minimising $\|\mathbf{s}\|_2$ & $\|\mathbf{d}\|_2$.

4 Discussion and Conclusions

Examining Tables 1–4, it can be seen that $\|\mathbf{d}\|_2$ and $\|\mathbf{s}\|_2$ increase with m for each mechanism. The trend for the planar $RRRR$ is towards convergence. It is interesting to note that the error results are identical for the spherical $RRRR$ and the spatial $RCCC$ linkages, except that α_{opt} and β_{opt} are different. In a sense, this is not surprising because of the symmetrical nature of the function in the $\psi - \phi$ plane. Moreover, the synthesis equations for these two linkages are, with the exception of sign, trigonometric complements in the form considered in this article. However, compared to the planar $RRRR$, we see

the errors converge near $m = 40$, but then diverge again for higher values of m. Fig. 1 shows the close agreement of the respective structural error curves for $m = 40$. In all cases treated, a number of prescribed I/O values of at least $m = 10$ is sufficient for the minimisation of the Euclidean norm of the design error to lead to the same norm of the structural error within a reasonable difference.

These results support our hypothesis that for a suitably large data-set cardinality linkage optimisation using design and structural error based objective functions result in virtually identical function-generating mechanisms. The obvious weakness is that the cardinality of the data-set for which convergence is obtained is not known *a priori*. Nonetheless, further pursuit of this result is worthwhile because of its computational simplicity.

5 Acknowledgements

The support of Canada's Natural Sciences and Engineering Research Council through a research grant to the third author and a graduate fellowship to the first author is highly acknowledged.

References:

Tinubu, S.O. and Gupta, K.C., Optimal Synthesis of Function Generators Without the Branch Defect, ASME, J. of Mech., Trans., and Autom. in Design, Vol. 106, Sept. 1984, pp. 348–354.

Wilde, D.J., Error Linearization in the Least-Squares Design of Function Generating Mechanisms, ASME, J. of Mech., Des., Vol. 104, Oct. 1982, pp. 881–884.

Freudenstein, F., Approximate Synthesis of Four-Bar Linkages, Trans. ASME, Vol. 77, Aug. 1955, pp. 853-861.

Hartenberg, R.S. and Denavit, J., Kinematic Synthesis of Linkages, McGraw-Hill Book Co., New York, N.Y., U.S.A., 1964.

Liu, Z., Kinematic Optimization of Linkages, Ph.D. Thesis, Dept. of Mech. Eng., McGill University, Montreal, Canada, 1993.

Liu, Z. and Angeles, J., Least-Square Optimization of Planar and Spherical Four-Bar Function Generator Under Mobility Constraints, ASME, J. of Mech. Des., Vol. 114, Dec. 1992, pp. 569–573.

Liu, Z. and Angeles, J., Data Conditioning in the Optimization of Function-Generating Linkages, ASME, Adv. in Design Auto., DE-Vol 65-1, Vol. 1, 1993, pp. 419–425.

Golub, G.H. and Van Loan, C.F., Matrix Computations, The Johns Hopkins University Press, Baltimore, U.S.A., 1989.

Dahlquist, G. and Björck, Å., Numerical Methods, translated by Anderson, N., Prentice-Hall, Inc., 1969, pp. 248–251, 442–446.

Mechanism and Machine Theory 101 (2016) 158–167

Contents lists available at ScienceDirect

Mechanism and Machine Theory

journal homepage: www.elsevier.com/locate/mechmt

Continuous approximate synthesis of planar function-generators minimising the design error

Alexis Guigue[a], M. John D. Hayes[b,*]

[a] Softree Technical Systems Inc., Vancouver, British Columbia, Canada
[b] Mechanical and Aerospace Engineering, Carleton University, Ottawa, Ontario, Canada

ARTICLE INFO

Article history:
Received 3 December 2015
Received in revised form 17 March 2016
Accepted 18 March 2016
Available online 6 April 2016

Keywords:
Approximate and continuous
kinematic synthesis
Design error
Structural error
Function-generating linkage

ABSTRACT

It has been observed in the literature that as the cardinality of the prescribed discrete input–output data set increases, the corresponding four-bar linkages that minimise the Euclidean norm of the design and structural errors tend to converge to the same linkage. The important implication is that minimising the Euclidean norm, or any p-norm, of the structural error, which leads to a nonlinear least-squares problem requiring iterative solutions, can be accomplished implicitly by minimising that of the design error, which leads to a linear least-squares problem that can be solved directly. Apropos, the goal of this paper is to take the first step towards proving that as the cardinality of the data set tends towards infinity the observation is indeed true. In this paper we will integrate the synthesis equations in the range between minimum and maximum input values, thereby reposing the discrete approximate synthesis problem as a continuous one. Moreover, we will prove that a lower bound of the Euclidean norm, and indeed of any p-norm, of the design error for planar RRRR function-generating linkages exists and is attained with continuous approximate synthesis.

1. Introduction

Design and structural errors are important performance indicators in the assessment and optimisation of function-generating linkages arising by means of approximate synthesis. The *design error* indicates the error residual incurred by a specific linkage in satisfying its synthesis equations. The *structural error*, in turn, is the difference between the prescribed linkage output value and the actual generated output value for a given input value [1]. From a design point of view it may be successfully argued that the structural error is the one that really matters, for it is directly related to the performance of the linkage.

It was shown in Ref. [2] that as the cardinality of the prescribed discrete input–output (I/O) data-set increases, the corresponding linkages that minimise the Euclidean norms of the design and structural errors tend to converge to the same linkage. The important implication of this observation is that the minimisation of the Euclidean norm of the structural error can be accomplished indirectly via the minimisation of the corresponding norm of the design error, provided that a suitably large number of I/O pairs is prescribed. The importance arises from the fact that the minimisation of the Euclidean norm of the design error leads to a linear least-squares problem whose solution can be obtained directly as opposed to iteratively [3,4], while the minimisation of the same norm of the structural error leads to a nonlinear least-squares problem, and hence, calls for an iterative solution [1].

* Corresponding author.
E-mail address: John.Hayes@carleton.ca (M. Hayes).

http://dx.doi.org/10.1016/j.mechmachtheory.2016.03.012
0094-114X/

Several issues have arisen in the design error minimisation of four-bar linkages. First, the condition number of the synthesis matrix may lead to design parameters that poorly approximate the prescribed function [5]. This problem can be addressed through careful selection of the I/O pairs used to generate the synthesis matrix. It has also been suggested to introduce dial zeros whose values are chosen to minimise the condition number of the synthesis matrix [6]. Second, the identified design parameters have a dependence on the I/O set cardinality. As the number of I/O pairs grows, the magnitude of the design error tends to converge to a lower bound. Hence, the I/O set cardinality might be fixed as soon as the magnitude of the design error reaches some pre-defined minimum value [2].

Diverse interesting and useful optimisation strategies have been proposed recently for structural error minimisation in planar four-bar function-generators. For example, in Ref. [7] the authors define the least squares error between the desired and generated functions as the objective function for a sequential quadratic programming (SQP) approach. The proposed method solves a sequence of optimisation subproblems, each of which optimises a quadratic model of the objective function subject to a linearisation of the constraints based on the distribution of a finite set of precision points. Another novel approach which considers the minimisation of the structural error of the link lengths is described in Ref. [8]. The method treats one of the dyads as having fixed distances between joint centres, while the other dyad has links of variable length. The adjustable link lengths are varied using a discrete set of precision points as benchmarks. A completely different approach is used in Ref. [9] to develop a probabilistic, time-dependent function-generator synthesis method. The authors introduce the concept of "interval reliability synthesis". The dimensions of the link lengths are treated as random variables while their mean values become the design variables, and the probability of failure to produce the function within a prescribed tolerance is minimised over a defined time interval and corresponding position level interval of the function. While these methods achieve excellent results, they do not shed any light on the curious tendency observed in Ref. [2]. What the vast body of literature reporting investigations into function-generator synthesis optimisation is missing is a systematic study of what the implications are of allowing the cardinal number of the I/O data set to tend towards infinity.

Hence, the goal of this paper is to take the first step towards proving that the convergence observed in Ref. [2] is true for planar four-bar function-generators. More precisely, a proof will be given for the design error that as the cardinality of the I/O data set increases from discrete numbers of I/O pairs to an infinite number between minimum and maximum pairs that a lower bound for any p-norm of the design error exists, and corresponds to that of the infinite I/O set, thereby changing the discrete approximate synthesis problem to a continuous approximate synthesis problem. To this end, the design error minimisation occurs in the space of a continuous function possessing an L_p norm defined later in this paper. However, our study is currently restricted to the planar RRRR function-generating linkage, where R denotes *revolute joint*, synthesised using the kinematic model defined in Ref. [10].

2. Design error minimisation: the discrete approximate approach

The synthesis problem of planar four-bar function-generators consists of determining all relevant design parameters such that the mechanism can produce a prescribed finite set of m I/O pairs, $\{\psi_i, \varphi_i\}_1^m$, where ψ_i and φ_i represent the i^{th} input and output variables, respectively, and m is the cardinality of the finite data-set. We define n to be the number of independent design parameters required to fully characterise the mechanism. For planar RRRR linkages, $n = 3$ [10]. If $m = n$, the problem is termed *exact synthesis* and may be considered a special case of approximate synthesis where $m > n$.

We consider the optimisation problem of planar four-bar function-generators as the approximate solution of an overdetermined linear system of equations with the least error. The synthesis equations that are used to establish the linear system for a four-bar function-generator are the *Freudenstein equations* [10]. Consider the mechanism in Fig. 1. The i^{th} configuration is governed by:

$$k_1 + k_2 \cos(\varphi_i) - k_3 \cos(\psi_i) = \cos(\psi_i - \varphi_i), \tag{1}$$

where the k's are the *Freudenstein parameters* , which are the following link length ratios:

$$k_1 = \frac{(a_1^2 + a_2^2 + a_4^2 - a_3^2)}{2a_2a_4}; \quad k_2 = \frac{a_1}{a_2}; \quad k_3 = \frac{a_1}{a_4}. \tag{2}$$

Given a set of three Freudenstein parameters, the corresponding set of link lengths, scaled by a_1, are:

$$a_1 = 1; \quad a_2 = \frac{1}{k_2}; \quad a_4 = \frac{1}{k_3}; \quad a_3 = (1 + a_2^2 + a_4^2 - 2a_2a_4k_1)^{1/2}. \tag{3}$$

The finite set of I/O equations can be written in the following form, using Eq. (1)

$$\mathbf{Sk} = \mathbf{b}, \tag{4}$$

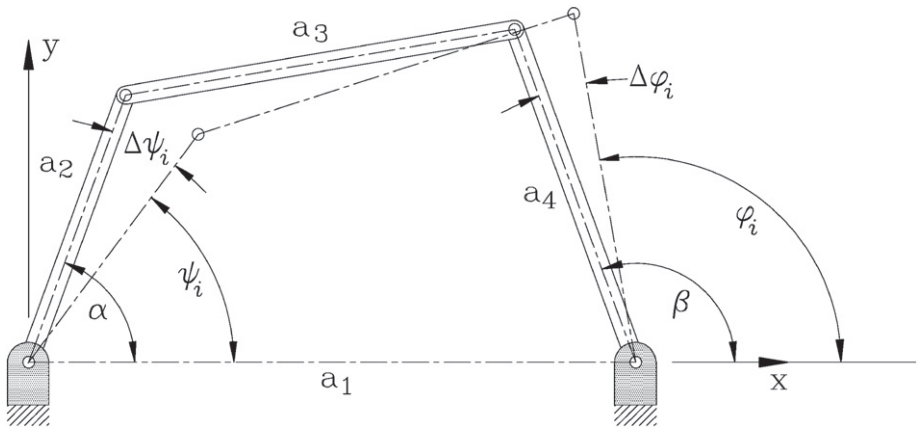

Fig. 1. A four-bar linkage in two configurations.

where $\mathbf{S}$ is the $m \times 3$ *synthesis matrix*, whose i^{th} row is the 1×3 array $\mathbf{s}_i$, $\mathbf{b}$ is an m-dimensional vector, whereas $\mathbf{k}$ is the 3-dimensional vector of design variables called the *Freudenstein parameters* [10]. For the planar RRRR mechanism we have:

$$\mathbf{s}_i = [1 \cos\varphi_i - \cos\psi_i], \quad i = 1, \ldots, m, \tag{5}$$

$$b_i = \cos(\psi_i - \varphi_i), \quad i = 1, \ldots, m, \tag{6}$$

$$\mathbf{k} = [k_1 k_2 k_3]^T. \tag{7}$$

The synthesised linkage will only be capable of generating the desired function approximately. The design error is the algebraic difference of the left-hand side of Eq. (4) less the right-hand side. Because we will be comparing errors associated with different cardinalities, we now include the cardinality m in the definition. The m-dimensional design error vector $\mathbf{d}_m$ for a finite discrete set of $m > 3$ I/O pairs, $\{(\psi_i, \varphi_i)_{i=1\ldots m}\}$, is defined as:

$$\mathbf{d}_m = \mathbf{S}_m \mathbf{k} - \mathbf{b}_m. \tag{8}$$

If the output values prescribed by the functional relationship, $\varphi_{pres,i}$, correspond precisely to the output values generated by the mechanism, i.e., $\varphi_{gen,i}$, then, $\| \mathbf{d}_m \| = 0$. However, for a general prescribed function $\varphi_{pres}(\psi)$, $\| \mathbf{d}_m \| \neq 0$ and we seek the Freudenstein parameter vector that minimises the norm of the design error vector. In general, the weighted Euclidian norm is used:

$$\| \mathbf{d}_m \|^2_{\mathbf{W}_m,2} = \frac{1}{2} \quad \mathbf{d}_m^T \mathbf{W}_m \mathbf{d}_m, \tag{9}$$

where $\mathbf{W}_m$ is an $m \times m$ diagonal matrix with strictly positive elements. In a typical design problem, $\mathbf{W}_m$ is used to adjust the impact on the optimisation of specific I/O pairs. However, for the purposes of this work, $\mathbf{W}_m$ will be set to the identity matrix, $\mathbf{I}_m$. The optimal Freudenstein parameters $\mathbf{k}^*_m$ for this norm are:

$$\mathbf{k}^*_m = \mathbf{S}^+_m \mathbf{b}_m, \tag{10}$$

where $\mathbf{S}^+_m$ is the Moore–Penrose generalised inverse of the synthesis matrix, and the corresponding minimal design error is:

$$\rightarrow \min_{\mathbf{k}} \| \mathbf{d}_m \|_2 = \| \mathbf{d}^*_m \|_2 = \| (\mathbf{I}_m - \mathbf{S}_m \mathbf{S}^+_m) \mathbf{b}_m \|_2. \tag{11}$$

In general, for any matrix, square or rectangular, the condition number κ is a measure of how invertible the matrix is: it is the ratio of the largest to smallest singular values. Consider the system of linear equations represented by $\mathbf{Ax} = \mathbf{b}$. The matrix $\mathbf{A}$ may be viewed as a map from vector space $\mathbf{x}$ to vector space $\mathbf{b}$. A very large condition number of $\mathbf{A}$ implies that the smallest singular value of the matrix is very small, meaning that $\mathbf{b}$ is poorly approximated by $\mathbf{Ax}$. This also implies that $\mathbf{A}^{-1}\mathbf{b}$ very poorly approximates $\mathbf{x}$. Extremely large condition numbers indicate that there is a near linear dependency among some of the rows of $\mathbf{A}$, meaning that one, or more, of its singular values is very close to zero. Such matrices are termed ill-conditioned. The

condition number κ is a property of the matrix **A** and entirely independent of the vector spaces **x** and **b**. For numerical stability considerations, it is always desirable to have a well-conditioned synthesis matrix, otherwise the numerical values of $\mathbf{S}_m^+$ may be significantly distorted by very small singular values, or singular values identically equal to zero, leading to optimised **k** that imply a mechanism which very poorly approximates the function. Hence, the dial zeros α and β, illustrated in Fig. 1, have been introduced to minimise the condition number, κ, of $\mathbf{S}_m$:

$$\psi_i = \alpha + \Delta\psi_i; \quad \varphi_i = \beta + \Delta\varphi_i. \tag{12}$$

When the dial zeros are substituted into Eq. (1), the synthesis equation becomes:

$$k_1 + k_2\cos(\beta + \Delta\varphi_i) - k_3\cos(\alpha + \Delta\psi_i) = \cos(\alpha + \Delta\psi_i - \beta - \Delta\varphi_i), \tag{13}$$

and, the I/O pairs are regarded as a discrete set of incremental angular changes $\{(\Delta\psi_i, \Delta\varphi_i)_{i=0..m}\}$. The arrays $\mathbf{d}_m^*$, $\mathbf{k}_m^*$ and $\mathbf{S}_m$ are now also functions of the dial zeros. With this modification, the design error minimisation problem can be efficiently solved in a least squares sense in two steps:

1. determine the dial zeros to minimise the condition number $\kappa_m(\alpha, \beta)$ of the synthesis matrix $\mathbf{S}_m$;
2. determine the corresponding optimal Freudenstein parameters using Eq. (10).

3. Design error minimisation: the continuous approximate approach

A major issue associated with the discrete approach to the design error minimisation is the appropriate choice for the cardinality of the discrete I/O pair data set such that the minimisation of the structural error is implied. Indeed, the choice of m depends on the prescribed function $\Delta\varphi_{pres}(\Delta\psi)$ and m is generally fixed when some level of convergence is observed. For the example used in Ref. [2] $m = 40$ was observed to be a good choice. We now propose to evaluate the design error over the continuous range between minimum and maximum, or initial and final, input values of the prescribed function, denoted $[\Delta\psi_0, \Delta\psi_f]$. We only consider functions that are continuous over $[\Delta\psi_0, \Delta\psi_f]$, that are defined in a function space, denoted $\mathcal{C}^0([\Delta\psi_0, \Delta\psi_f])$, whereupon the following L_p-norm has been defined for any continuous function f on the closed interval $[\Delta\psi_0, \Delta\psi_f]$:

$$\forall f \in \mathcal{C}^0([\Delta\psi_0, \Delta\psi_f]), \|f\|_p = \left(\int_{\Delta\psi_0}^{\Delta\psi_f} |f(\psi)|^p d\psi\right)^{1/p}, \tag{14}$$

where p is an integer such that $p \geq 1$. Imposing the L_p-norm upon this function space makes $\mathcal{C}^0([\Delta\psi_0, \Delta\psi_f])$ an L_p-space. Such L_p-spaces are defined using a generalisation of the vector norm for finite-dimensional vector spaces [4]. Vector norms are special cases of the family of L_p-norms, often denoted by l_p while L_p is reserved for norms in function spaces [4]. The most common L_p-norms for a continuous function f on a closed interval $[a, b]$, and in fact, the most commonly used vector norms [11], are the *maximum* or *Chebyshev* norm, the Euclidean norm, and the so called Manhattan norm[1] which are respectively defined by:

$$\|f\|_\infty = \max_{x\in[a,b]} |f(x)|; \tag{15}$$

$$\|f\|_2 = \left(\int_a^b f(x)^2 dx\right)^{1/2}; \tag{16}$$

$$\|f\|_1 = \int_a^b |f(x)| dx. \tag{17}$$

The Manhattan and Chebyshev norms are the limiting cases ($p = 1$ and $p = \infty$, respectively) of the family of L_p-norms [4]. The L_p-norms obey the following relationship:

$$\|f\|_\infty \leq \cdots \leq \|f\|_2 \leq \|f\|_1. \tag{18}$$

Typically, the most appropriate norm must be selected to evaluate the magnitude of the objective function for the error minimisation, given a function that is to be approximated by the resulting linkage. However, it turns out that Lawson's

[1] The term Manhattan norm arises because the vector norm corresponds to sums of distances along the basis vector directions, as one would travel along a rectangular street plan.

algorithm [12,13] can be used to sequentially minimise the Chebyshev norm via the minimisation of the Euclidean norm [14]. This means that the continuous approximate approach to the design error minimisation is independent of the L_p-norm because it applies to both the Chebyshev and Euclidean norms, and hence all intermediate ones. Therefore, without loss in generality the Euclidean norm will be used in the example in Section 5, which follows the development of the approach.

Assuming that the prescribed function belongs to $\mathcal{C}^0([\Delta\psi_0, \Delta\psi_f])$, the design error is defined using the Euclidean norm, though any L_p-norm could be used [14]:

$$\| \mathbf{d}(\alpha,\beta)\|_2 = \left(\int_{\Delta\psi_0}^{\Delta\psi_f} (k_1 + k_2\cos(\beta+\Delta\varphi) - k_3\cos(\alpha+\Delta\psi) - \cos(\alpha+\Delta\psi-\beta-\Delta\varphi))^2 d\Delta\psi \right)^{\frac{1}{2}}. \tag{19}$$

After some algebraic manipulation, it can be shown that the square of Eq. (19) is a quadratic function in terms of the Freudenstein parameters:

$$\| \mathbf{d}(\alpha,\beta) \|_2^2 = \mathbf{k}^T\mathbf{A}(\alpha,\beta)\mathbf{k} - 2\mathbf{e}(\alpha,\beta)^T\mathbf{k} + c(\alpha,\beta). \tag{20}$$

The matrix $\mathbf{A}(\alpha,\beta)$ is a 3 × 3 a symmetric positive semidefinite matrix whose six distinct elements a_{ij} are:

$$\begin{aligned}
a_{11} &= \int_{\Delta\psi_0}^{\Delta\psi_f} d\Delta\psi = \Delta\psi_f - \Delta\psi_0;\\
a_{12} &= \int_{\Delta\psi_0}^{\Delta\psi_f} \cos(\beta+\Delta\varphi)d\Delta\psi;\\
a_{13} &= -\int_{\Delta\psi_0}^{\Delta\psi_f} \cos(\alpha+\Delta\psi)d\Delta\psi;\\
a_{22} &= \int_{\Delta\psi_0}^{\Delta\psi_f} \cos^2(\beta+\Delta\varphi)d\Delta\psi\\
a_{23} &= -\int_{\Delta\psi_0}^{\Delta\psi_f} \cos(\beta+\Delta\varphi)\cos(\alpha+\Delta\psi)d\Delta\psi\\
a_{33} &= \int_{\Delta\psi_0}^{\Delta\psi_f} \cos^2(\alpha+\Delta\psi)d\Delta\psi;
\end{aligned}$$

while $\mathbf{e}(\alpha,\beta)$ is a 3-dimensional vector whose elements are:

$$\begin{aligned}
e_1 &= \int_{\Delta\psi_0}^{\Delta\psi_f} \cos(\alpha+\Delta\psi-\beta-\Delta\varphi)d\Delta\psi;\\
e_2 &= \int_{\Delta\psi_0}^{\Delta\psi_f} (\cos(\beta+\Delta\varphi)\cos(\alpha+\Delta\psi-\beta-\Delta\varphi))d\Delta\psi;\\
e_3 &= -\int_{\Delta\psi_0}^{\Delta\psi_f} (\cos(\alpha+\Delta\psi)\cos(\alpha+\Delta\psi-\beta-\Delta\varphi))d\Delta\psi;
\end{aligned}$$

and finally $c(\alpha,\beta)$ is a scalar having the form:

$$c = \int_{\Delta\psi_0}^{\Delta\psi_f} \cos^2(\alpha+\Delta\psi-\beta-\Delta\varphi)d\Delta\psi.$$

When $\mathbf{A}(\alpha,\beta)$ is positive definite, the optimal Freudenstein parameters $\mathbf{k}^*(\alpha,\beta)$ which minimise $\| \mathbf{d}(\alpha,\beta) \|_2^2$ (or equivalently $\|\mathbf{d}(\alpha,\beta) \|_2$) are:

$$\mathbf{k}^*(\alpha,\beta) = \mathbf{A}^{-1}(\alpha,\beta)\mathbf{e}(\alpha,\beta), \tag{21}$$

and the square of the minimal design error is:

$$\min_{\mathbf{k}} \| \mathbf{d}(\alpha,\beta) \|_2^2 = \| \mathbf{d}^*(\alpha,\beta) \|_2^2 = c(\alpha,\beta) - \mathbf{e}(\alpha,\beta)^T\mathbf{A}^{-1}(\alpha,\beta)\mathbf{e}(\alpha,\beta). \tag{22}$$

The assumption of positive definiteness for $\mathbf{A}(\alpha,\beta)$ will be discussed in Section 4. However, a necessary condition for $\mathbf{A}(\alpha,\beta)$ to be positive definite is that it is non-singular. This justifies *a posteriori* why we use the dial zeros. In this case, as in Section 2, the design error minimisation problem is solved in two steps:

1. determine the dial zeros to minimise the condition number $\kappa(\alpha,\beta)$ of $\mathbf{A}(\alpha,\beta)$;
2. determine the corresponding optimal Freudenstein parameters using Eq. (21).

Intuitively, the continuous approximate approach should correspond to the limit of the discrete approximate approach. This is proven to be so in the next section.

4. The design error of the discrete approximate approach is lower bounded by that of the continuous approximate approach

In this section, we assume that $\Delta\varphi_{pres}(\Delta\psi)$ is a continuously differentiable function, however Propositions 1, 2, and 3, which follow, only require continuity. With this assumption and using the notation introduced in the previous sections, the following propositions hold.

Proposition 1. *$\boldsymbol{A}(\alpha,\beta)$ is positive semidefinite, and*

$$\lim_{m\to\infty} \kappa_m(\alpha,\beta) = \kappa(\alpha,\beta).$$

Proposition 2. *If $\boldsymbol{A}(\alpha,\beta)$ possesses full rank, then,*

$$\lim_{m\to\infty} \mathbf{k}_m^*(\alpha,\beta) = \mathbf{k}^*(\alpha,\beta).$$

Recall that $\mathbf{k}^*(\alpha,\beta)$ minimises the design error under the condition that $\mathbf{A}(\alpha,\beta)$ is positive definite. Now, from Proposition 1, we can claim that $\mathbf{A}(\alpha,\beta)$ is at least positive semidefinite. However, the positive definitiveness is not guaranteed and it justifies the need for the assumption in Proposition 2.

Proposition 3. *If $\boldsymbol{A}(\alpha,\beta)$ possesses full rank, then,*

$$\lim_{m\to\infty} \frac{\Delta\psi_f - \Delta\psi_0}{m} \parallel \mathbf{d}_m^*(\alpha,\beta)\parallel_2 = \parallel \mathbf{d}^*(\alpha,\beta)\parallel_2.$$

Proposition 4. *Let (α^*,β^*) be the dial zero pair that minimises $\kappa(\alpha,\beta)$. If the optimal solution (α^*,β^*) is unique, then,*

$$\lim_{m\to\infty} (\alpha_m^*,\beta_m^*) = (\alpha^*,\beta^*).$$

Proposition 5. *If the optimal solution (α^*,β^*) is unique, then,*

$$\lim_{m\to\infty} \kappa_m(\alpha_m,\beta_m) = \kappa(\alpha^*,\beta^*).$$

Moreover, if $\boldsymbol{A}(\alpha^*,\beta^*)$ possesses full rank, then,

$$\lim_{m\to\infty} \mathbf{k}_m^*(\alpha_m,\beta_m) = \mathbf{k}^*(\alpha^*,\beta^*),$$

and

$$\lim_{m\to\infty} \frac{\Delta\psi_f - \Delta\psi_0}{m} \parallel \mathbf{d}_m^*(\alpha_m,\beta_m)\parallel_2 = \parallel \mathbf{d}^*(\alpha^*,\beta^*)\parallel_2.$$

Proposition 5 is our main result. It essentially states that the optimal Freudenstein parameters and the minimal design error for the discrete approach converge to the optimal Freudenstein parameters and the minimal design error for the continuous approach.

4.1. Proofs

Proof of Proposition 1. the proof of Proposition 1 requires the following result.

Proposition 6. *Let f be a continuous function on some interval*$[a,b]$, *then* [4]

$$\lim_{n\to+\infty}\sum_{i=0}^{n-1}\frac{b-a}{n}f(a+i\frac{b-a}{n})=\int_a^b f(x)dx.$$

From Proposition 6, the elements of $\mathbf{A}_m(\alpha,\beta)=\frac{\Delta\psi_f-\Delta\psi_0}{m}\mathbf{S}_m^T(\alpha,\beta)\mathbf{S}_m(\alpha,\beta)$ converge to the elements of $\mathbf{A}(\alpha,\beta)$.

Recall the definitions for positive definiteness and positive semidefiniteness: a real $n\times n$ matrix $\mathbf{A}$ is positive definite if, for all vectors $\mathbf{x}\in\mathbb{R}$, $\mathbf{x}^T\mathbf{A}\mathbf{x}>0$, and positive semidefinite if, for all vectors $\mathbf{x}\in\mathbb{R}$, $\mathbf{x}^T\mathbf{A}\mathbf{x}\geq 0$. Now, from the definitions of the elements a_{ij} of $\mathbf{A}(\alpha,\beta)$ we have

$$\mathbf{A}(\alpha,\beta)=\int_{\Delta\psi_0}^{\Delta\psi_f}\mathbf{B}d\Delta\psi, \tag{23}$$

where $\mathbf{B}$ is a symmetric 3×3 matrix:

$$\mathbf{B}=\begin{bmatrix}1 & \cos(\beta+\Delta\varphi) & -\cos(\alpha+\Delta\psi)\\ \cos(\beta+\Delta\varphi) & \cos^2(\beta+\Delta\varphi) & -\cos(\beta+\Delta\varphi)\cos(\alpha+\Delta\psi)\\ -\cos(\alpha+\Delta\psi) & -\cos(\beta+\Delta\varphi)\cos(\alpha+\Delta\psi) & \cos^2(\alpha+\Delta\psi)\end{bmatrix}. \tag{24}$$

Matrix $\mathbf{B}$ has the special property that it is the vector product of vector $\mathbf{v}$ and its transpose, where

$$\mathbf{v}=\begin{bmatrix}1\\ \cos(\beta+\Delta\varphi)\\ -\cos(\alpha+\Delta\psi)\end{bmatrix}, \tag{25}$$

such that

$$\mathbf{v}\mathbf{v}^T=\mathbf{B}. \tag{26}$$

Then, for each vector $\mathbf{x}=[x_1,x_2,x_3]^T$ in $\mathbb{R}^3$ the function

$$f(\mathbf{x},\Delta\psi)=\mathbf{x}^T\mathbf{B}\mathbf{x}$$

has only non-negative values, as

$$f(\mathbf{x},\Delta\psi)=\mathbf{x}^T\mathbf{B}\mathbf{x}\ =\ \mathbf{x}^T(\mathbf{v}\mathbf{v}^T)\mathbf{x}=\ (\mathbf{x}^T\mathbf{v})^2\geq\ 0.$$

From this result, it necessarily follows that

$$\mathbf{x}^T\mathbf{A}\mathbf{x}=\mathbf{x}^T\left(\int_{\Delta\psi_0}^{\Delta\psi_f}\mathbf{B}d\Delta\psi\right)\mathbf{x}=\ \int_{\Delta\psi_0}^{\Delta\psi_f}(\mathbf{x}^T\mathbf{B}\mathbf{x})d\Delta\psi=\ \int_{\Delta\psi_0}^{\Delta\psi_f}f(\mathbf{x},\Delta\psi)d\Delta\psi\geq\ 0,$$

which completes the proof. Now, given an arbitrary function, the function-generator designer need only check that the eigenvalues of the matrix $\mathbf{A}$ defined by the given function are all greater than zero.

Proof of Proposition 2. the proof of Proposition 2 requires the following proposition.

Proposition 7. *If a sequence of matrices* $\mathbf{M}_n$ *converges to a matrix* $\mathbf{M}$ *and* $\mathbf{M}$ *is invertible then,* $\mathbf{M}_n^{-1}$ *converges to* $\mathbf{M}^{-1}$ [15].

From Proposition 1, $\mathbf{A}_m(\alpha,\beta)$ converges towards $\mathbf{A}(\alpha,\beta)$. $\mathbf{A}(\alpha,\beta)$ possesses full rank by hypothesis, then there must be some index m_0 such that $\forall m\geq m_0$ and $\mathbf{A}_m(\alpha,\beta)$ possesses full rank. Hence, $\forall m\geq m_0\mathbf{S}_m(\alpha,\beta)$ possesses full rank and the pseudo-inverse $\mathbf{S}_m^+(\alpha,\beta)$ is:

$$\mathbf{S}_m^+(\alpha,\beta)=(\mathbf{S}_m^T(\alpha,\beta)\mathbf{S}_m(\alpha,\beta))^{-1}\mathbf{S}_m^T(\alpha,\beta)=\frac{\Delta\psi_f-\Delta\psi_0}{m}\mathbf{A}_m^{-1}(\alpha,\beta)\mathbf{S}_m^T(\alpha,\beta). \tag{27}$$

Eq. (10) then becomes:

$$\mathbf{k}_m^*(\alpha,\beta) = \mathbf{A}_m^{-1}(\alpha,\beta)\left(\frac{\Delta\psi_f - \Delta\psi_0}{m}\mathbf{S}_m^T(\alpha,\beta)\mathbf{b}_m(\alpha,\beta))\right). \tag{28}$$

From Proposition 6, $\left(\frac{\Delta\psi_f-\Delta\psi_0}{m}\mathbf{S}_m^T(\alpha,\beta)\mathbf{b}_m(\alpha,\beta)\right)$ converges to $\mathbf{e}(\alpha,\beta)$. From Proposition 7, $\mathbf{A}_m^{-1}(\alpha,\beta)$ converges towards $\mathbf{A}^{-1}(\alpha,\beta)$, hence $\mathbf{k}_m^*(\alpha,\beta)$ converges towards $\mathbf{A}^{-1}(\alpha,\beta)\mathbf{e}(\alpha,\beta)$ which is equal to $\mathbf{k}^*(\alpha,\beta)$ in Eq. (21). This completes the proof.

Proof of Proposition 3. Eq. (11) can be rewritten:

$$\| \mathbf{d}_m^*(\alpha,\beta) \|_2^2 = \mathbf{b}_m^T(\alpha,\beta)\mathbf{b}_m(\alpha,\beta) - \left(\mathbf{S}_m^T(\alpha,\beta)\mathbf{b}_m(\alpha,\beta)\right)^T \mathbf{k}_m^*(\alpha,\beta). \tag{29}$$

Multiply Eq. (29) by $\frac{\Delta\psi_f-\Delta\psi_0}{m}$. From Proposition 6, $\left(\frac{\Delta\psi_f-\Delta\psi_0}{m}\mathbf{S}_m^T(\alpha,\beta)\mathbf{b}_m(\alpha,\beta)\right)$ converges to $\mathbf{e}(\alpha,\beta)$ and $\left(\frac{\Delta\psi_f-\Delta\psi_0}{m}\mathbf{b}_m^T(\alpha,\beta)\mathbf{b}_m(\alpha,\beta)\right)$ converges to $c(\alpha,\beta)$. From Proposition 2, $\mathbf{k}_m^*(\alpha,\beta)$ converges towards $\mathbf{k}^*(\alpha,\beta)$. This completes the proof.

Proof of Proposition 4. the proof of Proposition 4 requires the following proposition:

Proposition 8. *Letfbe a function continuously differentiable on*$[a,b]$, *then* [16]

$$\left|\int_a^b f(x)dx - \lim_{n\to+\infty}\sum_{i=0}^{n-1}\frac{b-a}{n}f(a+i\frac{b-a}{n})\right| \le \frac{(b-a)\max\{f'(x), x\in[a,b]\}}{n}.$$

The dial zeros are members of a compact set defined by the Cartesian product $K = [-\pi,\pi]\times[-\pi,\pi]$. Hence, the maximum of the first derivative of any entry of $\mathbf{A}_m(\alpha,\beta)$ is bounded uniformly relative to (α,β). From Proposition 8, it follows that the elements of $\mathbf{A}_m(\alpha,\beta)$ converge uniformly relative to (α,β) towards the elements of $\mathbf{A}(\alpha,\beta)$.

The sequence (α_m^*,β_m^*) belongs to K. Hence, there exists a subsequent $(\alpha_{\varphi(m)}^*,\beta_{\varphi(m)}^*)$ which converges to some $(\alpha_\varphi^*,\beta_\varphi^*)$. From the uniform convergence of $\mathbf{A}_m(\alpha,\beta)$, it follows that the elements of $\mathbf{A}_{\varphi(m)}(\alpha_{\varphi(m)}^*,\beta_{\varphi(m)}^*)$ converge towards the elements of $\mathbf{A}(\alpha_\varphi^*,\beta_\varphi^*)$. Following the same arguments used in the proof of Proposition 1, we get:

$$\lim_{m\to\infty}\kappa_{\varphi(m)}(\alpha_{\varphi(m)}^*,\beta_{\varphi(m)}^*) = \kappa(\alpha_\varphi^*,\beta_\varphi^*), \tag{30}$$

or $(\alpha_{\varphi(m)}^*,\beta_{\varphi(m)}^*)$ minimises the condition number of $\mathbf{A}_{\varphi(m)}(\alpha,\beta)$, hence:

$$\forall(\alpha,\beta)\in K, \kappa_{\varphi(m)}(\alpha_{\varphi(m)}^*,\beta_{\varphi(m)}^*) \le \kappa_{\varphi(m)}(\alpha,\beta).$$

From Eq. (30) and Proposition 1, taking the limit on both sides of this inequality gives:

$$\forall(\alpha,\beta)\in K, \kappa(\alpha_\varphi^*,\beta_\varphi^*) \le \kappa(\alpha,\beta).$$

Hence, $(\alpha_\varphi^*,\beta_\varphi^*)$ minimises the condition number of $\mathbf{A}(\alpha,\beta)$. In other words, each convergent (α_m^*,β_m^*) converges to a minimum of the condition number of $\mathbf{A}(\alpha,\beta)$. By hypothesis, this minimum is unique. Hence, $\forall\varphi,(\alpha_\varphi^*,\beta_\varphi^*) = (\alpha^*,\beta^*)$ and the whole sequence (α_m^*,β_m^*) converges to (α^*,β^*). This completes the proof.

Proof of Proposition 5. the first statement of Proposition 5 has been proved in the proof of Proposition 4, see Eq. (30). From the uniform convergence arising from Proposition 8 the convergence in Proposition 2 and Proposition 3 is in fact uniform. The last two statements of Proposition 5 follow. To be completely rigorous, Proposition 7 should be modified to uniform convergence, but doing so introduces no contradictions.

5. Example

The preceding results for continuous approximate synthesis that minimises the design error are now illustrated with an example. Let the prescribed function be the Ackerman steering condition for terrestrial vehicles. The steering condition can be expressed as a trigonometric function whose variables are illustrated in Fig. 2:

$$\sin(\Delta\varphi_{pres} - \Delta\psi) - \rho\sin(\Delta\psi)\sin(\Delta\varphi_{pres}) = 0, \tag{31}$$

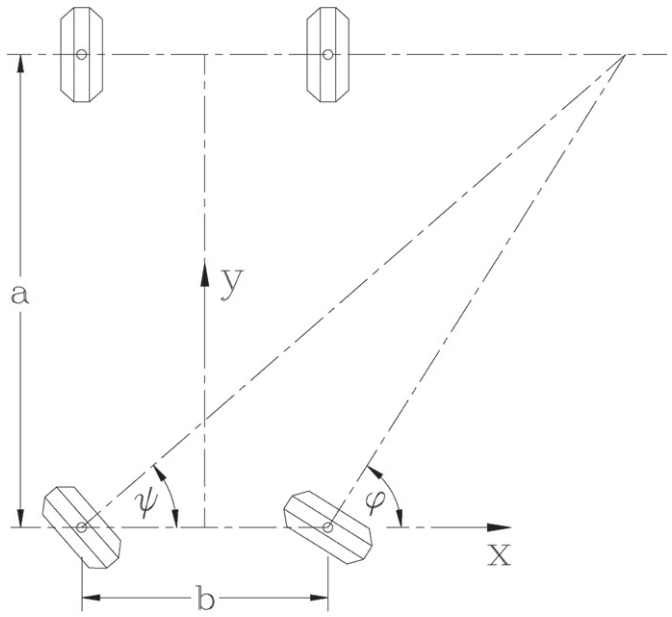

Fig. 2. Graphical illustration of the *Ackerman steering condition*.

with ρ denoting the length ratio b/a, where a is the distance between front and rear axles, and b the distance between the pivots of the wheel-carriers, which are coupled to the chassis. With the dial zeros, the expression for the steering condition becomes:

$$\sin(\beta + \Delta\varphi_{pres} - \alpha - \Delta\psi) - \rho \sin(\alpha + \Delta\psi)\sin(\beta + \Delta\varphi_{pres}) = 0. \tag{32}$$

For our example, $\rho = 0.5$ and $[\Delta\psi_0, \Delta\psi_f] = [-40.00, 30.00]$, where angles are specified in degrees. With these values, the prescribed function, i.e. the steering condition, is continuously differentiable. Hence, Proposition 5 must apply.

5.1. Establishing the optimal dial zeros and Freudenstein parameters

The multi-dimensional Nelder–Mead downhill simplex algorithm [17] is employed to find the optimal values for the dial zeros. Table 1 lists (α^*_m, β^*_m) for different values of m, as well as (α^*, β^*). From the optimal dial zeros obtained in Table 1, it is now possible to compute the optimal Freudenstein parameters. Table 2 lists the optimised Freudenstein parameters, k_i, synthesis matrix condition numbers κ_m, and design error norms which have been normalised by dividing by $\sqrt{m}$ for comparison for different values of m as well as the values using the continuous approach.

Continuous approximate synthesis eliminates the problem of determining an appropriate cardinal number for the data-set because it evaluates the case for $m \to \infty$. Hence there is no need to search for some convergence in order to set the proper value of m, which eliminates a source of error. However, the continuous approach requires numerical integrations, which itself is a source of error. These errors are in fact of the same nature. Indeed, from the development of Section 4, it is clear that discrete approximate synthesis is essentially a numerical integration method itself: Romberg's method for example, which is an extrapolation on the trapezoidal rule [4]. Hence, comparing the errors arising from the discrete approximate synthesis with continuous approximate synthesis is equivalent to comparing the error terms of two different numerical integration methods. The example presented above employed the Matlab function *quadl*, which employs recursive adaptive Lobatto quadrature [18].

Table 1
Optimal dial zeros.

m	α^*_m	β^*_m	α^*	β^*
10	−61.80	67.320	–	–
40	−62.17	68.73	–	–
100	−62.23	69.03	–	–
400	−62.26	69.17	–	–
1000	−62.27	69.20	–	–
∞	–	–	−62.27	69.22

Table 2
Optimised Freudenstein parameters, condition numbers, and normalised design errors.

m	k_1	k_2	k_3	κ_m	κ^*	$\| \mathbf{d}_m \|_2$	$\| \mathbf{d}^* \|_2$
10	−0.993	0.412	−0.429	18.24	–	6.93×10^{-4}	–
40	−1.001	0.406	−0.425	20.79	–	6.44×10^{-4}	–
100	−1.003	0.405	−0.424	21.38	–	6.31×10^{-4}	–
400	−1.003	0.404	−0.424	21.69	–	6.24×10^{-4}	–
1000	−1.004	0.404	−0.424	21.75	–	6.23×10^{-4}	–
∞	−1.004	0.404	−0.424	–	475.03	–	6.23×10^{-4}

6. Conclusions and future work

In this paper a proof has been given that the design error of planar RRRR function-generating linkages synthesised using over-constrained systems of equations established with discrete I/O data sets is bounded by a minimum value established using continuous approximate synthesis between minimum and maximum I/O values. Evaluating the design error over the entire continuous range of the function requires the use of a functional normed space, thereby changing the discrete approximate synthesis problem to a continuous approximate synthesis problem. Assuming that the prescribed function $\Delta\varphi_{pres}(\Delta\psi)$ is continuously differentiable, it is shown that the dial zeros, the optimal Freudenstein parameters, and the minimal design error for discrete approximate synthesis converge towards the dial zeros, the optimal Freudenstein parameters and the minimal design error for continuous approximate synthesis. In other words, the continuous approach corresponds to the discrete approach after setting the cardinality of the I/O set to $m \to \infty$, and represents the bounding optimal values.

The extension of this work is to investigate how the structural error as defined in Ref. [2] bounds the design error. First, it should be determined whether the structural error minimisation problem can be formulated and, more importantly solved, using the continuous approach. Second, it should be investigated whether in this case too, the continuous approach corresponds to the discrete approach with $m \to \infty$. This is certainly much more challenging due to the increased complexity of the continuous structural error minimisation problem, which is a non-linear problem with equality constraints, compared to the continuous design error minimisation problem, which is a quadratic problem without any constraints. Finally, one might ask whether our developments could be applied to other mechanism topologies, such as planar mechanisms possessing prismatic joints, as well as spherical, or spatial linkages.

Acknowledgments

The authors gratefully acknowledge partial financial support for this work provided by a research grant from the *Natural Sciences and Engineering Research Council of Canada* (NSERC) (250012-2011).

References

[1] S.O. Tinubu, K.C. Gupta, Optimal synthesis of function generators without the branch defect, ASME, J. of Mech., Trans., and Autom. in Design 106 (1984) 348–354.
[2] M.J.D. Hayes, K. Parsa, J. Angeles, The effect of data-set cardinality on the design and structural errors of four-bar function-generators, Proceedings of the Tenth World Congress on the Theory of Machines and Mechanisms, Oulu, Finland, 1999, 437–442.
[3] D.J. Wilde, Error synthesis in the least-squares design of function generating mechanisms, ASME, J. of Mechanical Design 104 (1982) 881–884.
[4] G. Dahlquist, Å. Björck, Numerical Methods, translated by Anderson, Prentice-Hall, Inc., U.S.A. 1969.
[5] Z. Liu, J. Angeles, Data conditioning in the optimization of function-generating linkages, Advances in Design Automation: Proc. 19th Annual ASME Design Automation Conference, 1993, 419–426.
[6] Z. Liu, Kinematic Optimization of Linkages, Dept. of Mech. Eng., McGill University, Montréal, QC, Canada, 1993. (Ph.D. thesis)
[7] M. Shariati, M. Norouzi, Optimal synthesis of function generator of four-bar linkages based on distribution of precision points, Mechanica 46 (5) (2011) 1007–1021.
[8] C. Peng, R.S. Sohdi, Optimal synthesis of adjustable mechanisms generating multi-phase approximate paths, Mech. Mach. Theory 45 (7) (2010) 989–996.
[9] J. Zhang, J. Wang, X. Du, Time-dependent probabilistic synthesis for function generator mechanisms, Mech. Mach. Theory 46 (9) (2011) 1236–1250.
[10] F. Freudenstein, Approximate synthesis of four-bar linkages, Trans. ASME 77 (1955) 853–861.
[11] J.E. Gentle, Numerical Linear Algebra for Applications in Statistics, Springer, New York, U.S.A. 1998.
[12] C.L. Lawson, Contributions to the Theory of Linear Least Maximum Approximations, UCLA, Los Angeles, California, U.S.A., 1961. (Ph.D. thesis)
[13] J.R. Rice, K.H. Usow, The Lawson algorithm and extensions, Math. Comput. 22 (101) (December 1967) 118–126.
[14] F. Angeles, J. Angeles, Synthesis of function-generating linkages with minimax structural error: the linear case, Proc. 13th IFToMM World Congress, June 2011.
[15] J. Ercolano, Golden sequences of matrices with application to Fibonacci algebra, The Fibonacci Quarterly 15 (5) (December 1976) 419–426.
[16] N.B. Haaser, J.A. Sullivan, Real Analysis, Van Nostrand Reinhold Co., New York, U.S.A. 1971.
[17] J.A. Nelder, R. Mead, A simplex method for function minimization, Computer Journal 7 (4) (1965) 308–313.
[18] L.F. Shampine, Vectorized adaptive quadrature in MATLAB, J. Comput. Appl. Math. 211 (February 2008) 131–140.

Proceedings of DETC/CIE'02
2002 ASME Design Engineering Technical Conferences
September 29 - October 02, 2002, Montréal , Québec, Canada

DETC2002/MECH-34378

SOLVING THE BURMESTER PROBLEM USING KINEMATIC MAPPING

M.J.D. Hayes*
Carleton University
Deptartment of Mechanical &
Aerospace Engineering
1125 Colonel By Drive
Ottawa, Ontario,
Canada, K1S 5B6
Email: jhayes@mae.carleton.ca

P.J. Zsombor-Murray
McGill University
Dept. of Mechanical Engineering
Centre for Intelligent Machines
817 Sherbrooke St. W.
Montréal, Québec,
Canada, H3A 2K6
Email: paul@cim.mcgill.ca

ABSTRACT

Planar kinematic mapping is applied to the five-position Burmester problem for planar four-bar mechanism synthesis. The problem formulation takes the five distinct rigid body poses directly as inputs to generate five quadratic constraint equations. The five poses are on the fourth order curve of intersection of up to four hyperboloids of one sheet in the image space. Moreover, the five poses uniquely specify these two hyperboloids. So, given five positions of any reference point on the coupler and five corresponding orientations, we get the fixed revolute centres, the link lengths, crank angles, and the locations of the coupler attachment points by solving a system of five quadratics in five variables that always factor in such a way as to give two pairs of solutions for the five variables (when they exist).

1 Introduction

The determination of a planar four-bar mechanism that can guide a rigid-body through five finitely separated *poses* (position and orientation) is known as the *five-position Burmester problem*, see Burmester (1888). It may be stated as follows. Given five positions of a point on a moving rigid body and the corresponding five orientations of some line on that body, design a four-bar mechanism whose coupler crank pins are located on the moving body and is assemblable upon these five poses. The coupler must assume the five required poses, however sometimes not all five may lie in the same assembly branch.

The problem formulation engenders as many variables as equations so the synthesis is exact. However, most approaches to synthesizing a mechanism that can guide the rigid body exactly through the five positions are rooted in the Euclidean geometry of the plane in which the rigid body must move. From time to time this problem has been revisited (Chang, *et al*, 1991). Readers are refered to this document which contains a recent solution method and a quite adequate and relevant bibliography. More recently, classical finite position synthesis has been reviewed by McCarthy (2000).

We propose a solution obtained in a three-dimensional projective image space of the rigid body motion. An algebraic approach to this exact problem based on quaternions is to be found in Murray and McCarthy (1996). Instead, we use planar kinematic mapping. The planar kinematic mapping was introduced independently by Blaschke and Grünwald in 1911 (Blaschke, 1911; Grünwald, 1911). But, their writings are difficult. In North America Roth, De Sa, Ravani (De Sa and Roth, 1981; Ravani and Roth, 1983), as well as others, have made contributions. However, we choose to build upon interpretations by Husty (1995, 1996), who used the accessible language of Bottema and Roth (1990).

Kinematic synthesis of four-bar mechanisms using kinematic mapping was discussed in Bottema and Roth (1990), originally published in 1979, and expanded upon in great detail by Ravani (1982), and Ravani and Roth (1983). In this early work, Ra-

*Address all correspondence to this author.

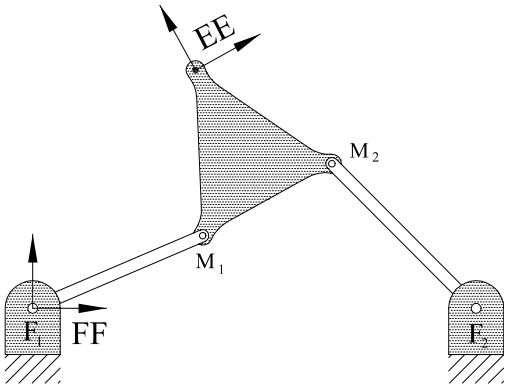

Figure 1. A FOUR-BAR LINKAGE.

vani and Roth developed the framework for performing *approximate* dimensional synthesis. While *exact* dimensional synthesis for the Burmester problem may have been implied, it has never, to our knowledge, been implemented. Results are so elegantly obtained in the kinematic mapping image space that we are compelled to expose the methodology and procedure by which these are produced.

In this image space, the kinematic constraint implied by the motion of a point bound to move upon a circle of fixed centre and radius maps to a hyperboloid of one sheet. Thus, the motion of the coupler of a planar four-bar mechanism connected with four revolute (R) pairs can be characterized by the fourth order curve of intersection of two distinct hyperboloids of one sheet in the image space.

When the kinematic constraint dictates a point moving on a line with fixed line coordinates, as with a prismatic (P) pair, the constraint surface is a hyperbolic paraboloid. Hyperboloids of one sheet and hyperbolic paraboloids are the only types of constraint surfaces associated with planar mechanisms containing only lower pair joints (Hayes and Husty, 2001). Here, we assume solutions of the five-position Burmester problem confined to four-bar mechanisms jointed with four R-pairs, not slider-cranks. Thus only image space hyperboloids of one sheet will apply.

2 Planar Kinematic Mapping

One can consider the relative displacement of two rigid-bodies in the plane as the displacement of a Cartesian reference coordinate frame EE attached to one of the bodies with respect to a Cartesian reference coordinate frame FF attached to the other. Without loss of generality, FF may be considered as fixed while EE is free to move, as is the case with the four-bar mechanism illustrated by Figure 1. Then the position of a point in EE in terms of the basis of FF can be expressed compactly as

$$\mathbf{p}' = \mathbf{R}\mathbf{p} + \mathbf{d}, \tag{1}$$

where, $\mathbf{p}$ is the 2×1 position vector of a point in EE, $\mathbf{p}'$ is the position vector of the same point in FF, $\mathbf{d}$ is the position vector of the origin of frame EE in FF, and $\mathbf{R}$ is a 2×2 proper orthogonal rotation matrix (*i.e.*, its determinant is $+1$) defined by the orientation of EE in FF indicated by ϕ.

Equation (1) can always be represented as a linear transformation by making it *homogeneous* (see McCarthy (1990), for example). Let the homogeneous coordinates of points in the fixed frame FF be the ratios $[X : Y : Z]$, and those of points in the moving frame EE be the ratios $[x : y : z]$. Then Equation (1) can be rewritten as

$$\begin{bmatrix} X \\ Y \\ Z \end{bmatrix} = \begin{bmatrix} \cos\phi & -\sin\phi & a \\ \sin\phi & \cos\phi & b \\ 0 & 0 & 1 \end{bmatrix} \begin{bmatrix} x \\ y \\ z \end{bmatrix}. \tag{2}$$

Equation (2) clearly reflects the fact that a general displacement in the plane is fully characterized by three parameters, in this case a, b, and ϕ.

2.1 Image Space Coordinates and Pole Position

The essential idea of the kinematic mapping introduced by Blashke (1911) and Grünwald (1911)is to map the three homogeneous coordinates of the pole of a planar displacement, in terms of (a, b, ϕ), to the points of a three dimensional projective image space.

The pole, P, of a planar displacement may be described in the following way. Any planar displacement that is a combination of translation and rotation may be represented by a single rotation through a finite angle about a unique fixed axis normal to the plane. Even a pure translation can be considered a rotation through an infinitesimal angle about a point at infinity on a line perpendicular to the direction of the translation. The coordinates of the piercing point of this axis with the plane of the displacement describe the pole, P. If EE and FF are initially coincident, then the coordinates of P are invariant under the its related displacement. That is, P has the same coordinates in both EE and FF. This is illustrated in Figure 2.

By using the dehomogenized form of Equation (2) one may immediately write, after setting $X_P = x_P$ and $Y_P = y_P$ and solving the resulting two simultaneous equations

$$x_P = \frac{a}{2} - \frac{b\sin\phi}{2(1-\cos\phi)}; \quad y_P = \frac{a\sin\phi}{2(1-\cos\phi)} + \frac{b}{2}.$$

The value of the homogenizing coordinate is arbitrary and may, without loss of generality, be set to $z = 2\sin\phi/2$. This means that

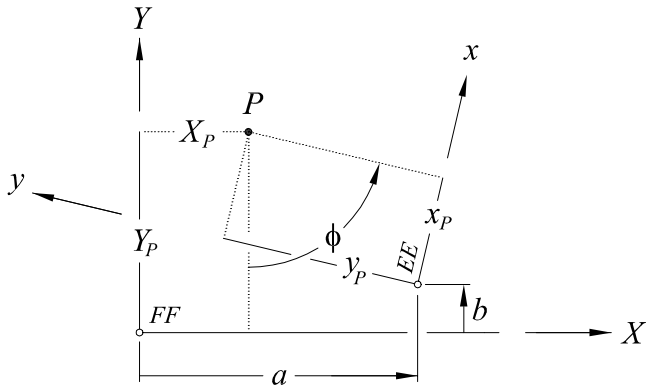

Figure 2. POLE POSITION.

both x_P and y_P must also be multiplied by this value. Then the double angle relationships

$$\sin 2\phi = 2\sin\phi\cos\phi; \quad \cos 2\phi = \cos^2\phi - \sin^2\phi$$

can be used to obtain the following homogeneous coordinates of the pole:

$$\begin{aligned} X_P = x_P &= a\sin(\phi/2) - b\cos(\phi/2) \\ Y_P = y_P &= a\cos(\phi/2) + b\sin(\phi/2) \\ Z_P = z_P &= 2\sin(\phi/2) \end{aligned} \tag{3}$$

The kinematic mapping image coordinates are defined, with respect to the pole P as follows.

$$\begin{aligned} X_1 &= a\sin(\phi/2) - b\cos(\phi/2) \\ X_2 &= a\cos(\phi/2) + b\sin(\phi/2) \\ X_3 &= 2\sin(\phi/2) \\ X_4 &= 2\cos(\phi/2). \end{aligned} \tag{4}$$

Since each distinct displacement described by (a,b,ϕ) has a corresponding unique image point, the inverse mapping can be obtained from Equation (4): for a given point of the image space, the displacement parameters are

$$\begin{aligned} \tan(\phi/2) &= X_3/X_4, \\ a &= 2(X_1X_3 + X_2X_4)/(X_3^2 + X_4^2), \\ b &= 2(X_2X_3 - X_1X_4)/(X_3^2 + X_4^2). \end{aligned} \tag{5}$$

Equations (5) give correct results when either X_3 or X_4 is zero. Caution is in order, however, because the mapping is injective, not bijective: *there is at most one pre-image for each image point*. Thus, not every point in the image space represents a displacement. It is easy to see that any image point on the real line $X_3 = X_4 = 0$ has no pre-image and therefore does not correspond to a real displacement of EE. From Equation (5), this condition renders ϕ indeterminate and places a and b on the line at infinity.

Armed with Equations (4) and (5) any displacement in terms of X_1, X_2, X_3, X_4 can be conveniently converted to the displacement of EE in terms of FF.

2.2 Representing Planar Displacements in Terms of Image Space Coordinates

By virtue of the relationships expressed in Equation (4), the transformation matrix from Equation (2) may be expressed in terms of the homogeneous coordinates of the image space. This yields a linear transformation to express a displacement of EE with respect to FF in terms of the image point:

$$\lambda \begin{bmatrix} X \\ Y \\ Z \end{bmatrix} = \begin{bmatrix} X_4^2 - X_3^2 & -2X_3X_4 & 2(X_1X_3 + X_2X_4) \\ 2X_3X_4 & X_4^2 - X_3^2 & 2(X_2X_3 - X_1X_4) \\ 0 & 0 & X_3^2 + X_4^2 \end{bmatrix} \begin{bmatrix} x \\ y \\ z \end{bmatrix}, \tag{6}$$

where λ is a proportionality constant arising from the use of homogeneous coordinates. The inverse transformation can be obtained with the inverse of the 3×3 matrix in Equation (6) as follows.

$$\mu \begin{bmatrix} x \\ y \\ z \end{bmatrix} = \begin{bmatrix} X_4^2 - X_3^2 & 2X_3X_4 & 2(X_1X_3 - X_2X_4) \\ -2X_3X_4 & X_4^2 - X_3^2 & 2(X_2X_3 + X_1X_4) \\ 0 & 0 & X_3^2 + X_4^2 \end{bmatrix} \begin{bmatrix} X \\ Y \\ Z \end{bmatrix}, \tag{7}$$

with μ being another proportionality constant. The product of these matrices is homogeneously proportional to a unit matrix:

$$\begin{bmatrix} (X_3^2 + X_4^2)^2 & 0 & 0 \\ 0 & (X_3^2 + X_4^2)^2 & 0 \\ 0 & 0 & (X_3^2 + X_4^2)^2 \end{bmatrix}.$$

Clearly, by construction in Equation (4), $X_3^2 + X_4^2 \equiv 2$.

2.3 Planar Constraint Equations

Consider the case of an R-R joint dyad. A point on EE moves on a circle on FF, whose homogeneous equation may be expressed by:

$$C_0(X^2 + Y^2) + 2C_1XZ + 2C_2YZ + C_3Z^2 = 0. \tag{8}$$

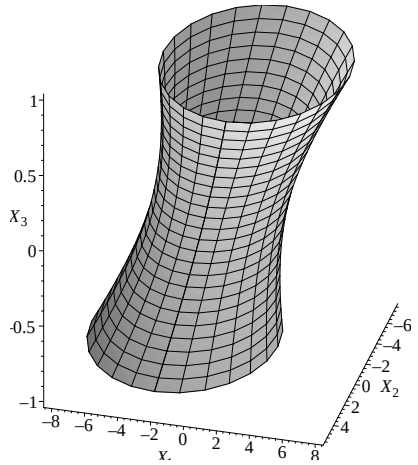

Figure 3. A HYPERBOLOID OF ONE SHEET.

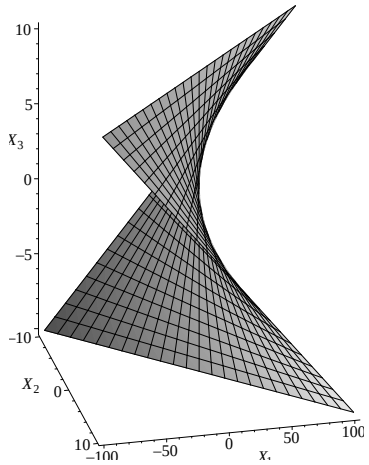

Figure 4. A HYPERBOLIC PARABOLOID.

In Equation (8) $C_0 = k$, an arbitrary constant, while $C_1 = -X_m$, $C_2 = -Y_m$, the circle centre coordinates, and $C_3 = X_m^2 + Y_m^2 - r^2$ with r being the circle radius.

Expanding Equation (6) and substituting the expressions for X, Y, and Z into Equation (8) produces a hyperboloid of one sheet in the image space, see Figure 3. The hyperboloid takes the form:

$$\begin{aligned} &C_0 z^2(X_1^2+X_2^2)+(-C_0x+C_1z)zX_1X_3 \\ &+(-C_0y+C_2z)zX_2X_3+(-C_0y-C_2z)zX_1X_4 \\ &+(C_0x+C_1z)zX_2X_4+(-C_1y+C_2x)zX_3X_4 \\ &+\frac{1}{4}[C_0(x^2+y^2)-2C_1xz-2C_2yz+C_3z^2]X_3^2 \\ &+\frac{1}{4}[C_0(x^2+y^2)+2C_1xz+2C_2yz+C_3z^2]X_4^2=0. \end{aligned} \tag{9}$$

Recall that the coordinates of a point in the moving frame EE are $(x:y:z)$. The hyperboloid is specified when a reference point $(x:y:z)$ is given together with the circle coordinates $(C_0 : C_1 : C_2 : C_3)$. The points $(X_1 : X_2 : X_3 : X_4)$ represent all possible displacements of EE relative to FF under the constraint that one point in FF moves on a circle in EE.

We can generalize the constraint hyperboloid by considering the kinematic inversion: a point on FF bound to move on a circle in EE. We thus expand Equation (5) and substitute the expressions for x, y, and z into Equation (8) and make the following simplifications. For the given circular constraint it is clear that $C_0 = 1$. We may also set $z = X_4 = 1$. The general constraint hyperboloid then becomes

$$\begin{aligned} &(X_1^2+X_2^2)+(C_1-x)X_1X_3+(C_2-y)X_2X_3 \\ &\mp(C_2+y)X_1\pm(C_1+x)X_2\pm(C_2x-C_1y)X_3 \\ &+\frac{1}{4}[(x^2+y^2)-2C_1x-2C_2y+C_3]X_3^2 \\ &+\frac{1}{4}[(x^2+y^2)+2C_1x+2C_2y+C_3]=0. \end{aligned} \tag{10}$$

When (x,y) are the coordinates of the moving point expressed in EE with $z=1$ the *upper* signs apply. If the constraint is intended to express the inverse, a point on FF bound to a circle in EE, then the *lower* signs apply *and* x, y or z is substituted wherever X, Y or Z appears. The situation of a circle moving on a point is never required in problem formulation.

However if a point is bound to a line, *i.e.*, in the case of a prismatic joint, and if one desires to treat inversions, the line may be either on FF *or* EE. Equation (10) reduces to Equation (11) if a point is bound to a line and $C_0 = 0$. This produces a hyperbolic paraboloid in the image space, see Figure 4:

$$\begin{aligned} &C_1X_1X_3+C_2X_2X_3\mp C_2X_1\pm C_1X_2\pm(C_2x-C_1y)X_3 \\ &-\frac{1}{4}[2C_1x+2C_2y-C_3]X_3^2+\frac{1}{4}[2C_1x+2C_2y+C_3]=0. \end{aligned} \tag{11}$$

The above constraint surfaces completely describe the displacements of all possible planar dyads constructed with lower pairs.

3 The Five-Position Burmester Problem

The goal of the dimensional synthesis problem for rigid body guidance of a 4R planar mechanism is to find the *moving*

circle points, M_1 and M_2 of the coupler, i.e., the revolute centres that move on fixed centred, fixed radii circles as a reference coordinate system, EE, attached to the coupler, passes through the desired poses. The *fixed centre points* for each circle are the fixed, or grounded revolute centres, F_1 and F_2, respectively. The circle and centre points are illustrated with the four-bar mechanism shown in Figure 1. For these constraints, the synthesis equations are determined using Equation (10).

What we set out to do here is to use the methods of planar kinematic mapping outlined in (Zsombor-Murray, *et al*, 2002) and set up five simultaneous constraint equations, each of which represents the image space constraint surface for a rigid body moving freely in the plane except that one point is bound to the circumference of a fixed circle. These equations are expressed in terms of the following eight variables.

i. X_1, X_2, X_3, $X_4 = 1$, the dehomogenized coordinates of the coupler pose in the image space.
ii. C_1, C_2, C_3, the coefficients of a circle equation ($C_0 = 1$).
iii. x, y, $z = 1$,the coordinates of the moving crank-pin revolute centre, on the coupler, which moves on a circle.

Since X_1, X_2, X_3 are given for five desired coupler poses, one may in principle solve for the remaining five variables (C_1, C_2, C_3, x, y) . The geometric interpretation is, five given points in space are common to, at most, four hyperboloids on one sheet. Each hyperboloid represents a 2R dyad. If two real solutions occur then all 4R mechanism design information is available (there are two circles in a feasible mechanism design result):

i. Circle centre is at $X_m = -C_1$, $Y_m = -C_2$.
ii. Circle radius is given by $r^2 = C_3 - (X_m^2 + Y_m^2)$.
iii. Coupler length is given by $L^2 = (x_2 - x_1)^2 + (y_2 - y_1)^2$.

4 Analysis

4.1 Converting Pose to Image Space Coordinates

Examine Equations (4) and divide by X_4.

$$X_1 = \frac{\left(a\tan\frac{\phi}{2} - b)\right)}{2},\ X_2 = \frac{\left(a + b\tan\frac{\phi}{2}\right)}{2},\ X_3 = \tan\frac{\phi}{2},\ X_4 = 1.$$

The five given poses being specified as (a_i, b_i, ϕ_i), $i \in \{1, ..., 5\}$, the planar coordinates of the moving point and the orientation of a line on the moving rigid body, all with respect to $(0, 0, 0^\circ)$ expressed in FF. Note that the location of the origin of FF is arbitrary, it is only shown on the fixed revolute centre in Figure 1 for convenience.

4.2 Crank Angles

If the desired five poses can be realized with a planar 4R four-bar mechanism, then at least two real solutions in

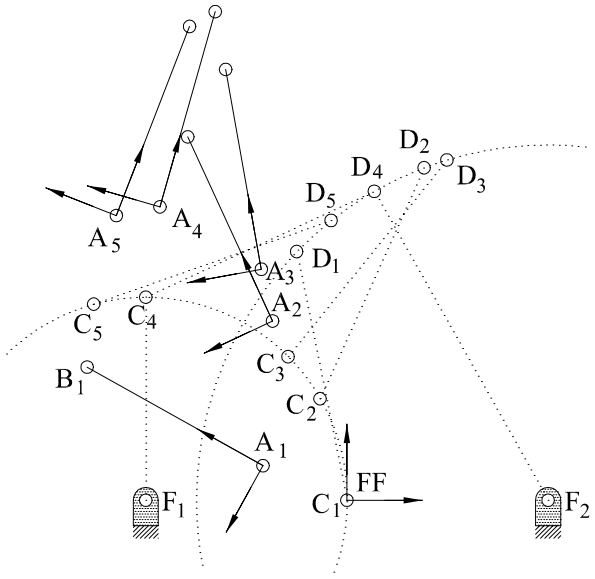

Figure 5. GENERATING THE FIVE DESIRED POSES.

(C_1, C_2, C_3, x, y) will be obtained, defining two 2R dyads sharing the coupler. To construct the mechanism in its five configurations the crank angles must be determined. To obtain the crank angles one just takes (x_1, y_1) and (x_2, y_2) and performs the linear transformation, expressed in image space coordinates, five times.

$$\begin{bmatrix} X \\ Y \\ 1 \end{bmatrix} = \begin{bmatrix} 1 - X_3^2 & -2X3 & 2(X_1X_3 + X2) \\ 2X_3 & 1 - X_3^2 & 2(X_2X_3 - X_1) \\ 0 & 0 & 1 + X_3^2 \end{bmatrix} \begin{bmatrix} x \\ y \\ 1 \end{bmatrix}.$$

(X, Y) come in five pairs because five poses are specified. These are the Cartesian coordinates of the moving revolute centres expressed in FF, and implicitly define the crank angles. For a practical design one must check that the solution did not separate crank pin coordinates in unconnected mechanism branches.

4.3 Pose Constraint Equation

Given the constraints imposed by four revolute joints, the pose constraint equation (synthesis equation) is given by Equation (10) with the upper signs used. For each of the five poses we obtain:

$$\begin{aligned} &(X_1^2 + X_2^2) + (C_1 - x)X_1X_3 + (C_2 - y)X_2X_3 \\ &-(C_2 + y)X_1 + (C_1 + x)X_2 + (C_2x - C_1y)X_3 \\ &+\tfrac{1}{4}[(x^2 + y^2) - 2C_1x - 2C_2y + C_3]X_3^2 \\ &+\tfrac{1}{4}[(x^2 + y^2) + 2C_1x + 2C_2y + C_3] = 0. \end{aligned} \tag{12}$$

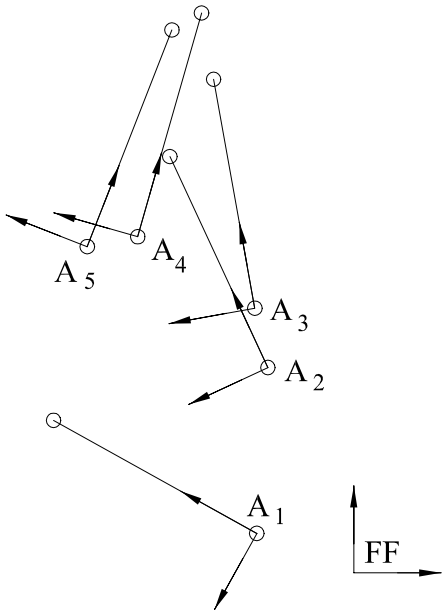

Figure 6. THE FIVE DESIRED POSES.

Parameter	Value
F_1	(-8,0)
F_2	(8,0)
F_1F_2	16
F_1C	8
CD	10
DF_2	14

Table 1. THE GENERATING MECHANISM

i^{th} Pose, A_i	a	b	φ (deg)
1	-3.339	1.360	150.94
2	-2.975	7.063	114.94
3	-3.405	9.102	100.22
4	-7.435	11.561	74.07
5	-9.171	11.219	68.65

Table 2. FIVE RIGID BODY POSES IN FF.

5 Example and Verification

The kinematic mapping solution to the five-position Burmester problem is illustrated with the following example problem. In order to verify our synthesis results, we started with Figure 5, wherein one sees a four-bar mechanism design represented by dotted crank pin circles and a coupler CD which has been placed in five feasible poses. Then an arbitrary point A and orientation line AB were specified. These were used to specify the given five poses, listed in Table 2. The fixed revolute centres and link lengths of the four-bar mechanism used to generate the poses, which we can check for verification, are listed in Table 1, all coordinates given relative to FF. The coordinate information obtained from these were inserted into the five synthesis equations. The results at the end constitute obvious confirmation concerning the effectiveness of the kinematic mapping approach to solving the Burmester problem.

Given the Cartesian coordinates of five positions of a reference point on a rigid body, together with five orientations of the rigid body which correspond to the positions, all relative to an arbitrary fixed reference frame, FF. The reference point is the origin of a coordinate system, A, attached to the rigid body. In Figure 6 the five poses are indicated by the position of A and the orientation of a line in the direction x_A axis. The coordinates and orientations are listed in Table 2.

The given five poses are mapped to five sets of coordinates in the image space. Using a computer algebra software package, we substitute the corresponding values for X_1, X_2, X_3, together with $X_4 = 1$ into Equation (12) yields the following five quadratics in C_1, C_2, C_3, x, and y:

$$\begin{aligned} &51.62713350 - 26.52347891C_1 + 28.43187273x \\ &+3.439909575y + 10.80321393C_2 + 3.971769828y^2 \\ &+3.971769828x^2 - 6.943539655C_1x + 3.971769828C_3 - \\ &6.943539655C_2y - 3.858377808C_1y + 3.858377808C_2x = 0 \end{aligned} \quad (13)$$

$$\begin{aligned} &50.78111719 - 5.144112496C_1 + 13.24300208x \\ &-.485305000y + 12.21272826C_2 + .8645567222y^2 \\ &+.8645567222x^2 - .7291134440C_1x + .8645567222C_3 \\ &-.7291134440C_2y - 1.567873365C_1y + 1.567873365C_2x = 0 \end{aligned} \quad (14)$$

$$\begin{aligned} &57.40558942 - 4.139456673C_1 + 11.62418825x \\ &+2.110482435y + 11.06529652C_2 + .6078497318y^2 \\ &+.6078497318x^2 - .2156994635C_1x + .6078497318C_3 \\ &-.2156994635C_2y - 1.196410852C_1y + 1.196410852C_2x = 0 \end{aligned} \quad (15)$$

$$\begin{aligned} &74.12376162 - 5.833830775C_1 + 7.121746695x \\ &+8.099525062y + 9.071273378C_2 + .3923221773y^2 \\ &+.3923221773x^2 + .2153556452C_1x + .3923221773C_3 \\ &+.2153556452C_2y - .7545122328C_1y + .7545122328C_2x = \end{aligned} \quad (16)$$

$$\begin{aligned} &76.96602922 - 6.723290851C_1 + 5.212549019x \\ &+9.256210937y + 8.224686519C_2 + .3665516768y^2 \\ &+.3665516768x^2 + .2668966465C_1x + .3665516768C_3 \\ &+.2668966465C_2y - .6827933120C_1y + .6827933120C_2x = 0 \end{aligned} \quad (17)$$

Solving the system of Equations (13)-(17) yields four sets of values for C_1, C_2, C_3, x, and y, two being real, and the remaining two being complex conjugates. The two real sets of hyperboloid coefficients are listed in Table 3. The corresponding synthesized four-bar fixed revolute centres and link lengths are listed in Table 4, rounded to same three decimal places as the graphically determined generating mechanism listed in Table 1.

Coefficient	Solution 1	Solution 2
C_1	-7.983138944	7.997107716
C_2	-.027859304	-.000953257
C_3	-131.4773813	-.022545268
x	2.932070052	-3.579426217
y	-8.023883728	-.435620093

Table 3. THE HYPEBOLOID COEFFICIENTS

Parameter	Value
F_1	(-7.997,0.001)
F_2	(7.983,-0.023)
F_1F_2	15.980
F_1C	7.999
CD	10.003
DF_2	13.972

Table 4. THE SYNTHESIZED MECHANISM

While the synthesized mechanism link lengths and centre coordinates are affected by the numerical resolution of the graphical construction of the generating mechanism, we believe this example demonstrates the utility of kinematic mapping to solving the five-position Burmester problem.

6 Computational Pathology

Notice that feasible slider-crank solutions were implicitly excluded by choosing to set $C_0 = z = 1$ rather than, say, $C_2 = y = 1$. This is similar to excluding half-turn EE orientations by setting $X_4 = 1$ rather than, say, $X_3 = 1$. It is recommended that algorithmic implementation should retain $X_4 = 2\cos(\phi/2)$ and contain features to replace $C_0 = 1$ with C_1, C_2 or $C_3 = 1$ and $z = 1$ with x or $y = 1$ should results where $x \to y \to \infty$ with $C_0 = z = 1$ occur.

7 Conclusions

We have used kinematic mapping to solve the five position planar Burmester problem. Five rigid body poses are mapped to points in a three dimensional projective image space and are used directly as inputs to generate five quadratic constraint surface equations in that space. The solutions, when they exist, give the coefficients of the hyperboloids having the five points in common. Each hyperboloid yields a fixed revolute centre, link lengths, crank angles, and coupler attachment points. This method is elegant in that the design task for any composition of R and P joints (open RR, PR, and RP chains) can be treated with a single formulation with no special cases.

REFERENCES

1. Blaschke, W., 1911, "Euklidische Kinematik und nichteuklidische Geometrie", *Zeitschr. Math. Phys.*, Vol. 60, pp. 61-91 and 203-204.
2. Bottema, O. & Roth, B., 1990, *Theoretical Kinematics*, Dover, ch.XI, pp.393-445.
3. Burmester, L., 1888, *Lehrbuch der Kinematik*, A. Felix, Leipzig.
4. Ching Yu Chang, Angeles, J., González-Palacios, M., 1991, "A Semi-graphical Method for the Solution of the Burmester Problem", *ASME Adv. in Des. Auto.*, DE-Vol. 32-2, pp 321-326.
5. Grünwald, J., 1911, "Ein Abbildungsprinzip, welches die ebene Geometrie und Kinematik mit der räumlichen Geometrie verknüpft", *Sitzber. Ak. Wiss. Wien*, Vol. 120, pp. 677-741.
6. De Sa, S., Roth, B., 1981, "Kinematic Mappings. Part 1: Classification of Algebraic Motions in the Plane", *ASME, J. of Mech. Design*, Vol. 103, pp. 585-591.
7. Hayes, M.J.D., Husty, M.L., 2001, "On the Kinematic Constraint Surfaces of General Three-Legged Planar Robot Platforms", submitted to *Mechanism and Machine Theory*.
8. Husty, M.L., 1995, "Kinematic Mapping of Planar Tree(*sic.*)-Legged Platforms, *Proc. of 15th Cdn. Conf. of Appl. Mech.*, Victoria, v.2, ISBN 0920049-06, pp. 876-877.
9. Husty, M.L., 1996, "An Algorithm for Solving the Direct Kinematics of General Stewart-Gough Platforms", *Mechanism and Machine Theory*, Vol. 31, No. 4, pp. 365-379.
10. McCarthy, J.M., 1990, *An Introduction to Theoretical Kinematics*, The M.I.T. Press, Cambridge, Mass., U.S.A..
11. McCarthy, J.M., 2000, *Geometric Design of Linkages*, Springer, New York, NY., U.S.A..

12. Murray, A.P., McCarthy, J.M., August 1996, *Constraint Manifold Synthesis of Planar Linkages*, Proceedings of ASME DETC: Mechanisms Conference, Irvine CA.
13. Ravani, B., 1982, *Kinematic Mappings as Applied to Motion Approximation and Mechanism Synthesis*, Ph.D. Dissertation, Stanford University, Stanford, Ca., U.S.A..
14. Ravani, B., Roth, B., 1983, "Motion Synthesis Using Kinematic Mappings", ASME, *J. of Mechanisms, Transmissions, & Automation in Design*, Vol. 105, pp. 460-467.
15. Zsombor-Murray, P.J., Chen, C. & Hayes M.J.D., 2002, "Direct Kinematic Mapping for General Planar Parallel Manipulators", to appear in *Proc. CSME Forum*, Kingston, ON, Canada.

Quadric Surface Fitting Applications to Approximate Dimensional Synthesis

M. John D. Hayes* S. Radacina Rusu†
Mechanical and Aerospace Engineering,
Carleton University,
Ottawa, ON., Canada

Abstract— *An approximate synthesis method is presented that takes a given set of n desired poses of the coupler of a four-bar planar mechanism and finds the "best" mechanism that can achieve them. This is accomplished by solving an equivalent unconstrained non-linear minimization problem. The hyperboloids of one sheet or hyperbolic paraboloids that minimize the distance between the given n poses in the kinematic mapping image space and n corresponding points that belong to the quadric surfaces, represent the "best" mechanism that can achieve the desired poses. The procedure is tested successfully on an RRRR mechanism.*

Keywords: kinematic mapping; quadric surface fitting; approximate dimensional synthesis.

I. Introduction

Kinematic synthesis of planar four-bar mechanisms for rigid body guidance was first proposed by Burmester [1]. Burmester theory states that five finitely separated poses (positions and orientations) of a rigid body define a planar four-bar mechanism that can guide a rigid body exactly through those five poses. Burmester showed that the problem leads to at most four dyads that, when paired, determine at most six different four-bar mechanisms that can guide the rigid body exactly through the poses.

Although the solution to the five-pose Burmester problem yields mechanisms that have no deviation from the prescribed poses, a major disadvantage is that only five positions and associated orientations may be prescribed. The designer has no control over how the mechanism behaves for any intermediate pose. This can be a difficult challenge in confined and crowded operating spaces. To gain a measure of control over the intermediate poses it is necessary to have a means by which to synthesize a mechanism that guides a rigid body through n prescribed poses, with $n > 5$. In general, an exact solution does not exist to this problem. The problem is known as *approximate synthesis*, where the mechanism determined to be the solution will guide a rigid-body through the prescribed poses with the smallest error, typically in a least-squares sense. The approximate solution will be unique up to the error minimization criteria. The literature is rich with a large variety of numerical approaches to pure approximate kinematic synthesis of this type, see [2], [3], [4], [5] for example.

A possibly much more intuitive approach is to build the approximation algorithm in the kinematic mapping image space introduced simultaneously, but independently in 1911 in [6] and [7]. In this paper, a novel approach to approximate kinematic synthesis for rigid body guidance is presented that uses the geometry of the image space to fit a set of points, representing desired positions and orientations, to quadric surfaces representing mechanism dyads. It is important to note that the optimization considers only kinematics. Dynamics and static force issues such as transmission angle and mechanical advantage are not considered. Such a restriction still applies to a vast array of planar four bar mechanism applications [8]. A very detailed summary of the geometry on the kinematic mapping image space can be found in [9], but a brief description of properties germane to algorithm presented in this paper is presented below.

II. Kinematic Mapping

One can consider the relative displacement of two rigid-bodies in the plane as the displacement of a Cartesian reference coordinate frame E attached to one of the bodies with respect to a Cartesian reference coordinate frame Σ attached to the other. Without loss of generality, Σ may be considered fixed with E free to move.

The homogeneous coordinates of points represented in E are given by the ratios $(x : y : z)$. Those of the same points represented in Σ are given by the ratios $(X : Y : Z)$. The position of a point $(X : Y : Z)$ in E in terms of the basis of Σ can be expressed compactly as

$$\begin{bmatrix} X \\ Y \\ Z \end{bmatrix} = \begin{bmatrix} \cos\varphi & -\sin\varphi & a \\ \sin\varphi & \cos\varphi & b \\ 0 & 0 & 1 \end{bmatrix} \begin{bmatrix} x \\ y \\ z \end{bmatrix}, \qquad (1)$$

where the pair (a, b) are the $(X/Z, Y/Z)$ Cartesian coordinates of the origin of E expressed in Σ, and φ is the orientation of E relative to Σ, respectively.

The essential idea of kinematic mapping is to map the three homogeneous coordinates of the pole of a planar displacement, in terms of (a, b, φ), to the points of a three dimensional projective image space. The image space coordinates are defined as:

*jhayes@mae.carleton.ca
†srrusu@connect.carleton.ca

$$X_1 = a\sin(\varphi/2) - b\cos(\varphi/2); \qquad X_3 = 2\sin(\varphi/2)$$
$$X_2 = a\cos(\varphi/2) + b\sin(\varphi/2); \qquad X_4 = 2\cos(\varphi/2). \quad (2)$$

The mapping is injective, not bijective: *there is at most one pre-image for each image point*. Any image point on the real line l, defined by the intersection of the coordinate planes $X_3 = X_4 = 0$, has no pre-image and therefore does not correspond to a real displacement of E. See [9], for a detailed analysis of the geometry of the image space.

To be practical, we can remove the one parameter family of image points for coupler orientations of $\varphi = \pi$, and normalize the image space coordinates by setting $X_4 = 1$. Conceptually, this implies dividing the X_i by $X_4 = 2\cos(\varphi/2)$ giving

$$X_1 = \frac{1}{2}\left(a\tan(\varphi/2) - b\right); \qquad X_3 = \tan(\varphi/2)$$
$$X_2 = \frac{1}{2}\left(a + b\tan(\varphi/2)\right); \qquad X_4 = 1. \quad (3)$$

Since each distinct displacement described by (a, b, φ) has a corresponding unique image point, the inverse mapping can be obtained from Eqs. (3): for a given point of the image space, the displacement parameters are

$$\begin{aligned} \tan(\varphi/2) &= X_3, \\ a &= 2(X_1X_3 + X_2)/(X_3^2 + 1), \\ b &= 2(X_2X_3 - X_1)/(X_3^2 + 1). \end{aligned} \quad (4)$$

By virtue of the relationships expressed in Eqs. (3), the transformation matrix from Eq. (1) may be expressed in terms of the homogeneous coordinates of the image space. After setting $z = 1$, which is done because no practical coupler will have a point at infinity, one obtains a linear transformation to express a displacement of E with respect to Σ in terms of the coordinates of the image point:

$$\begin{bmatrix} X \\ Y \\ Z \end{bmatrix} = \begin{bmatrix} 1 - X_3^2 & -2X_3 & 2(X_1X_3 + X_2) \\ 2X_3 & 1 - X_3^2 & 2(X_2X_3 - X_1) \\ 0 & 0 & X_3^2 + 1 \end{bmatrix} \begin{bmatrix} x \\ y \\ 1 \end{bmatrix}. \quad (5)$$

A. Planar Constraint Equations

Corresponding to the kinematic constraints imposed by RR- and PR-dyads are quadric constraint surfaces in the image space. A general equation is obtained when $(X : Y : Z)$ from Eqs. (5) are substituted into the general equation of a circle, the form of the most general constraint, [10]:

$$K_0(X^2 + Y^2) + 2K_1XZ + 2K_2YZ + K_3Z^2 \quad = \quad 0. \quad (6)$$

The result is that the constraint surfaces corresponding to RR, and PR-dyads can be represented by *one* equation (see [10], for how to include RP- and PP-dyads as well). After re-arranging in terms of the constraint surface *shape* parameters K_0, K_1, K_2, K_3, x, and y, treating the image space coordinates X_1, X_2, and X_3 as constants yields Eq. (7).

$$\begin{gathered} \left[\tfrac{1}{4}(X_3^2 + 1)x^2 + (X_2 - X_1X_3)x + \tfrac{1}{4}(X_3^2 + 1)y^2 - \right. \\ \left. (X_1 + X_2X_3)y + X_2^2 + X_1^2\right] K_0 + \\ \left[\tfrac{1}{2}(1 - X_3^2)x - X_3y + X_1X_3 + X_2\right] K_1 + \\ \left[X_3x + \tfrac{1}{2}(1 - X_3^2)y - X_1 + X_2X_3\right] K_2 + \\ \tfrac{1}{4}(X_3^2 + 1)K_3 = 0. \end{gathered} \quad (7)$$

For a particular dyad the associated $[K_0 : K_1 : K_2 : K_3]$, along with the design values of the coordinates of the coupler attachment point (x, y), expressed in reference frame E, are substituted into Eq. (7) revealing the image space constraint surface for the given dyad. The K_i in Eqs. (6) and (7) depend on the constraints imposed by the dyad.

For RR-dyads $K_0 = 1$ and the surface is a hyperboloid of one sheet, when projected into the hyperplane $X_4 = 1$, that intersects planes parallel to $X_3 = 0$ in circles, [11]. The K_i are termed *circular coefficients* and are defined as:

$$[K_0 : K_1 : K_2 : K_3] = [1 : -X_c : -Y_c : (K_1^2 + K_2^2 - r^2)], \quad (8)$$

where the ungrounded R-pair in an RR-dyad is constrained to move on a circle of constant radius, r, and fixed centre coordinates in Σ, (X_c, Y_c).

Linear constraints result when PR-dyads are employed. In this case $K_0 = 0$ and the constraint surface is an hyperbolic paraboloid, when projected into the hyperplane $X_4 = 1$, with one regulus ruled by skew lines that are all parallel to the plane $X_3 = 0$, [11]. The *linear coefficients* are defined as

$$[K_0 : K_1 : K_2 : K_3] = [0 : \tfrac{1}{2}L_1 : \tfrac{1}{2}L_2 : L_3], \quad (9)$$

where the L_i are line coordinates obtained by Grassmann expansion of the determinant of any two distinct points on the line, [12]. We obtain

$$\begin{gathered} [K_0 : K_1 : K_2 : K_3] = \\ [0 : -\tfrac{1}{2}\sin\vartheta_\Sigma : \tfrac{1}{2}\cos\vartheta_\Sigma : F_{X/\Sigma}\sin\vartheta_\Sigma - F_{Y/\Sigma}\cos\vartheta_\Sigma] \end{gathered} \quad (10)$$

where ϑ_Σ is the angle the direction of translation makes with respect to the X-axis, expressed in Σ, $F_{X/\Sigma}$, $F_{Y/\Sigma}$, represent the homogeneous coordinates $(X : Y : 1)$, expressed in reference frame Σ, of a point on the line that is fixed relative to Σ.

III. Fitting Displacements (Image Space Points) to Constraint Surfaces

To use kinematic mapping for approximate synthesis requires the best approximation, in a least squares sense, of the constraint surface coefficients K_0, K_1, K_2, K_3, x, and y given a suitably over constrained set of image space coordinates X_1, X_2, X_3, and X_4 which represent the desired set of positions and orientations of the coupler. The given image space points are on some space curve. The points on this curve must be projected onto the *best* fourth order curve of intersection of two constraint surfaces corresponding to two possible dyads from which a mechanism can be constructed which possesses motion characteristics *closest* to those specified. The solution to this problem *is* the solution to the approximate synthesis problem using kinematic mapping for rigid body guidance.

We may begin the search for a solution by generating a set of image space points that satisfy a known image space constraint hyperboloid. If the cardinality of the set of points is much larger than the number of constants required to define the hyperboloid then we should be able to fit the points to the surface. In other words, identify the equation, in a least squares sense, that the points satisfy.

One possibility is to identify the implicit quadric surface equations in the nullspace of the set of equations. That is, an arbitrary quadric surface has the following implicit second order equation:

$$c_0X_4^2 + c_1X_1^2 + c_2X_2^2 + c_3X_3^2 + c_4X_1X_2 + c_5X_2X_3 + c_6X_3X_1 + c_7X_1X_4 + c_8X_2X_4 + c_9X_3X_4 = 0. \quad (11)$$

Given a sufficiently large set of points, one may be able to identify the 10 coefficients $c_0 \ldots c_9$ that define the quadric surface that is closest, in some sense, to the given points. But, two surfaces are required, one for each of the two dyads comprising the mechanism.

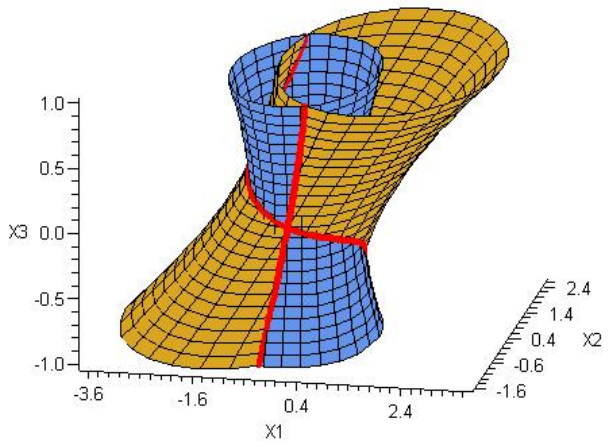

Fig. 1. Intersection curve of two RR hyperboloids of one sheet.

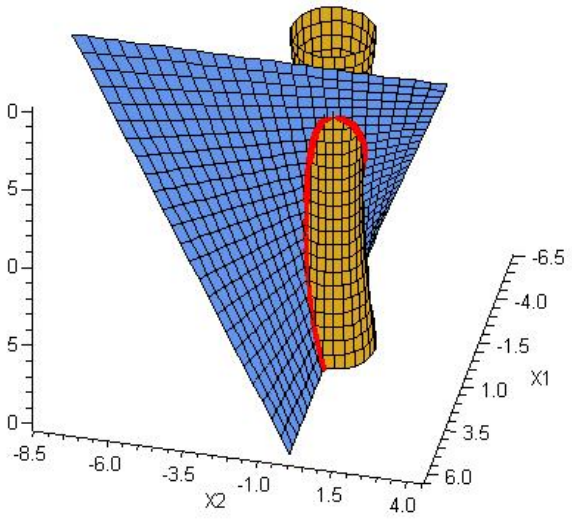

Fig. 2. Intersection curve of one RR hyperboloid of one sheet and one RP hyperbolic paraboloid.

The *best* four bar mechanism will be composed of RR, PR or RP-dyads. Due to their motion constraints, RR-dyads map to hyperboloids of one sheet, while PR and RP-dyads map to hyperbolic paraboloids in the image space [9], [11]. The two constraint surfaces that intersect in the curve closest to the reference curve will yield the best mechanism for the given set of desired poses in some sense. The curve of intersection of the quadric surfaces of the dyad pairs for $RRRR$, $RRRP$ and $PRRP$ mechanisms are illustrated in Figures 1, 2, and 3. Considering that the curve closest, in the least squares sense, to the reference curve must be the intersection of two quadric surfaces as shown above, it is obvious that the curve belongs to each of those

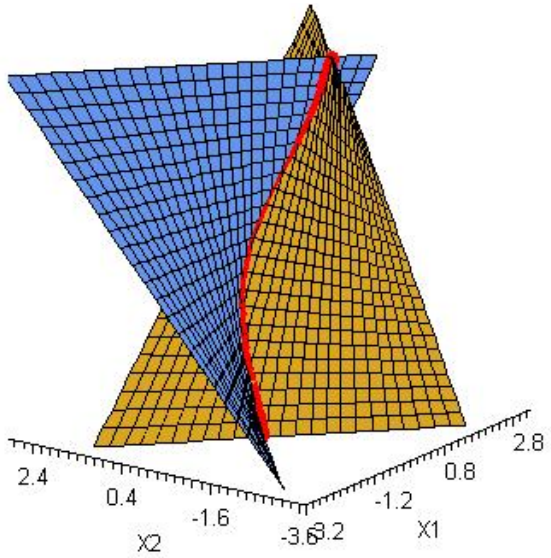

Fig. 3. Intersection curve of two PR hyperbolic paraboloids.

two quadric surfaces. Thus the solution to the approximate synthesis problem is finding the best two quadric surfaces (hyperboloid of one sheet or hyperbolic paraboloid) that contain a curve that is closest to the reference curve, in a least squares sense.

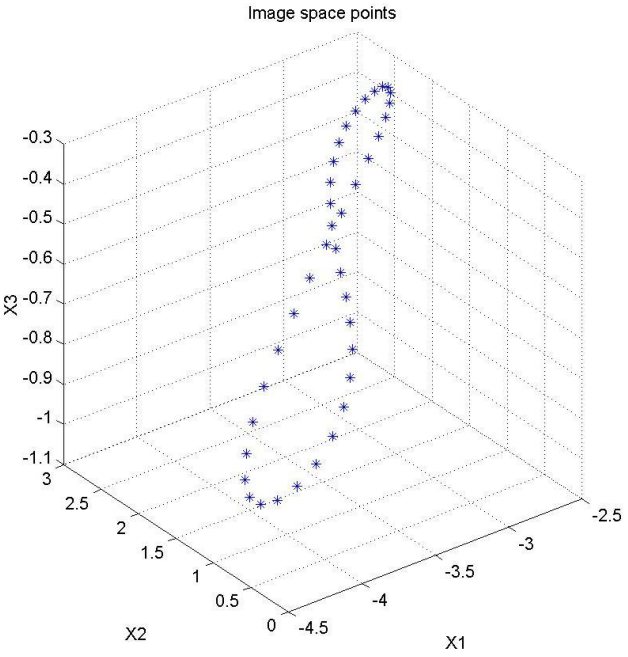

Fig. 4. Points on 4^{th}-order curve of intersection of two image space quadric constraint hyperboloids.

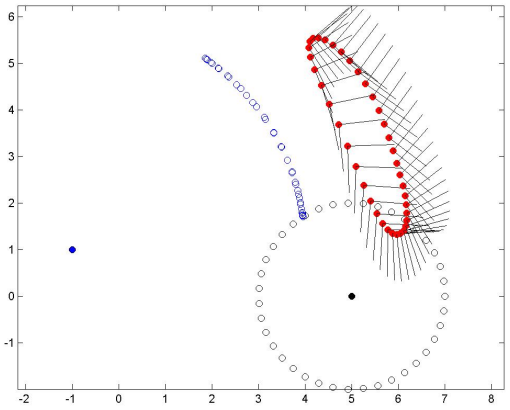

Fig. 5. The mechanism used to generate the poses.

IV. Example

The way the algorithm will be described is through an example. To generate a set of points that lie exactly on one of these constraint surfaces a parametric equation of the surface is required. It is a simple matter to parametrize Eq. (7), see [11]. Note the typo in this paper in Eq. (7): the $-$ signs should be replaced by $+$ signs so that it reads $K_0(X^2+Y^2)+2K_1XZ+2K_2YZ+K_3Z^2$. The parametrization is

$$\begin{bmatrix} X_1 \\ X_2 \\ X_3 \end{bmatrix} = \frac{1}{2}\begin{bmatrix} ([x-K_1]t+K_2+y)+(r\sqrt{t^2+1})\cos\zeta \\ ([y-K_2]t-K_1-x)+(r\sqrt{t^2+1})\sin\zeta \\ 2t \end{bmatrix}, \quad \begin{array}{c}\zeta\in\{0,\ldots,2\pi\},\\ t\in\{-\infty,\ldots,\infty\},\end{array} \tag{12}$$

where x and y are the coordinates of the moving revolute centre expressed in the moving frame E, K_1 and K_2 are the coordinates of the fixed revolute centre expressed in Σ multiplied by -1 (i.e., $K_1=-X_c$ and $K_2=-Y_c$), r is the length between the moving and fixed revolute centres, while t and ζ are free parameters. To simplify the coefficients begin with the surface having the following shape parameters: $K_0=X_4=z=1$, $K_1=K_2=x=y=0$, $r=2$, $K_3=-4$ (recall that $K_3=K_1^2+K_2^2-r^2$). A set of 40 image space points, shown in Figure 4 was generated by the linkage geometry, illustrated in Figure 5

Using the general quadric surface equation, Eq. (11), the image space coordinates of the 40 poses generate a set of 40 synthesis equations in terms of the 10 surface shape parameters $\{c_0,c_1,\cdots,c_9\}$. The two quadric surfaces that best fit the given points lie in the null space of the synthesis matrix $\mathbf{A}$, whose same numbered elements in each row are the terms of the $X_i, i\in\{1,2,3,4\}$ scaled by the surface shape parameters, $c_i, i\in\{0,1,\cdots,9\}$. The two surfaces closest, in a least squares sense, to the null space of $\mathbf{A}$ can be identified using singular value decomposition (SVD). Applying SVD to the overconstrained set of synthesis equations $\mathbf{Ac}=\mathbf{0}$ reveals that the matrix $\mathbf{A}$ is rank deficient by two. That is, two of its singular values are zero, or computationally close to zero. In this case the two smallest singular values are 1.0×10^{-15}, and 3.0×10^{-15}. Hence, the two smallest singular values may be considered to be effectively zero, and near the numerical resolution of the computer. The next smallest singular value is 6.5×10^{-3}, which is five orders of magnitude smaller than the largest singular value of 88.8. It is a simple matter to identify the array of surface shape parameters, $\mathbf{c}$, that correspond to the two smallest singular values of the synthesis matrix $\mathbf{A}$ [13]. The coefficients are listed as Surfaces M, N and O in Table I, with M corresponding to the smallest, N the second smallest, and O the third smallest singular value.

The quadric surface type information is embedded in its coefficients. The implicit equation of the quadric surface can be classified according certain invariants of its discriminant and quadratic form [14]. Written in discriminant form,

Surface	c_0	c_1	c_2	c_3	c_4	c_5	c_6	c_7	c_8	c_9
M	1.0000	0.1380	0.0738	-0.3967	-0.0962	0.1201	0.0473	0.8249	-0.3372	-0.2950
N	1.0000	0.2603	0.5297	2.1392	0.0424	-0.0456	0.0145	0.7035	-1.0782	3.9373
O	1.0000	-0.3583	-0.3583	-0.0271	0.0000	-0.4448	0.1494	-0.9881	0.1732	0.0509

TABLE I. The surface shape parameters identified with SVD.

Surface	rank($\mathbf{D}$)	rank($\mathbf{Q}$)	sign of det($\mathbf{Q}$)	sign of T_1	sign of T_2	Quadric surface
M	4	3	+	+	-	Hyperboloid of one sheet
N	4	3	-	+	+	Hyperboloid of two sheets
O	3	3	+	-	+	Hyperboloid of one sheet

TABLE II. Quadric constraint surface type.

Eq. (11) becomes:

$$\begin{bmatrix} X_1 \\ X_2 \\ X_3 \\ X_4 \end{bmatrix}^T \begin{bmatrix} c_1 & \frac{1}{2}c_4 & \frac{1}{2}c_6 & \frac{1}{2}c_7 \\ \frac{1}{2}c_4 & c_2 & \frac{1}{2}c_5 & \frac{1}{2}c_8 \\ \frac{1}{2}c_6 & \frac{1}{2}c_5 & c_3 & \frac{1}{2}c_9 \\ \frac{1}{2}c_7 & \frac{1}{2}c_8 & \frac{1}{2}c_9 & c_0 \end{bmatrix} \begin{bmatrix} X_1 \\ X_2 \\ X_3 \\ X_4 \end{bmatrix} = \mathbf{X^T D X}. \quad (13)$$

The associated quadratic form is:

$$\mathbf{Q} = \begin{bmatrix} c_1 & \frac{1}{2}c_4 & \frac{1}{2}c_6 \\ \frac{1}{2}c_4 & c_2 & \frac{1}{2}c_5 \\ \frac{1}{2}c_6 & \frac{1}{2}c_5 & c_3 \end{bmatrix}. \quad (14)$$

Both the discriminant, $\mathbf{D}$, and the quadratic form, $\mathbf{Q}$, are square symmetric matrices. It can be shown [14] that quadric surfaces can be classified by conditions on the rank of the discriminant, rank($\mathbf{D}$), the rank of the quadriatic form, rank($\mathbf{Q}$), the sign of the determinant of the discriminant, det($\mathbf{D}$), the sign of the product of det($\mathbf{Q}$) with the trace of $\mathbf{Q}$ (indicated by T_1), and the sign of the sum of the two-rowed principal minors of $\mathbf{Q}$ (indicated by T_2). This last invariant is more precisely defined as

$$T_2 = \sum_{i=1,j=2,i<j}^{3} \begin{vmatrix} q_{ii} & q_{ij} \\ q_{ij} & q_{jj} \end{vmatrix}, \quad (15)$$

where the q_{ij} are the elements of $\mathbf{Q}$.

A quadric surface is an hyperboloid of one sheet if rank($\mathbf{D}$) $= \mathbf{4}$, rank($\mathbf{Q}$) $= \mathbf{3}$, det($\mathbf{D}$) $> \mathbf{0}$, and either $T_2 \leq 0$, or both $T_1 \leq 0$ and $T_2 > 0$. A quadric surface is an hyperboloid of two sheets if all the above conditions on the invariants are met, with the exception that det($\mathbf{D}$) $< \mathbf{0}$. A quadric surface is an hyperbolic paraboloid if rank($\mathbf{D}$) $= \mathbf{4}$ and rank($\mathbf{Q}$) $= \mathbf{2}$. The values of these parameters for each of Surfaces M, N, and O are listed in Table II.

Surfaces M and O are two hyperboloids of one sheet, while Surface N is a hyperboloid of two sheets. Since a hyperboloid of two sheets does not represent a planar dyad constraint surface, the conclusion is that the quadric surfaces that best fit the reference curve, in the least squares sense, are two hyperboloids of one sheet. Despite the fact that the second RR-dyad constraint surface is far removed from the null space of the synthesis matrix, it nevertheless indicates that an $RRRR$ mechanism will best approximate the desired coupler poses.

A. *Minimization*

Points on a hyperboloid of one sheet can be obtained using Eq. (12), where K_1, K_2, K_3, x, and y are the constraint surface shape parameters described in Section II-A. The approximate synthesis problem can be solved using an equivalent unconstrained non-linear minimization problem. This problem can be stated in the following way: find the set of surface shape parameters (K_1, K_2, K_3, x, y) that minimize the total spacing between all 40 points on the reference curve and 40 points that lie on the surface of a hyperboloid of one sheet where $t = X_3 = X_{3_{ref}}$:

$$d = \sum_{i=1}^{40} \sqrt{(X_{1ref_i} - X_{1_i})^2 + (X_{2ref_i} - X_{2_i})^2}. \quad (16)$$

The two sets of parameters that minimize d represent the two *best* constraint surfaces that intersect *closest* to the reference curve. Therefore, they represent the *best* dyad pair that approximate the desired 40 poses. This formulation results from the fact that $t = X_3$ is a free parameter in the parametric equation for the hyperboloid of one sheet, Eq. (12). Thus, for any hyperboloid of one sheet there exist 40 points with the same $t = X_3$ coordinates as the 40 points on the reference curve. Furthermore X_1 and X_2 have the same form in Eq. (12), so the distance between each point on the reference curve and each corresponding point on the quadric surface in the hyperplane $t = X_3$ can be simply measured on the X_1X_2 hyperplane. Hence, d can be defined.

The second free parameter, ζ, in Eq. (12) is found by a minimization sub routine, which runs for each corresponding point generated on the quadric surface with the same $t = X_3$ coordinate as a point on the reference curve. This simply implies that for a constraint hyperboloid of one sheet

cut by a plane corresponding to $t = X_3$ there is only one point on the circular trace of the hyperboloid of one sheet in that hyperplane that is closest to the corresponding point on the reference curve and that the (X_1, X_2) coordinates of the closest point are only a function of ζ. Another implication is that the distance between the point generated with coordinates (X_1, X_2) and the corresponding point on the reference curve is only dependent on the surface shape parameters K_1, K_2, K_3, x, and y.

B. Initial Guesses

In order for the algorithm to converge to the solution that minimizes d, decent initial guess for the shape parameters are required. While initial guesses may be good or bad, the minimization algorithm above allows for each of them to converge to the best solution and to quantify the deviation of the poses generated by the identified mechanism. Out of the 40 points on the reference curve five points spaced relatively widely apart are arbitrarily chosen giving five equations in the five unknown surface shape parameters, after setting $K_0 = 1$ in Eq. (7), knowing that the surface should be a hyperboloid of one sheet. Seven initial guesses are tabulated in Table III.

The idea behind this technique is that the curve that is closest to the reference curve is by definition also closest to the points on the reference curve and thus a curve that exactly passes through five of the points may also be relatively close to the best curve being sought. The minimization algorithm will iteratively jump to the closest curve from curves that may be close to the reference curve by minimizing d. Furthermore, the initial guess procedure could be repeated for a different set of points on the reference curve and more initial guesses can be found. Statistics and heuristics could be used to actually narrow down the initial guesses. For the sake of testing this approximate synthesis method, this is not done, and all initial guesses are considered equal and all resulting solutions are evaluated.

C. Minimization Results

Non-linear unconstrained programming methods such as the Nelder-Mead simplex method [15] and the Hookes-Jeeves method [16] have been used with similar outcomes. The results of the minimization corresponding to each initial guess can be observed in Figures 6-12.

In each figure, the solid dots represent the desired 40 poses in the projection of the kinematic mapping image space into the hyperplane $X_4 = 1$. These 40 reference points lie on the solid reference curve. The small circles are the corresponding 40 points generated by the mechanism identified from the minimization algorithm. These points lie on the surface of a constraint hyperboloid of one sheet that the algorithm converged to starting from the particular initial guess. The results can now be visually compared. In each figure, the images on the left are the results and reference curve projected onto the plane $X_3 = 0$.

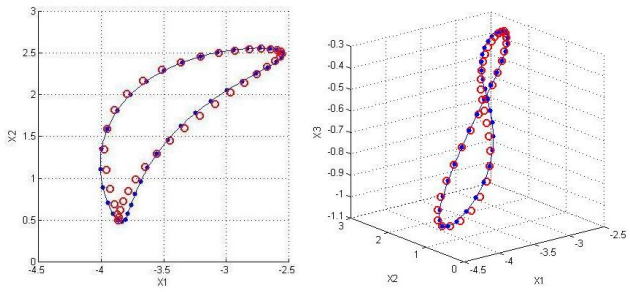

Fig. 6. Graphical results for Initial Guess 1.

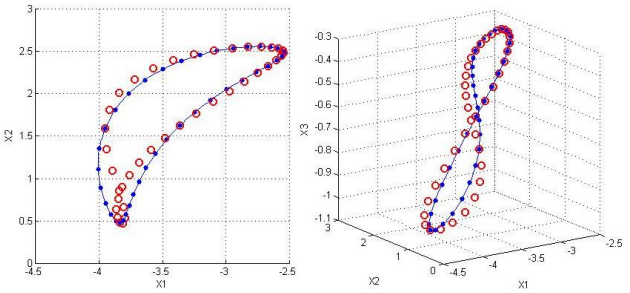

Fig. 7. Graphical results for Initial Guess 2.

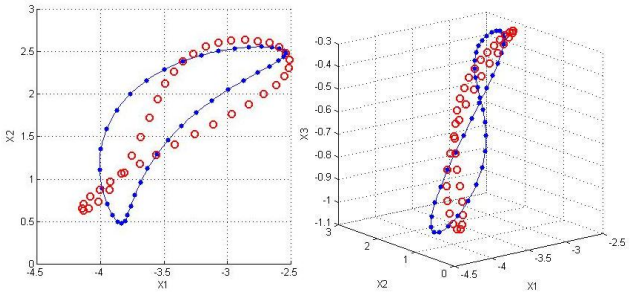

Fig. 8. Graphical results for Initial Guess 3.

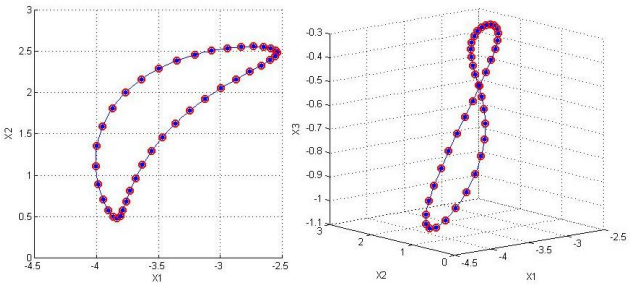

Fig. 9. Graphical results for Initial Guess 4.

Guess	K_1	K_2	K_3	x	y
1	-73.59218	-21.00890	5467.99420	23.99357	56.20798
2	-7.08742	-5.53320	46.84468	-1.58544	-3.19723
3	9.75170	5.29780	27.84599	-2.29188	-7.86290
4	-5.00000	0.00000	21.00000	3.00000	-2.00000
5	1.00000	-1.00000	-23.00000	-1.00000	-2.00000
6	-20.98570	-14.15501	297.79812	-1.28879	0.56361
7	-3.05304	-6.54866	48.44514	-3.82887	-1.05131

TABLE III. Initial Guesses.

Parameter	Guess 1	Guess 2	Guess 3	Guess 4	Guess 5	Guess 6	Guess 7
K_1	-97.720	-18.202	888.914	-5.000	1.000	-25.445	-1.398
K_2	-57.463	-12.363	432.395	0.000	-1.000	-17.073	-6.191
K_3	1491.757	261.650	-2374.375	21.000	-23.000	390.531	36.554
x	-1.133	-1.287	-0.894	3.000	-1.000	-1.309	-4.388
y	0.534	0.889	-5.375	-2.000	-2.000	1.030	-2.361
Iterations	450	623	718	101	176	745	436
d	1.1132	1.9333	6.726	0.0004	0.0010	1.5746	4.8138

TABLE IV. Results.

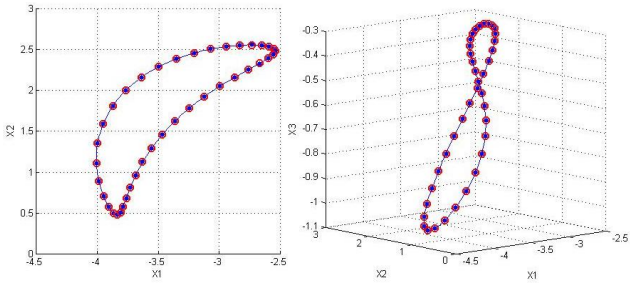

Fig. 10. Graphical results for Initial Guess 5.

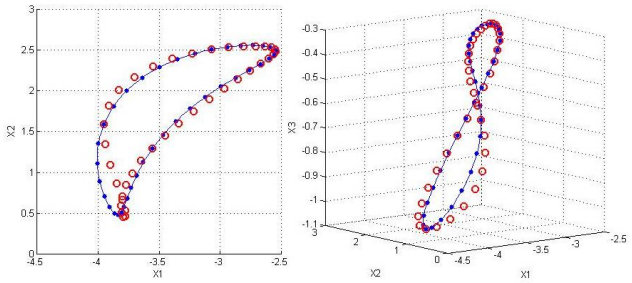

Fig. 11. Graphical results for Initial Guess 6.

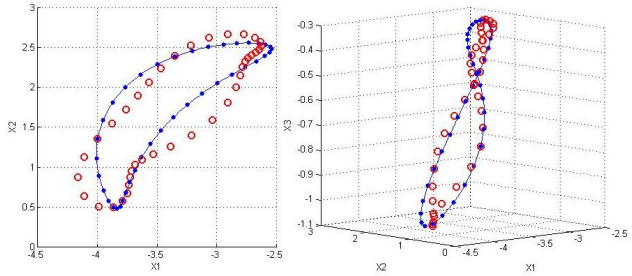

Fig. 12. Graphical results for Initial Guess 7.

The numerical results are tabulated in Table IV. The values of d that resulted from the minimization algorithm can now be compared. These values indicate how close the particular hyperboloid of one sheet obtained is to the reference curve. It is evident that Initial Guesses 4 and 5 generate the best hyperboloids of one sheet that intersect closest to the 40 points on the reference curve. The geometry of the best generating $RRRR$ mechanism can now be extracted using this pair of RR-dyads and their surface shape parameters.

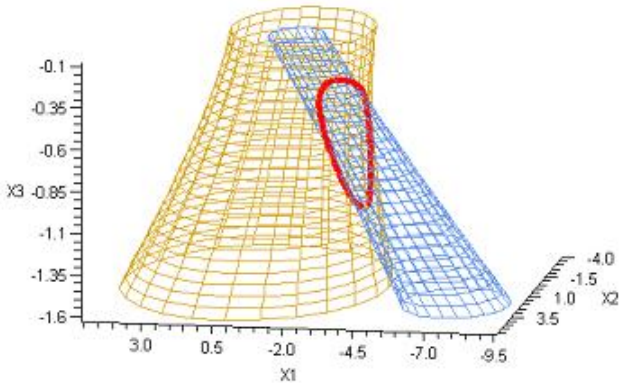

Fig. 13. Curve of intersection of *best* hyperboloids of one sheet.

It is to be noted that these are exactly the RR-dyads that were originally used to construct the initial given 40 poses, and hence the approximate synthesis was indeed successful. It should also be noted that the initial guess values for the shape parameters listed in Table III are completely different from the shape parameters that resulted from the minimization algorithm with the corresponding initial guess with the exception of Initial Guesses 4 and 5. This is not the case

for the other initial guesses because, even though the corresponding hyperboloid of one sheet fit the five arbitrarily chosen points on the reference curve well, the quadric surfaces very poorly fit the 40 points on the reference curve and the algorithm converged to a different, better solution. The curve of intersection of the best hyperboloids of one sheet corresponding to Initial Guesses 4 and 5 can be seen in Figure 13.

D. What Happens When Specified Poses are Not Perfect?

Arguably the example was contrived to be successful, but is also very illustrative of the importance of good initial guesses. The specified 40 poses lie exactly on the curve of intersection of two constraint hyperboloids of one sheet. To introduce poses that do not lie perfectly on such a 4^{th} order curve which lies exactly on two constraint hyperboloids of one sheet, the initial specified 40 poses were truncated to 2 decimal places to introduce error, and the approximate synthesis algorithm was rerun. The results obtained are listed in Table V.

Parameter	Truncated Guess 4	Truncated Guess 4
K_1	-5.01374158	1.00543179
K_2	0.00000497	-0.99534789
K_3	21.12526403	22.98658405
x	3.00653176	-1.00047287
y	-1.98696494	-2.01010896
Iterations	134	329
d	0.1194434	0.0740493

TABLE V. Truncated Results.

It is to be seen that the fit is worse than that for the mechanism identified from the results in Table IV, still the minimization converged to similar results in terms of the best RR-dyad pair.

V. Conclusions

Kinematic mapping of distinct displacement poles to distinct points in a 3D projective image space was successfully used for approximate kinematic synthesis for rigid body guidance. A new approximate synthesis method was developed and successfully tested, and could have a wide range of applications as it has been presented in a general way which can be further expanded or simplified.

For the case of a mechanism containing a PR-dyad, the same method can be used with the exception that the conditions on the identified quadratic form of the quadric that best satisfied the specified poses will indicate that the specified image space points best fit a constraint hyperbolic paraboloid. No heuristics are necessary and given the initial desired poses, the entire approximate synthesis can be carried out using software to return a list of the best generating mechanisms ranked according to d, their *closeness* to the given poses. The unconstrained non-linear programming problem developed has only five variables and is easily solved by several methods. A minimization algorithm could actually be further customized to "jump" from local minima to other local minima depending on the desired closeness to the given poses. Furthermore some relationships between the variables could be built in to the algorithm so it recognizes undesirable solutions from the perspective of surface shape parameters and avoids iterations in those directions.

The method developed drives the solution mechanism to achieve exactly the desired poses but not necessarily a line of best fit through the poses. This may be desirable for a mechanism designer who wants a point on the coupler to go through exactly some specified poses but does not care about the path in between them. If this is not satisfactory then the designer can simply specify more points where the path is not well defined and the approximate synthesis method will yield a more desirable solution.

References

[1] L. Burmester. *Lehrbuch der Kinematik*. Arthur Felix Verlag, Leipzig, Germany, 1888.

[2] J.E. Holte, T.R. Cahse, and A.G. Erdman. Mixed Exact-Approximate Position Synthesis of Planar Mechanisms. *ASME, J. of Mech. Des.*, 122: 278286, 2000.

[3] J. Yao and J. Angeles. Computation of All Optimum Dyads in the Approximate Synthesis of Planar Linkages for Rigid-Body Guidance. *Mechanism and Machine Theory*, 35(8): 10651078, 2000.

[4] A. Liu and T. Yang. Finding All Solutions to Unconstrained Nonlinear Optimization for Approximate Synthesis of Planar Linkages Using Continuation Method. *ASME, J. of Mech. Des.*, 121(3): 368374, 1999.

[5] X. Kong. Approximate Kinematic Synthesis of Linkages Using Generalized Inverse Matrix and Continuation. *Mechanical Science and Technology*, 18(1): 3840, 1999.

[6] W. Blaschke. Euklidische Kinematik und nichteuklidische Geometrie. *Zeit. Math. Phys.*, 60: 61-91 and 203-204, 1911.

[7] J. Grünwald. Ein Abbildungsprinzip, welches die ebene Geometrie und Kinematik mit der räumlichen Geometrie verknüpft. *Sitzber. Ak. Wiss. Wien*, 120: 677-741, 1911.

[8] A.G. Erdman, G.N. Sandor and S. Kota *Mechanism Design: Analysis and Synthesis, 4^{th} Ed.* Prentice Hall, 2001

[9] O. Bottema and B. Roth. *Theoretical Kinematics*. Dover Publications, Inc. New York, NY, U.S.A., 1990.

[10] M.J.D. Hayes, P.J. Zsombor-Murray, and C. Chen. "Kinematic Analysis of General Planar Parallel Manipulators". *ASME, Journal of Mechanical Design*, 126(5): 866-874, 2004.

[11] M.J.D. Hayes, M.L. Husty. "On the Kinematic Constraint Surfaces of General Three-Legged Planar Robot Platforms". *Mechanism and Machine Theory*, 38(5): 379-394, 2003.

[12] M.J.D. Hayes, T. Luu, X.-W. Chang. "Kinematic Mapping Application to Approximate Type and Dimension Synthesis of Planar Mechanisms". *9th Advances in Robotic Kinematics*, eds. Lenarčič, J. and Galletti, C., Kluwer Academic Publishers, Dordrecht, the Netherlands, pp. 41-48, 2004.

[13] W.H. Press, S.A. Teukolsky, W.T. Vetterling, and B.P. Flannery. *Numerical Recipes in C, 2nd Edition*. Cambridge University Press, Cambridge, England, 1992.

[14] A. Dresden. *Solid Analytical Geometry and Determinants*. Dover Publications, Inc. New York, NY, U.S.A., 1964.

[15] J.A. Nelder and R. Mead. "A Simplex Method for Function Minimization". *Computer Journal*, 7: 308-313, 1965.

[16] R. Hooke and T.A. Jeeves. "Direct Search Solution of Numerical and Statistical Problems". *Journal of the ACM (JACM)*, 8(2): 212-229, 1961.

Towards Integrated Type and Dimensional Synthesis of Mechanisms for Rigid Body Guidance

M.J.D. Hayes[1], P.J. Zsombor-Murray[2]

[1]*Department of Mechanical & Aerospace Engineering, Carleton University, 1125 Colonel By Drive, Ottawa, ON, K1S 5B6, Canada,*
jhayes@mae.carleton.ca

[2]*Centre for Intelligent Machines, McGill University, 817 Sherbrooke Street West, Montreal, QC, H3A 2K6, Canada*
paul@cim.mcgill.ca

In this paper kinematic mapping is used to take the first steps towards development of a general algorithm combining both type and dimensional synthesis of planar mechanisms for rigid body guidance. In the present work we develop an algorithm that can size link lengths, locate joint axes, and using heuristics decide between RR- and PR-dyads that, when combined, can guide a rigid body exactly through five specified positions and orientations, i.e., the five-position Burmester problem. An example is given providing proof-of-concept.

1 Introduction

The determination of a planar four-bar mechanism that can guide a rigid body through five finitely separated *poses* (position and orientation) is known as the *five-position Burmester problem*. It may be stated as follows: given five positions of a point on a moving rigid body and the corresponding five orientations of some line on that body, design a four-bar mechanism whose coupler is the moving body and is assemblable upon these five poses. The coupler must assume the five required poses, even though it may be that not all five lie in the same assembly branch. Burmester showed that the problem leads to, at most, four dyads that can be taken two at a time: there can be as many as six different four-bar mechanisms that can guide a rigid body exactly through five specified poses [1].

From time to time dimensional synthesis for the Burmester problem has been revisited, see for example [2]. More recently, classical finite position synthesis has been reviewed in [3]. An algebraic approach to this exact problem based on quaternions is to be found in [4]. Instead, we use planar kinematic mapping whose geometry is analogous to quaternions. The planar kinematic mapping was introduced independently by Blaschke and Grünwald in 1911 [5, 6], and is summarized in [7].

In general, dimensional synthesis for rigid body guidance assumes a mechanism *type*: i.e., planar $4R$; slider-crank; crank-slider; trammel, etc.. Our aim is to develop a completely general planar mechanism synthesis algorithm that integrates both *type* and *dimensional* synthesis for five-position exact synthesis. It was shown in [8] how kinematic mapping can be used for exact dimensional synthesis.

We employ the Blashke-Grünwald mapping of planar kinematics [5, 6] to regard the problem from a projective geometric perspective, thereby obtaining a system of five non-linear equations in five unknowns expressed in terms of a sixth *homogenizing*, or *influence coefficient*. The value of the sixth unknown determines *type*. The six unknowns represent one dyad. The solutions of the system of equations leads to, at most, four dyads, thereby agreeing with Burmester theory.

It is convenient to characterize rigid body displacements by a coordinate system E that moves relative to a fixed coordinate system Σ, see Figure 1. General planar displacements are then the transformation of points described in E to the coordinates of the same points described in Σ. The constraints on linkages imposed by different joint types can then be described geometrically.

Planar linkages contain either revolute (R-pairs), or prismatic (P-pairs). These kinematic pairs permit rotations about one axis, or translations parallel to one direction, respectively. In the kinematic mapping image space an RR-dyad (three binary links jointed end to end by two R-pairs) constraint involving a point with fixed coordinates in E forced to move on a circle with fixed radius and centre in Σ is a hyperboloid of one sheet. A PR-dyad (three binary links jointed in series by a P-pair and an R-

pair) imposes the constraint where a point with fixed coordinates in E is restricted to move on a line with fixed line coordinates in Σ. This constraint maps to a hyperbolic paraboloid in the image space. The RP-dyad is the kinematic inversion of the PR-dyad. It's constraints also map to hyperbolic paraboloids. The PP-dyad constraints map to a plane in the image space. These are the four possible lower pair dyads for planar mechanisms.

The algorithm that performs both type and dimensional synthesis for rigid body guidance must identify the constraint surfaces that intersect in the curve specified by the image space points of the five given poses. The way the constraints are formulated, the influence coefficient, mentioned earlier, can have either the value 1 or 0, indicating either an RR- or PR-dyad, respectively.

The planar $RRRP$ four-bar linkage shown in Figure 1 can be decomposed into an RR- and a PR-dyad. The RR-dyad is composed of the grounded R-pair centred at the base-fixed point F_1 and the moving R-pair centred at the point M_1. The PR-dyad is composed of the sliding P-pair and the R-pair connected to it with centre at M_2. In the PR-dyad, the P-pair slides on a line with fixed position and direction relative to the base-fixed R-pair centred at F_1. This $RRRP$ linkage is used to generate the five specified poses. Clearly, the algorithm must identify the constraint surfaces corresponding to the given RR- and PR-dyads. Using heuristics, we succeed in identifying these dyads, together with two additional RR-dyads, thereby agreeing with Burmester theory. These are the first steps towards the general algorithm.

2 Kinematic Mapping

The motion of the coupler in a four-bar mechanism can be described by the motion of a reference frame E that moves with the coupler, relative to a ground-fixed non moving reference frame Σ. The $RRRP$ linkage shown in Figure 1 illustrates these two coordinate reference frames. The homogeneous coordinates of points represented in E are given by the ratios $(x : y : z)$. Those of points represented in Σ are given by the ratios $(X : Y : Z)$.

The homogeneous transformation that maps the coordinates of points in E to Σ, which also describes the displacement of E relative to Σ, can be written:

$$\begin{bmatrix} X \\ Y \\ Z \end{bmatrix} = \begin{bmatrix} \cos\varphi & -\sin\varphi & a \\ \sin\varphi & \cos\varphi & b \\ 0 & 0 & 1 \end{bmatrix} \begin{bmatrix} x \\ y \\ z \end{bmatrix}. \qquad (1)$$

Equation (1) indicates that general planar displacements are characterized by the three parameters a, b, and φ, where the pair (a, b) are the $(X/Z, Y/Z)$ Cartesian coordinates of the origin of E expressed in Σ, and φ is the orientation of E relative to Σ, respectively.

All general planar displacements (*i.e.*, any combination of translations and rotations) may be represented by a single rotation through a finite angle about a fixed axis normal to the plane of the displacement. Even a pure translation may be considered a rotation through an infinitesimal angle about the point at infinity in the direction normal to the translation. The coordinates of the piercing point of the rotation axis with the plane of the displacement describe the *pole* of the displacement. The coordinates of the pole are invariant under the associated transformation described by Equation (1).

The pole coordinates for a particular displacement come from the eigenvector corresponding to the one real eigenvalue of Equation (1). Denoting them by the subscript p, the homogeneous pole coordinates, which are the same in both E and Σ, are:

$$\begin{aligned} X_p = \quad x_p = \quad & a\sin(\varphi/2) - b\cos(\varphi/2), \\ Y_p = \quad y_p = \quad & a\cos(\phi/2) + b\sin(\varphi/2), \\ Z_p = \quad z_p = \quad & 2\sin\varphi/2. \end{aligned}$$

Note that the value of the homogenizing coordinate is arbitrary. Without loss in generality it is set $Z_p = z_p = 2\sin\varphi/2$.

The essential idea of kinematic mapping is to map the three homogeneous coordinates of the pole of a planar displacement, in terms of three parameters that characterize it, (a, b, φ), to the points of a three dimensional projective image space. The kinematic mapping image coordinates are defined as:

$$\begin{aligned} X_1 &= a\sin(\varphi/2) - b\cos(\varphi/2) \\ X_2 &= a\cos(\varphi/2) + b\sin(\varphi/2) \\ X_3 &= 2\sin(\varphi/2) \\ X_4 &= 2\cos(\varphi/2). \end{aligned} \qquad (2)$$

Since each distinct displacement described by (a, b, φ) has a corresponding unique image point, the inverse mapping can be obtained from Equation (2): for a given point of the image space, the displacement parameters are

$$\begin{aligned} \tan(\varphi/2) &= X_3/X_4, \\ a &= 2(X_1X_3 + X_2X_4)/(X_3^2 + X_4^2), \\ b &= 2(X_2X_3 - X_1X_4)/(X_3^2 + X_4^2). \end{aligned} \qquad (3)$$

By virtue of the relationships expressed by Equations (2), the transformation matrix from Equation (1) may be expressed in terms of the homogeneous coordinates of the image space. This yields a

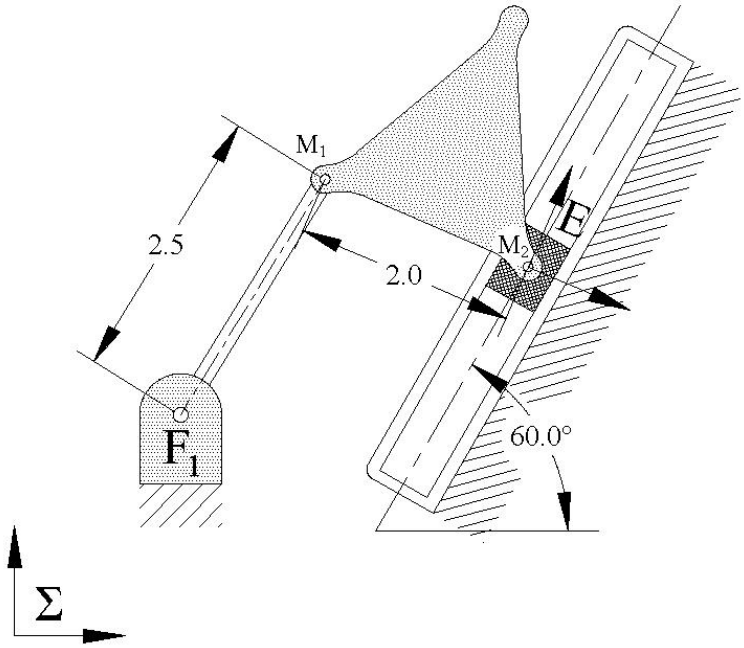

Figure 1: $RRRP$ linkage used to generate the five poses for the example.

linear transformation to express a displacement of E with respect to Σ in terms of the image point [7]:

$$\lambda \begin{bmatrix} X \\ Y \\ Z \end{bmatrix} = \boldsymbol{T} \begin{bmatrix} x \\ y \\ z \end{bmatrix}, \qquad (4)$$

where λ is some non-zero constant arising from the use of homogeneous coordinates and

$$\boldsymbol{T} = \begin{bmatrix} X_4^2 - X_3^2 & -2X_3X_4 & 2(X_1X_3 + X_2X_4) \\ 2X_3X_4 & X_4^2 - X_3^2 & 2(X_2X_3 - X_1X_4) \\ 0 & 0 & X_3^2 + X_4^2 \end{bmatrix}.$$

The inverse transformation can be obtained with the inverse of the matrix in Equation (4) as follows.

$$\gamma \begin{bmatrix} x \\ y \\ z \end{bmatrix} = \boldsymbol{T}^{-1} \begin{bmatrix} X \\ Y \\ Z \end{bmatrix}, \qquad (5)$$

with γ being another non-zero constant arising from the use of homogeneous coordinates and

$$\boldsymbol{T}^{-1} = \begin{bmatrix} X_4^2 - X_3^2 & 2X_3X_4 & 2(X_1X_3 - X_2X_4) \\ -2X_3X_4 & X_4^2 - X_3^2 & 2(X_2X_3 + X_1X_4) \\ 0 & 0 & X_3^2 + X_4^2 \end{bmatrix}.$$

2.1 Kinematic Constraints

There is a specific type of constrained motion corresponding to each type of planar lower-pair dyad: RR-type; PR-type; RP-type; and PP-type. Because a motion is a continuous set of displacements, and because a displacement maps to a point, a constrained motion will map to a continuous set of points in the image space. As shown in [9], the constraints imposed by the four different dyad types are quadric surfaces with special properties in the image space.

A clearer picture of the image space constraint surface that corresponds to the possible kinematic constraints emerges when $(X : Y : Z)$, or $(x : y : z)$ from Equations (4), or (5) are substituted into the general equation of a circle, the form of the most general constraint [10]:

$$K_0(X^2+Y^2)+2K_1XZ+2K_2YZ+K_3Z^2 = 0. \qquad (6)$$

The K_i in Equation (6) depend on the constraint imposed by the dyad. The result is that the constraint surfaces corresponding to RR, PR, and RP-dyads can be represented by *one* equation [10]. It is obtained by substituting the results from Equations (4), or (5) into Equation (6). However, the expression is greatly simplified under the following assumptions:

1. No mechanism of practical significance will have a point at infinity, so it is safe to set $z = 1$.

2. Coupler rotations of $\varphi = \pi$ (half-turns) have images in the plane $X_4 = 0$. Because the X_i are implicitly defined by Equation (2), setting $\varphi = \pi$ gives

$$(X_1 : X_2 : X_3 : X_4) = (a : b : 2 : 0). \qquad (7)$$

When we remove the one parameter family of image points for coupler orientations of $\varphi = \pi$ we can, for convenience, normalise the image space coordinates by setting $X_4 = 1$. Conceptually, this implies dividing the X_i by $X_4 = 2\cos\varphi/2$ giving

$$\begin{aligned} X_1 &= \frac{1}{2}\left(a\tan\left(\varphi/2\right) - b\right) \\ X_2 &= \frac{1}{2}\left(a + b\tan\left(\varphi/2\right)\right) \\ X_3 &= \tan\left(\varphi/2\right) \\ X_4 &= 1. \end{aligned} \tag{8}$$

Applying these assumptions to Equations (4), or (5) gives the simplified constraint surface equation upon substitution in Equation (6):

$$\begin{aligned} &K_0(X_1^2 + X_2^2) + (-K_0x + K_1)X_1X_3 \\ &+(-K_0y + K_2)X_2X_3 \mp (K_0y + K_2)X_1 \\ &\pm(K_0x + K_1)X_2 \mp (K_1y - K_2x)X_3 \\ &+\tfrac{1}{4}[K_0(x^2 + y^2) - 2(K_1x + K_2y) + K_3]X_3^2 \\ &+\tfrac{1}{4}[K_0(x^2 + y^2) + 2(K_1x + K_2y) + K_3] = 0. \end{aligned} \tag{9}$$

The X_i are the image space coordinates that represent a displacement of E relative to Σ. The x and y, after setting $z = 1$, are the Cartesian coordinates of the coupler attachment point in E. For both the RR- and PR-dyads the coupler and base-fixed link are joined by an R-pair, hence these coordinates are conveniently selected to be the rotation centre of the R-pair. The constraint surfaces for these dyads are obtained by using the *upper* signs in Equation (9). Note that for RP-dyads the kinematic constraint is inverted: instead of an R-pair centre constrained to move along a fixed line yielding a fixed range of points, we have a movable line constrained to move on a fixed point yielding a planar pencil of lines on the fixed point. For this case we use the alternate form of Equation (9) where the coordinates $(X : Y : 1)$ of the fixed R-pair centre are used in place of $(x : y : 1)$, and the *lower* signs are used. See [10] for a detailed explanation.

PP-dyads represent a special case. The image space constraint surface corresponding to possible displacements of a PP-dyad is a degenerate quadric that splits into a real and an imaginary plane. This is because only curvilinear motion of the coupler can result. Because φ is constant, the image space coordinates $X_3 = f(\varphi)$ and $X_4 = g(\varphi)$ must also be constant. Hence, the finite part of the two dimensional constraint manifold is linear and must be a hyper-plane. The plane is completely determined by the coupler orientation. When the image space is normalised by setting $X_4 = 1$, the surface equation is simply $X_3 = \tan\left(\varphi/2\right)$.

In what follows only RR- and PR-dyads will be considered to provide some degree of *proof-of-concept*. Development, refinement, and generalization of this approach will come in subsequent publications.

2.2 RR-type Circular Constraints

The ungrounded R-pair in an RR-dyad is constrained to move on a circle with a fixed centre. Meanwhile, the coupler can rotate about the moving R-pair when the coupler connection to the other dyad has been removed. This two parameter family of displacements corresponds to a two parameter hyperboloid of one sheet in the image space. An important property of the hyperboloid is that sections in planes parallel to $X_3 = 0$ are circles [9]. Each one of these image space circles represents possible coupler displacements with a fixed orientation. Thus the constraints imposed by RR-dyads are called *circular constraints*. The exact coefficients of the hyperboloid are determined by substituting in Equation (9) the appropriate values for the kinematic parameters:

$$\begin{aligned} K_0 &= 1, \\ K_1 &= -X_c, \\ K_2 &= -Y_c, \\ K_3 &= K_1^2 + K_2^2 - r^2, \end{aligned} \tag{10}$$

where (X_c, Y_c) are the Cartesian coordinates of the fixed circle centre in the reference frame that is considered to be non-moving, and r is the circle radius. If the kinematic constraint is a fixed point in E bound to fixed circle in Σ, then (x, y) are the Cartesian coordinates of the coupler reference point in E, and the upper signs apply. If the kinematic constraint is a fixed point in Σ bound to fixed circle in E, then (X, Y) are substituted for (x, y) as the coordinates of the coupler reference point in Σ, and the lower signs apply.

2.3 PR-type Linear Constraints

Linear constraints result when PR- and RP-dyads are employed. The linear coefficients are defined as

$$[K_0 : K_1 : K_2 : K_3] = [0 : \tfrac{1}{2}L_1 : \tfrac{1}{2}L_2 : L_3], \tag{11}$$

where the L_i are line coordinates obtained by Grassmann expansion of the determinant of any two distinct points on the line [11].

Of these in the present work we consider only PR-dyads. The direction of the line is a design constant, described by the angle it makes with respect to the fixed base frame Σ, indicated by ϑ_Σ. The point at infinity contained on the line is determined by the

direction of the line, and hence can be specified as $(\cos\vartheta_\Sigma : \sin\vartheta_\Sigma : 0)$. Additionally, the location of a fixed point on the line, also expressed in Σ, is given by the coordinates F_Σ. The line equation in Σ for a given PR-dyad is obtained from the Grassmann expansion:

$$\begin{vmatrix} X & Y & Z \\ F_{X/\Sigma} & F_{Y/\Sigma} & F_{Z/\Sigma} \\ \cos\vartheta_\Sigma & \sin\vartheta_\Sigma & 0 \end{vmatrix} = 0, \qquad (12)$$

where the notation $F_{X/\Sigma}$, $F_{Y/\Sigma}$, $F_{Z/\Sigma}$, represent the homogeneous coordinates $(X : Y : Z)$, expressed in reference frame Σ, of a fixed point on the line that is fixed relative to Σ. Applying Equations (11) and (12) we obtain

$$\begin{aligned} K_0 &= 0, \\ K_1 &= -\frac{F_{Z/\Sigma}}{2}\sin\vartheta_\Sigma, \\ K_2 &= \frac{F_{Z/\Sigma}}{2}\cos\vartheta_\Sigma, \\ K_3 &= F_{X/\Sigma}\sin\vartheta_\Sigma - F_{Y/\Sigma}\cos\vartheta_\Sigma. \end{aligned} \qquad (13)$$

The direction of the translation permitted by the P-pair is specified by the angle the line makes expressed in Σ, ϑ_Σ. When the coordinates of a fixed point on the line are known, we obtain the line coefficients $[K_0 : K_1 : K_2 : K_3]$. These, along with the design values of the coordinates of the coupler attachment point (x, y), expressed in reference frame E, substituted into Equation (9) reveals the image space constraint surface for the given PR-dyad. This surface is an hyperbolic paraboloid [9] with one regulus ruled by skew lines that are all parallel to the plane $X_3 = 0$.

2.4 The Burmester Problem in the Image Space

Each specified pose of E determines a point, $(X_1 : X_2 : X_3 : X_4)$, in the image space. If the displacements are feasible, the five points lie on the curve of intersection of the dyad constraint surfaces. The five points are enough to determine the intersecting quadrics. Recall that, in general, nine points are required to specify a quadric. The special nature of the constraint surfaces represent four constraints on these quadrics.

The hyperboloids, corresponding to RR-dyads, intersect planes parallel to $X_3 = 0$ in circles. Thus, all constraint hyperboloids contain the image space equivalent of the *imaginary circular points*, J_1 and J_2: $(1 : \pm i : 0 : 0)$. The points J_1 and J_2 are imaginary points on the real line, l, of intersection of the planes $X_3 = 0$ and $X_4 = 0$. This real line is the axis of a pencil of planes that includes the complex conjugate planes V_1 and V_2, defined by: $X_3 = \pm iX_4$. The hyperboloids all have V_1 and V_2 as tangent planes, though not necessarily at J_1 and J_2.

The hyperbolic paraboloids, corresponding to PR- and RP-dyads, contain l as a generator. Therefore all constraint hyperbolic paraboloids contain J_1 and J_2, moreover V_1 and V_2 are the tangent planes at these two points. Thus every constraint surface for RR-, PR-, and RP-dyads have these four conditions in common, reducing the number of independent parameters to five.

Our approach is to leave K_0 as an unspecified variable homogenizing coordinate and solve the synthesis equations in terms of K_0. In general, the constants K_1, K_2, and K_3 will depend on K_0. If these multipliers become very large (on the order of 10^6) indicating a very large crank radius then we set $K_0 = 0$ and use line coordinate definitions for K_1, K_2, and K_3 in Equation 13 giving a PR-dyad. Otherwise, $K_0 = 1$, and the circle coordinate definitions for K_1, K_2, and K_3 in Equation 10 are used yielding an RR-dyad.

3 Example

The mechanism illustrated in Figure 1 was used to generate the five poses listed in Table 1 and displayed in Figure 2. For this generating mechanism, the origin of reference frame E, O_E, is on the centre of the R-pair on the coupler point M_2. Homogeneous coordinates in E are described by the triples of ratios $(x : y : z)$. The coupler reference points M_1 and M_2 define the direction of the x-axis. The positive y-axis is as shown in Figures 1 and 2. Frame Σ is as shown in the same two figures. Reference frame E moves with the coupler. The fixed R-pair center is located on point F_1. The geometry of the generating mechanism is listed in the right hand side of Table 1.

The given five poses are mapped to the coordinates of five points in the image space. Using a computer algebra software package, we substitute the corresponding values for X_1, X_2, X_3, together with $X_4 = 1$ and $z = 1$ into Equation (9), effectively projecting the points onto the embedded Euclidean Space. This produces the following five nonlinear equations in terms of K_0, K_1, K_2, K_3, x, and y, which are quadratic when K_0 is considered constant:

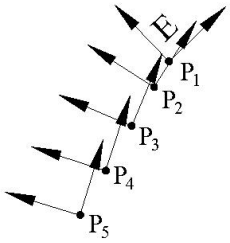

Figure 2: The five poses.

pose	a	b	φ (deg)	parameter	value
1	5.24080746	4.36781272	43.88348278	F_1	$(X:Y:Z)=(1.5:2:1)$
2	5.05087057	4.03883237	57.45578356	M_1	$(x:y:z)=(-2:0:1)$
3	4.76358093	3.54123213	66.99534998	M_2	$(x:y:z)=(0:0:1)$
4	4.43453496	2.97130779	72.10014317	M_1M_2	$l=2$
5	4.10748142	2.40483444	72.30529428	F_1M_1	$r=2.5$
				P-pair angle	$\vartheta_\Sigma=60$ (deg)

Table 1: Five poses of the $RRRP$ mechanism; Geometry of the $RRRP$ generating mechanism.

$$(13.52428430+3.954702976x-0.281732470y+0.2905708072x^2+0.2905708072y^2)K_0+$$
$$(3.045651308+0.4188583855x-0.4028439264y)K_1+$$
$$(2.538317736+0.4028439264x+0.4188583855y)K_2+0.2905708072K_3; \quad (14)$$

$$(13.59714292+3.980465638x-1.355748810y+0.3251080324x^2+0.3251080324y^2)K_0+$$
$$(3.284157186+0.3497839351x-0.5481168944y)K_1+$$
$$(2.626113690+0.3497839351y+0.5481168944x)K_2+0.3251080324K_3; \quad (15)$$

$$(12.66604850+3.682213684x-2.157608235y+0.3595038128x^2+0.3595038128y^2)K_0+$$
$$(3.425051014+0.2809923744x-0.6618272064y)K_1+$$
$$(2.546172905+0.6618272064x+0.2809923744y)K_2+0.3595038128K_3; \quad (16)$$

$$(10.89749412+3.205294435x-2.529259406y+0.3824518134x^2+0.3824518134y^2)K_0+$$
$$(3.391991875+0.2350963732x-0.7278785984y)K_1+$$
$$(2.272764106+0.7278785984x+0.2350963732y)K_2+0.3824518134K_3; \quad (17)$$

$$(8.686958330+2.714462017x-2.440453512y+0.3834517468x^2+0.3834517468y^2)K_0+$$
$$(3.150041851+0.2330965065x-0.7306209600y)K_1+$$
$$(+1.844275934+0.7306209600x+0.2330965065y)K_2+0.3834517468K_3; \quad (18)$$

Parameter	Surface 1	Surface 2	Surface 3	Surface 4
K_1	$-1.500K_0$	$-4.2909 \times 10^6 K_0$	$-15.6041K_0$	$-8.3011K_0$
K_2	$-2.0000K_0$	$2.4773 \times 10^6 K_0$	$3.4362K_0$	$-5.0837K_0$
K_3	$-2.5801 \times 10^{-6} K_0$	$2.3334 \times 10^7 K_0$	$107.3652K_0$	$93.4290K_0$
x	-2.0000	8.1749×10^{-7}	0.2281	3.7705
y	3.4329×10^{-7}	-1.3214×10^{-6}	-0.7845	-2.0319

Table 2: The identified constraint surface coefficients.

Parameter	Relation	Value
F_1	$(-K_{1_1}, -K_{2_1})$	$(1.500, 2.000)$
M_1	(x_1, y_1)	$(-2.000, 3.4329 \times 10^{-7})$
M_2	(x_2, y_2)	$(8.1749 \times 10^{-7}, -1.3214 \times 10^{-6})$
ϑ_Σ	$\arctan\left(\frac{-K_{1_1}}{K_{2_1}}\right)$	60.0°

Table 3: Geometry of one of six synthesized mechanisms that is a good approximation of the generating $RRRP$ linkage in Figure 1.

Solving the system of Equarions (14-18) for the unknowns K_1, K_2, K_3, x, and y in terms of K_0 yields the set of four solutions listed in Table 2. Substituting these values into Equation (9) gives four distinct constraint surfaces in the image space, in terms of the homogenizing circle, or line coordinate, K_0.

At the present time, heuristics must be used to select an appropriate value for K_0 by comparing the relative magnitudes of K_1 and K_2. Recall that the circle coordinates are defined to be $K_1 = -X_c$, and $K_2 = -Y_c$, the Cartesian coordinates of the fixed revolute centres, multiplied by -1, expressed in Σ. The crank radius is given by $r = +\sqrt{K_3^2 - (K_1^2 + K_2^2)}$. The coefficients for Surfaces 1, 3, and 4 represent RR-dyads with finite rotation centres when $K_0 = 1$. However, the coefficients for Surface 2, relative to the other three, have a rotation centre whose location approaches infinity, $(4.2909 \times 10^6, -2.4773 \times 10^6)$ with a crank radius of 4.9547×10^6, also approaching infinity, while the relative values of x and y indicate this attachment point is on O_E. This surface should clearly be recomputed as an hyperbolic paraboloid revealing the corresponding PR-dyad. Recall the line coordinate definition, with K_0 left unspecified:

$$\begin{aligned} K_0 &= K_0, \\ K_1 &= -\frac{F_{Z/\Sigma}}{2} \sin\vartheta_\Sigma, \\ K_2 &= \frac{F_{Z/\Sigma}}{2} \cos\vartheta_\Sigma, \\ K_3 &= F_{X/\Sigma} \sin\vartheta_\Sigma - F_{Y/\Sigma} \cos\vartheta_\Sigma. \end{aligned} \quad (19)$$

The angle of the direction of translation of the P-

Solution	Dyad surface pairing
1	Dyad 1 - Dyad 2
2	Dyad 2 - Dyad 3
3	Dyad 2 - Dyad 4
4	Dyad 1 - Dyad 3
5	Dyad 1 - Dyad 4
6	Dyad 3 - Dyad 4

Table 4: Dyad pairings yielding the six synthesized mechanisms.

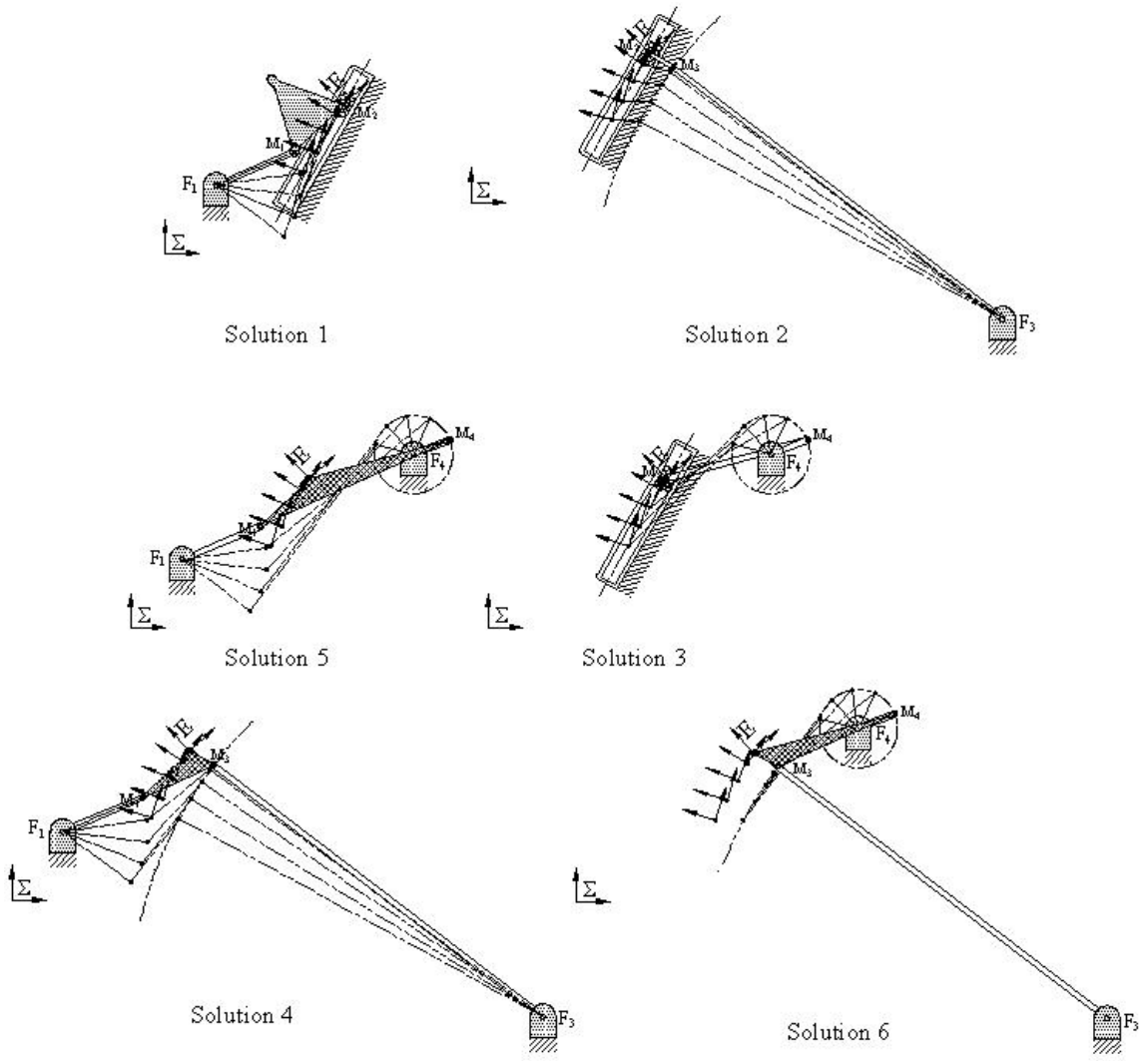

Figure 3: The six synthesized mechanisms.

pair relative to the X-axis of Σ is ϑ_Σ. The translation direction of a PR-dyad that could be combined with any of the three RR-dyads is thus

$$\begin{aligned} \vartheta_\Sigma &= \arctan\left(\frac{-K_1}{K_2}\right) \\ &= \arctan\left(\frac{4.2909\times10^6 K_0}{2.4773\times10^6 K_0}\right) \\ &= 60.0^\circ. \end{aligned} \tag{20}$$

Employing plane trigonometry, it is simple to extract the link lengths and joint locations of the dyad associated with each of the four constraint surfaces. The generating mechanism is reproduced when the dyads corresponding to Surfaces 1 and 2 are paired. We obtain the geometry listed in Table 3 (note, the second subscript refers to the particular surface). The six possible mechanisms are the combinations of the four dyads taken two at a time. These are listed in Table 4 and are illustrated in Figure 3.

4 Conclusions

The example presented herein illustrates that the general image space constraint surface equation, leaving K_0 unspecified, can be used for general type and dimensional synthesis for planar mechanisms. For a set of five poses generated by a particular slider-crank, we synthesized six mechanisms, including the one that generated the poses, that can guide the coupler through the five poses. Three of the six synthesized linkages are slider-cranks while

the remaining three are $4R$ mechanisms. The coupler point is the centre of the R-pair connecting the coupler to the P-pair. This coupler point is clearly bound to a line in the $RRRP$ linkages, but not in the case of the $4R$'s. This approach to planar four-bar mechanisms stands to offer the designer *all* possible linkages that can attain the desired poses, not just $4R$'s and not just slider-cranks, but *all* feasible four-bar linkage architectures along with their dimensions.

Outstanding issues involve the following. The heuristics must be rethought so that an algorithm for type selection can be developed. Moreover, the problem formulation must be reconsidered in such a way that both PR- and RP-dyads can be typed, and extracted from the solutions. The geometric reasoning explaining why five image space points are sufficient to define four unique quadrics must be formalized. Additionally, the geometric interpretation of K_0 must be investigated. How, for example, are the constraint hyperbolic paraboloids parameterized in the image space without setting $K_0 = 0$?

Finally, methods to apply this technique to approximate synthesis should be investigated. The resulting problem would involve fitting a suitable number of points to surfaces in the image space. More specifically, fitting points to the curve of intersection of constraint surfaces. To do this some form of least-squares error minimization would have to be employed. The outcome would be a single dyad pair: the one corresponding to the two constraint surfaces whose intersection best approximates the given set of desired poses

References

[1] L. Burmester. *Lehrbuch der Kinematik*. Arthur Felix Verlag, Leipzig, Germany, 1888.

[2] Y.C. Ching, J. Angeles, and M. González-Palacios. "A Semi-graphical Method for the Solution of the BurmesterProblem". *ASME Adv. in Des. Auto.*, DE-Vol. 32-2: pages 321–326, 1991.

[3] J.M. McCarthy. *Geometric Design of Linkages*. Springer-Verlag, New York, N.Y., U.S.A., 2000.

[4] A.P. Murray and J.M. McCarthy. "Constraint Manifold Synthesis of Planar Linkages". *Proceedings of ASME DETC: Mechanisms Conference, Irvine CA.*, 1996.

[5] W. Blaschke. "Euklidische Kinematik und Nichteuklidische Geometrie". *Zeitschr. Math. Phys.*, vol. 60: pages 61–91 and 203–204, 1911.

[6] J. Grünwald. "Ein Abbildungsprinzip, welches die ebene Geometrie und Kinematik mit der räumlichen Geometrie verknüpft". *Sitzber. Ak. Wiss. Wien*, vol. 120: pages 677–741, 1911.

[7] O. Bottema and B. Roth. *Theoretical Kinematics*. Dover Publications, Inc., New York, N.Y., U.S.A., 1990.

[8] M.J.D. Hayes and P.J. Zsombor-Murray. "Solving the Burmester Problem Using Kinematic Mapping". *Proc. of the ASME Design Engineering Technical Conferences: Mechanisms Conference*, Montréal, QC, Canada, on CD, Sept. 2002.

[9] M.J.D. Hayes and M.L. Husty. "On the Kinematic Constraint Surfaces of General Three-Legged Planar Robot Platforms". *Mechanism and Machine Theory*, vol. 38, no. 5: pages 379–394, 2003.

[10] M.J.D. Hayes, P.J. Zsombor-Murray, and C. Chen. "Kinematic Analyais of General Planar Parallel Manipulators". *ASME, Journal of Mechanical Design*, in-press, 2004.

[11] F. Klein. *Elementary Mathematics from an Advanced Standpoint: Geometry*. Dover Publications, Inc., New York, N.Y., U.S.A., 1939.

Integrated Type And Dimensional Synthesis of Planar Four-Bar Mechanisms

Tim J. Luu and M. John D. Hayes

Abstract A novel approach to integrated type and approximate dimensional synthesis of planar four-bar mechanisms (i.e. linkages comprised of any two of *RR*, *PR*, *RP*, and *PP* dyads) for rigid-body guidance is proposed. The essence is to correlate coordinates of the coupler attachment points in two different coordinate frames, thereby reducing the number of independent variables defining a suitable dyad for the desired rigid-body motion from five to two. After applying these geometric constraints, numerical methods are used to size link lengths, locate joint axes, and decide between *RR*, *PR*, *RP* and *PP* dyads that, when combined, guide a rigid body through the best approximation, in a least-squares sense, of n specified positions and orientations, where $n \geq 5$. No initial guesses of type or dimension are required. An example is presented illustrating the effectiveness and robustness of this new approach.

Key words: Approximate type and dimensional synthesis; planar four-bar mechanisms; rigid body guidance; singular value decomposition.

1 Introduction

Planar linkages contain either revolute (*R*-pairs), or prismatic (*P*-pairs). These kinematic pairs permit rotations about one axis, or translations parallel to one direction, respectively. In general, dimensional synthesis for rigid body guidance assumes a mechanism *type*: i.e., planar 4*R*; slider-crank; crank-slider; trammel, etc.. Our aim is to develop a completely general planar mechanism synthesis algorithm that in-

Tim J. Luu
Neptec Design Group Ltd., Ottawa, Ontario, Canada e-mail: tluu@neptec.com
M. John D. Hayes
Carleton University, Deptartment of Mechanical and Aerospace Engineering e-mail: jhayes@mae.carleton.ca

tegrates both *type* and *dimensional* synthesis for n-position approximate synthesis for rigid body guidance. The pairing of the two types leads to four possible dyads: revolute-revolute (RR), prismatic-revolute (PR), revolute-prismatic (RP), and prismatic-prismatic (PP).

There is an extensive body of literature reporting research on approximate dimensional kinematic synthesis of planar four-bar mechanisms for rigid-body guidance, see for example [12, 1, 6, 5, 4, 9]. However, there are no methods reported in the substantial body of literature that successfully integrate both type and approximate dimensional synthesis of planar four-bar mechanisms for rigid body guidance, without a priori knowledge or initial guesses with the exception of two special cases reported in [3, 2]. In this paper a method for doing so is presented for the first time.

The minimization criteria of the algorithm presented in this paper is purely mathematical: the condition number of the synthesis matrix. The algorithm will be enhanced when the transmission angle is incorporated as an optimization objective. It would be additionally beneficial to examine the order and branch defect problems. It may be that advances made in [10] can be incorporated into the integrated type-dimensional synthesis algorithm to address these issues. These issues notwithstanding, the algorithm presented in this paper is a robust foundation upon which to build. The algorithm is being adapted for synthesis of spatial motion platforms.

2 Kinematic Constraints: Circular and Linear

The motion of the coupler link in a four-bar planar mechanism is determined by the relative displacements of all links in the kinematic chain. The relative displacement of two rigid bodies in the plane can be considered as the displacement of a Cartesian reference coordinate frame E attached to one of the bodies with respect to a Cartesian reference coordinate frame Σ attached to the other. Without loss of generality, Σ may be considered fixed with E free to move, see Figure 2. The homogeneous coordinates of points represented in E are given by the ratios $(x : y : z)$. Those of the same points represented in Σ are given by the ratios $(X : Y : Z)$. The mapping between the coordinates of points expressed in the two reference frames is given by the homogeneous coordinate transformation

$$\begin{bmatrix} X \\ Y \\ Z \end{bmatrix} = \begin{bmatrix} \cos\theta & -\sin\theta & a \\ \sin\theta & \cos\theta & b \\ 0 & 0 & 1 \end{bmatrix} \begin{bmatrix} x \\ y \\ z \end{bmatrix}, \tag{1}$$

where (a,b) are the $(\frac{X}{Z}, \frac{Y}{Z})$ Cartesian coordinates of the origin of E with respect to Σ, and θ is the orientation of E relative to Σ. Any point $(x : y : z)$ in E can be mapped to $(X : Y : Z)$ in Σ using this transformation. For rigid body guidance, each pose is defined by the position and orientation of E with respect to Σ, which is specified by the ordered triple (a,b,θ). Dyads are connected through the coupler link at the coupler attachment points M_1 and M_2, see Figure 1.

There is a specific type of constrained motion corresponding to each one of the four types of planar lower-pair dyad. The ungrounded *R* pair in an *RR* dyad is constrained to move on a circle with a fixed centre. Because of this they are denoted *circular constraints*. *Linear constraints* result when *PR* and *RP* dyads are employed because the *R* pair attachment point is constrained to move on a line defined by the *P* pair translation direction. The *PP* dyad represents a planar constraint: the line of one *P* pair direction is constrained to translate on the direction line of the other.

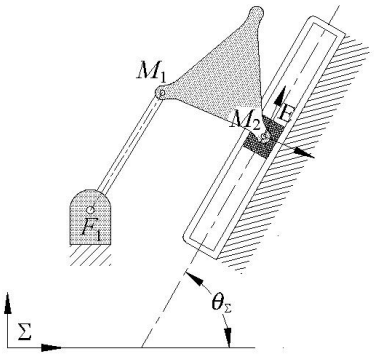

Fig. 1. Planar *RRRP* linkage.

It can be shown [2] that the model representing both circular and linear constraints for n Cartesian point coordinate pairs can be expressed in matrix form as

$$\mathbf{Ck} = \begin{bmatrix} X_j^2 + Y_j^2 & 2X_j & 2Y_j & 1 \end{bmatrix} \begin{bmatrix} K_0 \\ K_1 \\ K_2 \\ K_3 \end{bmatrix} = \mathbf{0}, \tag{2}$$

where $\mathbf{C}$ is an $n \times 4$ dimensional array with $j \in \{1, 2, \ldots, n\}$, with X and Y being the Cartesian coordinates of points on either a circle or line, and the K_i are constant shape parameters determined by the constraint imposed by the dyad [2].

For circular constraints the K_i are defined as

$$K_0 = 1, \;\; K_1 = -X_c, \;\; K_2 = -Y_c, \;\; K_3 = K_1^2 + K_2^2 - r^2, \tag{3}$$

where (X_c, Y_c) are the Cartesian coordinates of the circle centre expressed in Σ and r is the circle radius.

Linear constraints require $K_0 = 0$ and the remaining K_i are proportional to line coordinates defined by

$$K_1 = -\frac{1}{2} F_{Z/\Sigma} \sin\theta_\Sigma, \;\; K_2 = \frac{1}{2} F_{Z/\Sigma} \cos\theta_\Sigma, \;\; K_3 = F_{X/\Sigma} \sin\theta_\Sigma - F_{Y/\Sigma} \cos\theta_\Sigma, \tag{4}$$

where $(F_{X/\Sigma} : F_{Y/\Sigma} : F_{Z/\Sigma})$ are homogeneous coordinates of a fixed point, expressed in Σ, on the line that makes an angle θ_Σ with the positive X-axis in Σ.

In the definitions of the K_i, the parameter K_0 acts as a binary switch between circular and linear constraints. When $K_0 = 1$ Equation (2) represents the implicit equation of points on a circle, and when $K_0 = 0$ the equation becomes that of a line. Nonetheless, K_0 is still an homogenizing parameter whose value is arbitrary. The K_i can be normalized by K_0, but only when K_0 is nonzero.

3 Integrating Type and Approximate Dimensional Synthesis

Equations (2), (3), and (4) are used to integrate type and approximate dimensional synthesis of planar for-bar mechanisms for rigid-body guidance. Constructing the required synthesis matrix $\mathbf{C}$ based on the prescribed poses is done by relating the position of the two rigid body attachment points M_1 and M_2 in both reference frames E and Σ, see Figure 1. Reference frames Σ and E are correlated in two ways:

1. Points M_1 and M_2 move on circles or lines in Σ;
2. Points M_1 and M_2 have constant coordinates in E.

Let (x,y) be the coordinates expressed in E of one of the coupler attachment points, M, and (X,Y) be the coordinates of the same point expressed in Σ. Carrying out the matrix multiplication in Equation (1) yields

$$\begin{aligned} X &= x\cos\theta - y\sin\theta + az, \\ Y &= x\sin\theta + y\cos\theta + bz, \\ Z &= z. \end{aligned} \tag{5}$$

Ignoring infinitely distant coupler attachment points, it is reasonable to set $z = 1$ in Equation (5) and substituting the result into Equation (2), with $j \in \{1,2,\ldots,n\}$ yields

$$\mathbf{Ck} = \begin{bmatrix} (x\cos\theta_j - y\sin\theta_j + a_j)^2 + (x\sin\theta_j + y\cos\theta_j + b_j)^2 \\ 2\,(x\cos\theta_j - y\sin\theta_j + a_j) \\ 2\,(x\sin\theta_j + y\cos\theta_j + b_j) \\ 1 \end{bmatrix}^T \begin{bmatrix} K_0 \\ K_1 \\ K_2 \\ K_3 \end{bmatrix} = 0. \tag{6}$$

Prescribing $n > 5$ poses makes $\mathbf{C}$ an $n \times 4$ matrix. The parameters x and y possess constant values in E. The n-dimensional vector parameters $\mathbf{a}$, $\mathbf{b}$, and θ in $\mathbf{C}$ are all known a priori because they are the specified poses of E with respect to Σ.

The only unknown parameters in $\mathbf{C}$ are x and y. Determining the x and y that best satisfy Equation (6) will solve the problem. Once values for x and y are obtained $\mathbf{C}$ is fully determined, which allows the vector $\mathbf{k}$ to be identified. The problem is now a two dimensional search for x and y. However, at least two dyads are required to form a planar mechanism. This implies that there must be at least two distinct values for x and y in order for a complete solution to exist. The x and y are found such that they satisfy Equation (6). For equations of the form $\mathbf{Ck} = \mathbf{0}$ the only real $\mathbf{k}$ that satisfies the equation is the zero vector if $\mathbf{C}$ is not singular. In other words, for non-trivial $\mathbf{k}$ to exist, $\mathbf{C}$ must be rank deficient [11]. The task becomes finding values for x and y that make $\mathbf{C}$ rank deficient, or failing that, the most ill-conditioned.

The conditioning of a matrix is measured by the ratio of the largest and smallest singular values of the matrix, which is called the condition number κ. It is computationally more convenient to use is the inverse of the condition number, γ

$$\gamma \equiv \frac{1}{\kappa} = \frac{\sigma_{MIN}}{\sigma_{MAX}}, 0 \leq \gamma \leq 1, \tag{7}$$

because it is bounded both from above and below. A well conditioned matrix has $\gamma \approx 1$, while an ill-conditioned matrix has $\gamma \approx 0$. Therefore, selecting x and y that renders $\mathbf{C}$ the most rank deficient involves minimizing γ.

The Nelder-Mead *Downhill Simplex Method in Multidimensions* algorithm may be used for this minimization [7]. This method requires only function evaluations, not derivatives. It is not very efficient in terms of the evaluations it requires, but for the problem at hand the computational burden is relatively small. We will not discuss the convergence properties, because any optimization method may be employed.

Since the Nelder-Mead algorithm needs an initial guess, γ may be plotted in terms of x and y first, in the neighborhood of $(x,\ y) = (0,\ 0)$ up to a user-defined range of the maximum distance that the coupler attachment points can be from the moving frame E origin, denoted ε. As x and y represent the position of a coupler attachment point with respect to moving refernece frame E. The x and y parameters may then be selected approximately corresponding to the smallest value of γ. These points represent the local minima of the entire γ plot, that is, with $\varepsilon = \infty$. However, for practical reasons, with ε finite, these minima may be regarded as the global minima of the region of interest. At least two minima are required to obtain a planar four-bar mechanism, as each minimum corresponds to a single dyad. The Nelder-Mead algorithm is fed these approximate values as inputs, and converges to the values of x and y that minimize γ.

Once the values of x and y have been determined the matrix $\mathbf{C}$ in Equation (6) can be populated. The $\mathbf{k}$ parameters may then be estimated. We have elected to use singular value decomposition (SVD) because we are necessarily required to work with either singular, or numerically very-close-to-singular sets of equations. SVD decomposes any given $m \times n$ matrix $\mathbf{C}$ into the product of three matrix factors such that

$$\mathbf{C}_{m\times n} = \mathbf{U}_{m\times m}\mathbf{S}_{m\times n}\mathbf{V}^T_{n\times n}, \tag{8}$$

where $\mathbf{U}$ and $\mathbf{V}$ are orthogonal, and $\mathbf{S}$ is a rectangular matrix whose only non-zero elements are on the diagonal of the upper $n \times n$ sub-matrix. These diagonal elements are the singular values of $\mathbf{C}$ arranged in descending order, lower bounded by zero [8]. SVD constructs orthonormal bases spanning the range of $\mathbf{C}$ in $\mathbf{U}$ and the nullspace of $\mathbf{C}$ in $\mathbf{V}$. If $\mathbf{C}$ is rank deficient, then the last $n-\text{rank}(\mathbf{C})$ singular values of $\mathbf{C}$ are zero. Furthermore, the corresponding columns of $\mathbf{V}$ are unit basis vectors that span the nullspace of $\mathbf{C}$. As such, any linear combination of these columns is a non-trivial solution that best satisfies the system $\mathbf{Ck} = \mathbf{0}$.

For overconstrained systems, where the $m \times n$ matrix $\mathbf{C}$ has $m > n$, in general no non-trivial exact solution exists, because in general an overconstrained synthesis matrix possesses full rank. In this case, the optimal approximate solution in a least-squares sense is last column of $\mathbf{V}$, corresponding to the smallest singular value of $\mathbf{C}$. Furthermore, the more ill-conditioned $\mathbf{C}$ is, the closer the optimal approximate solution is to being an exact solution. Because the K_i are homogeneous, the scaling posses no problem because $\mathbf{k}$ will be normalized by dividing through by K_0. In the case where $K_0 \approx 0$, or $K_0 = 0$ the linear definitions for K_1, K_2, and K_3 from

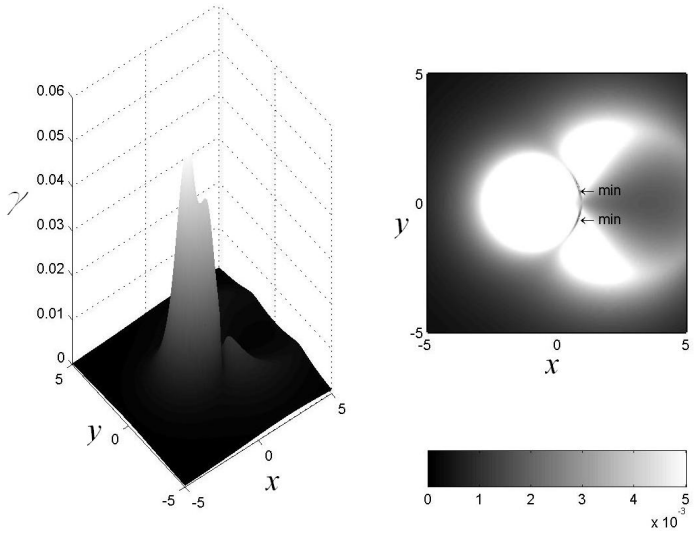

Fig. 2 The γ plot of the poses defining a square corner.

Equation (4) are used. The switching threshold for K_0 to represent either an *RR* or *PR* (or *RP*) dyad must be user defined based on the geometry of the problem.

Note that *PP* dyads are a special case. Two serial *P* pairs restricts the distal link from changing its orientation. For type synthesis, given any set of poses with non constant orientation, the *PP* dyad is immediately ruled out.

3.1 Example

Consider an example that requires completely general integrated type and approximate dimensional synthesis by defining poses that are impossible to generate exactly by any four-bar planar mechanism. The poses define a square corner. A point on a rigid body moves linearly between the Cartesian coordinates from (0, 1) to (1, 0) via (1,1). The orientation increases linearly from 0 to 90 degrees. The poses are listed in Table 1.

Pose	1	2	3	4	5	6	7	8	9	10	11	12	13	14	15	16	17	18
a	0.0	0.1	0.2	0.3	0.4	0.6	0.7	0.8	1.0	1.0	1.0	1.0	1.0	1.0	1.0	1.0	1.0	1.0
b	1.0	1.0	1.0	1.0	1.0	1.0	1.0	1.0	1.0	0.9	0.8	0.7	0.6	0.4	0.3	0.2	0.1	0.0
θ°	0.0	4.5	9.0	13.5	18.0	27.0	31.5	36.0	45.0	49.5	54.0	58.5	63.0	72.0	76.5	81.0	85.5	90.0

Table 1 Specified poses defining a square corner.

A planar four-bar mechanism cannot exactly replicate the motion defined above because points on the coupler generate either a 6^{th}, 4^{th}, or 2^{nd} order curve. The curve

$$x^n + y^n = 1 \tag{9}$$

approaches a square corner as $n \to \infty$. With $n \leq 6$ for planar four-bar mechanisms, it is impossible to exactly replicate the desired motion. Although a *PPPP* mechanism may be able to generate the desired point translation, the change in orientation rules out this type of mechanism.

The pose data are substituted into Equation (6) to populate **C**. The γ of **C** are then plotted as a function of x and y and are shown in Figure 2. As can be seen in this figure, two distinct minima occur at approximately (0.8, 0.6) and (0.8, -0.6). Using the Nelder-Mead minimization and the pair of approximate x and y as initial guesses, the exact values of the two minima are found, and listed in Figure 3. These values are then substituted into Equation (6) to completely determine **C**. SVD is then applied to **C** to find **k** corresponding to each minimum. The values of **k** thus determined are also listed in Figure 3. The resulting synthesized mechanism, illustrated in Figure 3, is composed of two *RR* dyads centred on (4.5843, -1.0539) and (-1.0539, 4.5843), both with links having length 1.7307.

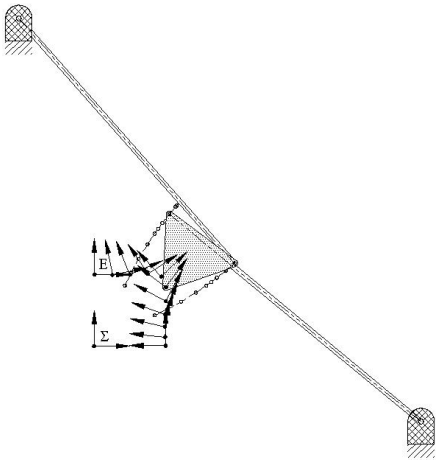

	Dyad 1	Dyad 2
x	0.8413	0.8413
y	0.5706	-0.5706
K_0	0.2010	0.2010
K_0/K_0	1	1
K_1/K_0	-4.5843	1.0549
K_2/K_0	1.0539	-4.5843
K_3/K_0	1.2704	1.2704

Fig. 3 Identified *RRRR* mechanism and corresponding dyads.

4 Conclusions

In this paper a novel method was presented that integrates type and approximate dimensional synthesis of planar four-bar mechanisms used for rigid-body guidance. Coupler attachment points are correlated between moving frame E and fixed frame

Σ thereby reducing the number of independent variables defining a suitable dyad for the desired poses from five to two. Numerical methods are then used to determine both mechanism type and approximate dimensions. A numerical example was presented, illustrating the utility of the algorithm.

References

[1] Akhras, R., Angeles, J.: "Unconstrained Nonlinear Least-Square Optimization of Planar Linkages for Rigid-Body Guidance". Mechanism and Machine Theory **25**(1), 97–118 (1990)

[2] Hayes, M.J.D., Luu, T., Chang, X.W.: "Kinematic Mapping Application to Approximate Type and Dimension Synthesis of Planar Mechanisms". In: 9th Advances in Robotic Kinematics, *eds. Lenarčič, J. and Galletti, C., Kluwer Academic Publishers, Dordrecht, the Netherlands*, pp. 41–48 (June 28 - July 1, 2004)

[3] Hayes, M.J.D., Zsombor-Murray, P.J.: "Towards Integrated Type and Dimensional Synthesis of Mechanisms for Rigid Body Guidance". In: Proceedings of the CSME Forum 2004, pp. 53–61. University of Western Ontario, London, ON, Canada (June 1-4, 2004)

[4] Kong, X.: "Approximate Kinematic Synthesis of Linkages Using Generalized Inverse Matrix and Continuation". Mechanical Science and Technology **18**(1), 38–40 (1999)

[5] Larochelle, P.: "Approximate Motion Synthesis of Open and Closed Chains Via Parametric Constraint Manifold Fitting: Preliminary Results". Proceedings of the ASME Design Engineering Technical Conferences and Computers and Information in Engineering Conference **2**, 1049–1057 (2003)

[6] Larochelle, P., McCarthy, J.M.: "Designing Planar Mechanisms Using a Bi-Invariant Metric in the Image Space of SO". ASME, Design Engineering Division, 23rd Biennial Mechanisms Conference **70**(1), 221–228 (1994)

[7] Nelder, J.A., Mead, R.: "A Simplex Method for Function Minimization". Computer Journal **7**, 308–313 (1965)

[8] Press, W., Teukolsky, S., Vetterling, W., Flannery, B.: Numerical Recipes in C, 2nd Edition. Cambridge University Press, Cambridge, England (1992)

[9] Ravani, B., Roth, B.: "Motion Synthesis Using Kinematic Mappings". Journal of Mechanisms, Transmissions, and Automation in Design **105**(3), 460–467 (1983)

[10] Schröcker, H.P., Husty, M., McCarthy, J.M.: "Kinematic Mapping Based Evaluation of Assembly Modes for Planar Four-Bar Synthesis". ASME, Journal of Mechanical Design **129**(9), 924–929 (2007)

[11] Strang, G.: Linear Algebra and its Applications. Academic Press (1980)

[12] Vallejo, J., Aviles, R., Hernandez, A., Amezua, E.: "Nonlinear Optimization of Planar Linkages for Kinematic Syntheses". Mechanism and Machine Theory **30**(4), 501–518 (1995)

Input-output Equation for Planar Four-bar Linkages

M. John D, Hayes[1], Manfred L. Husty[2], and Martin Pfurner[2]

[1] Carleton University, Ottawa, ON, Canada
john.hayes@carleton.ca,
WWW home page: https://carleton.ca/mae/people/m-john-d-hayes
[2] University of Innsbruck, Unit Geometry and CAD,
Innsbruck, Austria

Abstract. In this paper the generalised input-output (I-O) equation for planar 4*R* function generators is derived in a new way, leading to the algebraic form of the well known Freudenstein equation. The long term goal is to develop a generalised method to derive constraint based algebraic I-O equations that can be used for continuous approximate synthesis, where the synthesis equations are integrated between minimum and maximum input angle values resulting in a linkage whose objective function has been optimised over every output angle. In this paper we use a planar projection of Study's soma and the Cartesian displacement constraints for the dyads. These are mapped to the image space leading to four constraint equations in terms of the image space coordinates and the sines and cosines of the input and output angles. Using the tangent of the half angle substitution the trigonometric equations are converted to algebraic ones. Algebraic methods are used to eliminate the image space coordinates, then the polynomial resultants are found to obtain common roots leading to the desired equations.

Keywords: Function generators, continuous approximate synthesis, kinematic mapping, polynomial resultants.

1 Introduction

A planar 4*R* function generator correlates driver and follower angles in a functional relationship. The mechanism essentially generates the function $\varphi = f(\psi)$, or vice versa, see Fig. 1. Design methods typically employ the Freudenstein synthesis equations to identify link lengths required to generate the function [2,4]. For over-determined sets of prescribed input-output (I-O) angle pairs, these equations are linear in the three unknown Freudenstein parameters, which are ratios of the link lengths, and can be solved for using any least squares method to minimise a specified performance error. To the best of the authors knowledge, there are no alternative algebraic models of the function generator displacement equations in the accessible literature.

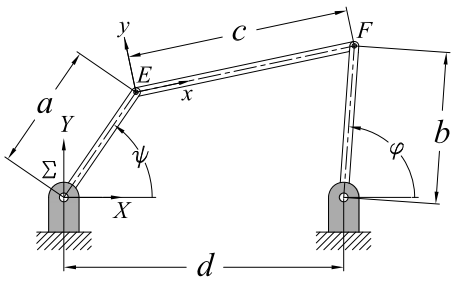

Fig. 1. 4*R* Function Generator.

It has been observed [7,5] that as the cardinality of the prescribed discrete I-O data set increases, the corresponding four-bar linkages that minimise the Euclidean norm of the design and structural errors tend to converge to the same linkage. The important implication is that minimising the Euclidean norm, or any p-norm, of the structural error can be accomplished indirectly by minimising the same norm of the design error. In [5] the trigonometric Freudenstein synthesis equations are integrated in the range between minimum and maximum input values, thereby reposing the discrete approximate synthesis problem as a continuous one whereby the objective function is optimised over the entire I-O range. Hence, our long-term goal is to determine a general method to derive motion constraint based algebraic I-O equations that may be used together with the method of continuous approximate synthesis [5] to obtain the very best linkage that can generate an arbitrary function. The goal of this paper is to develop one in the hope of providing new insight into the continuous approximate synthesis of function generators, while mitigating numerical integration error. Of course, the same equation will be obtained by making the tangent half-angle substitutions directly into the Freudenstein equation then collecting terms after factoring, normalising, and eliminating non-zero factors. But that must be the case since the geometric relations require that outcome, however this is irrelevant because the goal is to generalise a method to develop constraint based algebraic I-O equations for continuous approximate synthesis of planar, spherical, and spatial linkages. This paper represents the first step in that long journey.

2 Geometric and Algebraic Approach

The Freudenstein equation relating the input to the output angles of a planar $4R$ four-bar mechanism, with link lengths as in Fig. 1, was first put forward in [3]. In the equation the angle ψ is traditionally selected to be the input while φ is the output angle:

$$k_1 + k_2\cos(\varphi_i) - k_3\cos(\psi_i) = \cos(\psi_i - \varphi_i). \tag{1}$$

Equation (1) is linear in the k_i Freudenstein parameters, which are defined in terms of the link length ratios as

$$\left.\begin{aligned} k_1 &\equiv \frac{(a^2+b^2+d^2-c^2)}{2ab},\\ k_2 &\equiv \frac{d}{a},\\ k_3 &\equiv \frac{d}{b}. \end{aligned}\right\} \Leftrightarrow \begin{cases} d = & 1,\\ a = & \frac{1}{k_2},\\ b = & \frac{1}{k_3},\\ c = & (a^2+b^2+d^2-2abk_1)^{1/2}. \end{cases}$$

The new idea starts the same as with the Freudenstein method, writing the displacement constraints in terms of the I-O angles. Continuing with tradition, we select ψ to be the input angle and φ to be the output angle. Let Σ be a non moving Cartesian coordinate system with coordinates X and Y whose origin is located at the centre of the

ground fixed link R-pair with length a. Let E be a coordinate system that moves with the coupler of length c whose origin is at the centre of the distal R-pair of link a, having basis directions x and y.

The displacement constraints for the origin of E can be expressed as

$$\begin{aligned} X - a\cos\psi &= 0, \\ Y - a\sin\psi &= 0, \end{aligned} \tag{2}$$

while those for point F, located at the centre of the distal R-pair on the output link with length b are

$$\begin{aligned} X - d - b\cos\varphi &= 0, \\ Y - b\sin\varphi &= 0. \end{aligned} \tag{3}$$

Next, we use a planar projection of Study's soma coordinates [8] to establish the I-O equation. Any displacement in Euclidean space, E_3, can be mapped in terms of the coordinates of a 7-dimensional projective image space using the transformation [1]

$$\mathbf{T} = \begin{bmatrix} x_0^2+x_1^2+x_2^2+x_3^2 & 0 & 0 & 0 \\ 2(-x_0y_1+x_1y_0-x_2y_3-x_3y_2) & x_0^2+x_1^2-x_2^2-x_3^2 & 2(x_1x_2-x_0x_3) & 2(x_1x_3+x_0x_2) \\ 2(-x_0y_2+x_1y_3+x_2y_0-x_3y_1) & 2(x_1x_2+x_0x_3) & x_0^2-x_1^2+x_2^2-x_3^2 & 2(x_2x_3-x_0x_1) \\ 2(-x_0y_3-x_1y_2+x_2y_1+x_3y_0) & 2(x_1x_3-x_0x_2) & 2(x_2x_3+x_0x_1) & x_0^2-x_1^2-x_2^2+x_3^2 \end{bmatrix}. \tag{4}$$

This transforms the coordinates of any point described in a moving $3D$ coordinate system E to the coordinates of the same point in a relatively fixed $3D$ coordinate system Σ (assuming that the two frames are initially coincident) after a given displacement of E relative to Σ in terms of the coordinates of a point on the Study quadric, S_6^2. In order for a point in the image space to represent a real displacement, and therefore to be located on S_6^2, the non-zero condition of $x_1^2+x_2^2+x_3^2+x_4^2 \neq 0$ must be satisfied.

The transformation matrix $\mathbf{T}$ simplifies considerably when we consider displacements that are restricted to the plane. Three degrees of freedom are lost and hence four Study parameters vanish. The displacements may be restricted to any plane. Without loss in generality, we may select one of the principal planes in Σ. Thus, we arbitrarily select the plane $Z = 0$. Since E and Σ are assumed to be initially coincident, this means

$$\begin{bmatrix} W \\ X \\ Y \\ 0 \end{bmatrix} = \mathbf{T} \begin{bmatrix} w \\ x \\ y \\ 0 \end{bmatrix}, \tag{5}$$

leaving us with the four soma coordinates

$$(x_0 : x_3 : y_1 : y_2). \tag{6}$$

The non-zero condition is now $x_0^2 + x_3^2 \neq 0$, and the fourth row and column of the reduced $\mathbf{T}$ contains only this condition as the last element with zeros elsewhere leading to the trivial equation $Z = z = 0$. We can therefore eliminate the fourth row and column and normalise the coordinates with the nonzero condition giving the planar mapping

equation

$$\mathbf{T} = \frac{1}{x_0^2+x_3^2}\begin{bmatrix} x_0^2+x_3^2 & 0 & 0 \\ 2(-x_0y_1+x_3y_2) & x_0^2-x_3^2 & -2x_0x_3 \\ -2(x_0y_2+x_3y_1) & 2x_0x_3 & x_0^2-x_3^2 \end{bmatrix}. \tag{7}$$

We can now express a point in Σ in terms of the soma coordinates and the corresponding point coordinates in E as

$$\begin{bmatrix} 1 \\ X \\ Y \end{bmatrix} = \mathbf{T}\begin{bmatrix} 1 \\ x \\ y \end{bmatrix} = \frac{1}{x_0^2+x_3^2}\begin{bmatrix} x_0^2+x_3^2 \\ 2(-x_0y_1+x_3y_2)+(x_0^2-x_3^2)x-(2x_0x_3)y \\ -2(x_0y_2+x_3y_1)+(2x_0x_3)x+(x_0^2-x_3^2)y \end{bmatrix}. \tag{8}$$

The novelty of the approach begins with creating two Cartesian vector constraint equations containing the nonhomogeneous coordinates in Equations (2) and (3), but substituting the values in Equation (8) for (X,Y). These two vector equations are $\mathbf{F}_1 = \mathbf{0}$ and $\mathbf{F}_2 = \mathbf{0}$:

$$\mathbf{F}_1 = \frac{1}{x_0^2+x_3^2}\begin{bmatrix} 2(-x_0y_1+x_3y_2)+(x_0^2-x_3^2)x-2x_0x_3y-(a\cos\psi)(x_0^2+x_3^2) \\ -2(x_0y_2+x_3y_1)+2x_0x_3x+(x_0^2-x_3^2)y-(a\sin\psi)(x_0^2+x_3^2) \end{bmatrix} = \mathbf{0};$$

$$\mathbf{F}_2 = \frac{1}{x_0^2+x_3^2}\begin{bmatrix} 2(-x_0y_1+x_3y_2)+(x_0^2-x_3^2)x-2x_0x_3y-(b\cos\varphi+d)(x_0^2+x_3^2) \\ -2(x_0y_2+x_3y_1)+2x_0x_3x+(x_0^2-x_3^2)y-(b\sin\varphi)(x_0^2+x_3^2) \end{bmatrix} = \mathbf{0}.$$

Now we determine equations for the coupler. The coordinate system that moves with the coupler has its origin, point E, on the centre of the R-pair, as in Fig. 1, having coordinates $(x,y) = (0,0)$, while point F is on the R-pair centre on the other end having coordinates $(x,y) = (c,0)$. One more vector equation, $\mathbf{H}_1$ is obtained by substituting $(x,y) = (0,0)$ in $\mathbf{F}_1$, and another, $\mathbf{H}_2$ is obtained by substituting $(x,y) = (c,0)$ in $\mathbf{F}_2$. Next $\mathbf{H}_1$ and $\mathbf{H}_2$, two rational expressions, are converted to factored normal form. This is the form where the numerator and denominator are relatively prime polynomials with integer coefficients. The denominators for both $\mathbf{H}_1$ and $\mathbf{H}_2$ are the nonzero condition $x_0^2+x_3^2$, which can safely be factored out of each equation leaving the following two vector equations with polynomial elements:

$$\mathbf{H}_1 = \begin{bmatrix} -a\cos\psi(x_0^2+x_3^2)+2(-x_0y_1+x_3y_2) \\ -a\sin\psi(x_0^2+x_3^2)-2(x_0y_1+x_3y_2) \end{bmatrix} = \mathbf{0}; \tag{9}$$

$$\mathbf{H}_2 = \begin{bmatrix} -(b\cos\varphi+d)(x_0^2+x_3^2)+c(x_0^2-x_3^2)+2(-x_0y_1+x_3y_2) \\ -b\sin\varphi(x_0^2+x_3^2)+2c(x_0x_3)-2(x_0y_2+x_3y_1) \end{bmatrix} = \mathbf{0}. \tag{10}$$

The system of four displacement constraints on the I-O equations are $\mathbf{H}_1 = \mathbf{0}$ and $\mathbf{H}_2 = \mathbf{0}$. However, these are trigonometric equations. We convert them to algebraic ones using the tangent of the half-angle substitutions

$$u = \tan\frac{\psi}{2}, \quad v = \tan\frac{\varphi}{2},$$

and

$$\cos\psi = \frac{1-u^2}{1+u^2}, \quad \sin\psi = \frac{2u}{1+u^2},$$
$$\cos\varphi = \frac{1-v^2}{1+v^2}, \quad \sin\varphi = \frac{2v}{1+v^2}.$$

The usual constraint equations in the kinematic mapping image space are obtained by considering $\mathbf{H}_1$ and $\mathbf{H}_2$ with the tangent of the half-angles, giving four new algebraic polynomials when considering the individual elements converted to factored normal form. The denominators are u^2+1 and v^2+1 which can safely be factored out because they are always non-vanishing. The resulting four algebraic equations are expressed in terms of the elements of $\mathbf{K}_1 = \mathbf{0}$ and $\mathbf{K}_2 = \mathbf{0}$:

$$\mathbf{K}_1 = \begin{bmatrix} (au^2-a)(x_0^2+x_3^2)+2u^2(-x_0y_1+x_3y_2)+2(-x_0y_2+x_3y_1) \\ -2au(x_0^2+x_3^2)-2(1+u^2)(-x_0y_2+x_3y_1) \end{bmatrix} = \mathbf{0}; \quad (11)$$

$$\mathbf{K}_2 = \begin{bmatrix} (v^2(b-d)+b-d)(x_0^2+x_3^2)+(cv^2+c)(x_0^2-x_3^2)+ \\ 2(1+v^2)(-x_0y_1+x_3y_2) \\ 2cv^2x_0x_3-2(v^2+bv+1)(x_0^2+x_3^2)+2cx_0x_3 \end{bmatrix} = \mathbf{0}. \quad (12)$$

Factoring the resultant of the first and second elements of $\mathbf{K}_1 = \mathbf{0}$ with respect to u, as well as the first and second elements of $\mathbf{K}_2 = \mathbf{0}$ with respect to v yields the two displacement constraint equations in the image space:

$$a^2(x_0^2+x_3^2)-4(y_1^2+y_2^2) = 0,$$
$$(b^2-c^2-d^2)(x_0^2+x_3^2)+2cd(x_0^2-x_3^2)+4c(x_0y_1+x_3y_2)+ 4d(-x_0y_1+x_3y_2)-4(y_1^2+y_2^2) = 0.$$

Inspection of the quadratic forms of these two equations reveals that they are two hyperboloids of one sheet, which is exactly what is expected for two *RR* dyads [6]. But these are not the constraints we are looking for. We want to eliminate the image space coordinates using $\mathbf{K}_1 = \mathbf{0}$ and $\mathbf{K}_2 = \mathbf{0}$ to obtain an algebraic polynomial with the tangent half angles u and v as variables and link lengths as coefficients.

To obtain this algebraic polynomial we start by setting the homogenising coordinate $x_0 = 1$, which can safely be done since we are only concerned with real finite displacements. Next, observe that the two equations represented by the components of $\mathbf{K}_1 = \mathbf{0}$ (Equation (11)) have a simpler form than those of $\mathbf{K}_2 = \mathbf{0}$ (Equation (12)), and are linear in y_1 and y_2. Solving these two equations for y_1 and y_2 reveals that

$$y_1 = \frac{1}{2}\frac{a(u^2-2ux_3-1)}{u^2+1}, \quad (13)$$

$$y_2 = \frac{1}{2}\frac{a(u^2x_3+2u-x_3)}{u^2+1}. \quad (14)$$

Equations (13) and (14) reveal the common denominator of u^2+1, which can never be less than 1, and hence may be factored out. Now we back-substitute these expressions for y_1 and y_2 into the array components of Equation (12), thereby eliminating these image space coordinates, and factor the resultant with respect to x_3 which yields four factors. The first three are

$$4c^2,\ \ (u^2+1)^3,\ \ (v^2+1)^3.$$

None of these three factors can ever be zero and at the same time represent a real displacement constraint, hence they are eliminated. The remaining factor is a polynomial with only u and v as variables and link lengths a, b, c, and d, as coefficients. This is exactly the constraint equation we desire. It is factored, and the terms collected then distributed over u and v revealing

$$\begin{gathered}(a-b+c+d)(a-b-c+d)u^2v^2+(a+b-c+d)(a+b+c+d)u^2+\\ (a+b-c-d)(a+b+c-d)v^2-8abuv+(a-b+c-d)(a-b-c-d)=0.\end{gathered} \tag{15}$$

Equation (15) is an algebraic polynomial of degree four which represents the I-O equation for any planar 4R mechanism. It has two singular points at infinity, namely those of the X- and Y-axes. These two singular points are either double points, or acnodes, i.e. isolated, or hermit points in the solution set of a polynomial equation in two real variables. When both are double points the mechanism is a double crank, when both are acnodes the mechanism is a double rocker. In the event the mechanism is a folding four-bar then the degree of Equation (15) is less than four.

Freudenstein's equation [4] is linear in the ratios of the link lengths and therefore is ideally suited to identifying link lengths that minimise some mechanism performance error in a least squares sense for approximate synthesis. The corresponding algebraic form of Freudenstein's equation is Equation (15), which is quadratic in the link lengths a, b, c, and d, but still lends itself to linear least squares error minimisation subject to quadratic constraints, and the method presented in [5]. However, in the following example we shall use exact synthesis, using only three of the prescribed sets on I-O pairs, and leave the approximate case to future work.

3 Example

This example serves to demonstrate that Equation (15) can be used to identify link lengths to create a 4R mechanism to generate an arbitrary function. Here, the function is specified in terms of the tangent of the half angle parameters $v=f(u)$ as

$$v=2+\tan\left(\frac{u}{u^2+1}\right). \tag{16}$$

Eight I-O pairs $[u,v]$ were specified as, using Fig. 1 for reference,

$$[0,2],\left[\frac{1}{4},\frac{30055}{13419}\right],\left[\frac{1}{2},\frac{49597}{20471}\right],\left[\frac{3}{4},\frac{48857}{19383}\right],\left[1,\frac{64699}{25409}\right],\left[\frac{5}{4},\frac{25536}{10091}\right],\left[\frac{3}{2},\frac{110471}{44235}\right],\left[2,\frac{49597}{20471}\right].$$

Since a function generator is scalable, and hence only the ratios of the link lengths are needed, we set $d = 1$ and solve for the remaining three using the first, fourth, and eighth I-O pairs, giving, in generic units of length, $a = -0.23$, $b = 1.43$, and $c = 1.20$. Another linkage was identified using the second, fourth, and seventh I-O pairs giving nearly identical link lengths. Note that it is not uncommon in computational methods to obtain negative link lengths. These lengths are directed distances, and $a = -0.23$ means that the distance is directed from the distal R-pair in link a to the origin, instead of the other way around, as in [9].

In Fig. 2 the prescribed I-O function is plotted as the dashed curve, and the I-O function generated by the two identified linkages are plotted as the solid curves. The generated function shows good fidelity relative to the prescribed function over a reasonable range of I-O angles.

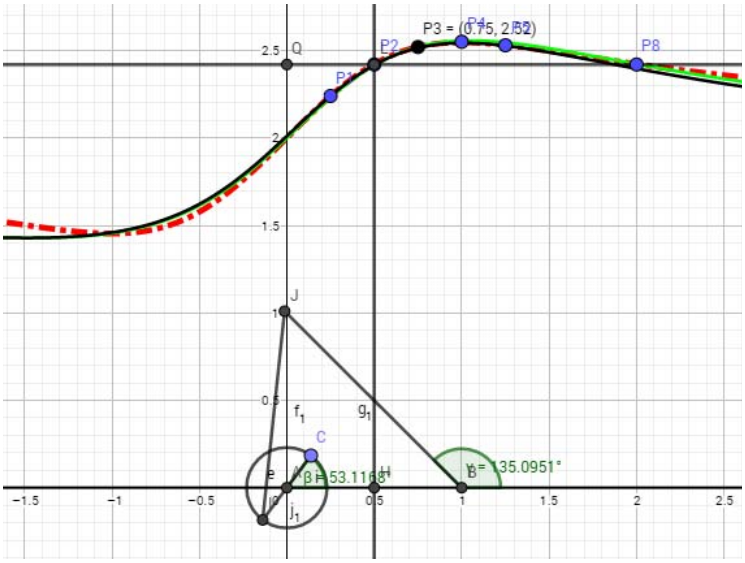

Fig. 2. Graphical representation of results.

4 Conclusions

In this paper a new method for deriving the I-O equations of planar 4R function generators was presented. The Cartesian displacement constraints of the two dyads comprising a planar 4R mechanism are expressed in terms of lengths and angles. This set of general constraint equations is mapped to a planar projection of Study's soma coordinates. The reason for using this unconventional form of planar kinematic mapping is to be able to apply these methods to spherical and spatial function generators in future work, where all eight soma coordinates will be needed. The result of this step is two arrays in terms

of the I-O angles, link lengths, and soma coordinates. The equations are converted from trigonometric expressions to algebraic ones with the tangent of the half angle substitutions. These equations are used to eliminate the soma coordinates. What remains is factored using resultants, and all non-zero factors are eliminated, ultimately leaving an algebraic polynomial that is of degree four in the tangent of the half angle parameters, and quadratic in the link lengths.

The I-O equation derived in this paper is an algebraic, however nonlinear, polynomial in terms of the link lengths. Regardless, this algebraic formulation will significantly mitigate the effect of round-off errors observed in the numerical integration of the trigonometric Freudenstein synthesis equations [5]. While the very same I-O equation is, necessarily, obtained starting from the Freudenstein equation, the point of the presented material is to generalise the derivation of function generator I-O equations. The ultimate goal is to use continuous I-O data sets to synthesise the very best linkage to generate an arbitrary planar, spherical, or spatial function. Derivation of the planar algebraic I-O equation is one of the first steps towards this goal.

References

1. Bottema, O., Roth, B.: Theoretical Kinematics. Dover Publications, Inc., New York, N.Y. (1990)
2. Freudenstein, F.: "An Analytical Approach to the Design of Fourlink Mechanisms.". Trans. ASME **vol 77**, pages 483–492 (1954)
3. Freudenstein, F.: Design of four-link mechanisms. Ph.D. thesis, Columbia University, New York, N.Y., USA (1954)
4. Freudenstein, F.: "Approximate Synthesis of Four-Bar Linkages". Trans. ASME **vol 77**, pages 853–861 (1955)
5. Guigue, A., Hayes, M.: "Continuous Approximate Synthesis of Planar Function-generators Minimising the Design Error". Mechanism and Machine Theory **vol 101**, pages 158–167, DOI: 10.1016/j.mechmachtheory.2016.03.012 (2016)
6. Hayes, M., Husty, M.: "On the Kinematic Constraint Surfaces of General Three-Legged Planar Robot Platforms". Mechanism and Machine Theory **vol 38, no 5**, pages 379–394 (2003)
7. Hayes, M.J.D., Parsa, K., Angeles, J.: "The Effect of Data-Set Cardinality on the Design and Structural Errors of Four-Bar Function-Generators". Proceedings of the Tenth World Congress on the Theory of Machines and Mechanisms, *Oulu, Finland*, pages 437-442 (1999)
8. Study, E.: Geometrie der Dynamen. Teubner Verlag, Leipzig, Germany (1903)
9. Todorov, T.: "Synthesis of Four Bar Mechanisms as Function Generators by Freudenstein-Chebyshev.". Journal of Robotics and Mechanical Engineering Research **vol 1, no 1**, pages 1–6 (2015)

An Algebraic Version of the Input-Output Equation of Planar Four-Bar Mechanisms

Manfred Husty and Martin Pfurner

University of Innsbruck, Austria
manfred.husty@uibk.ac.at, martin.pfurner@uibk.ac.at
WWW home page: http://geometrie.uibk.ac.at/

Abstract. This paper uses a formulation of the motion of the planar four-bar mechanism in the projective three-space of planar kinematic mapping and an algebraic version of the input-output relation is derived. This fourth order algebraic curve describes a new convenient form of the Freudenstein equation. Different geometric properties of the curve, independent of the design parameters, are carried out and their impact on the topology of the mechanism is shown. Furthermore the coefficients of this algebraic input-output curve are interpreted geometrically in the design parameter space which yields regions of parameter sets to the different topologies of four-bar mechanisms.

Keywords: Planar four-bar linkage, input-output equation, quartic algebraic curve, design parameter space.

1 Introduction

Planar four-bar linkages and their variants are probably the biggest kinematic success story of all time and are the practically most used planar mechanisms. Therefore it is not surprising that they are the best investigated mechanisms. Because of the simple design (Fig. 2), consisting of four bars connected via four revolute joints, they are introduced and analyzed in every basic course in kinematics. Four-bar mechanisms are used to transmit motion in many classical applications that range from moving windshield wiper blades, oil pumps to mountain bike suspensions. The analysis of these devices ranges from the discussion of coupler curves to the differential geometric properties of the whole motion (see e.g.[1]). Synthesis theory (see e.g. [9], [8], [7]) provides the designer with all the tools to design a mechanism for a specific motion or functional relation between the input and the output joint. It is well known that an exact functional relation between input and output can only be achieved for three or four positions of input and output link. In the early 1950s F. Freudenstein derived in his PhD thesis ([3]) an elegant equation that relates the input and output angle of a four-bar. This equation is widely used for function generation:

$$R_1 \cos\phi - R_2 \cos\psi + R_3 = \cos(\phi - \psi), \tag{1}$$

In Eq. (1), which is nowadays called "Freudenstein equation", R_i are functions of the dimensional parameters a, b, c and d of the mechanism (see Fig. 1), ϕ and ψ are the input and output angles.

Using complex numbers in the description of planar displacements K.H. Siecker [10] derived input-output relations of different designs of four-bars and plotted the resulting curves.

In this contribution an algebraic version of the input-output (IO) equation is presented which, to the best of the authors' knowledge, has never been derived before.

2 Input-Output Equation

Let the base of the four-bar be denoted by d, both arms a, b and the coupler c (Fig. 1, the sliders on the right side show the current values of the design variables a, b, c, d).

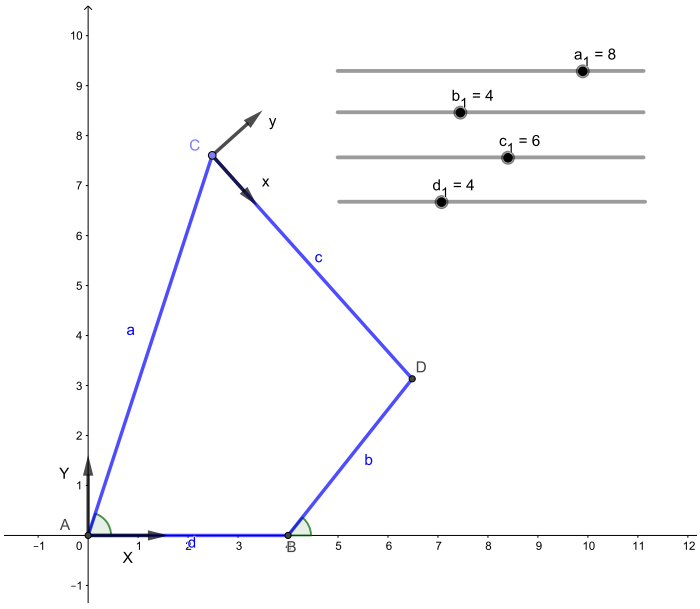

Fig. 1. Four-bar

To derive the algebraic version of the IO-equation it makes sense to use the algebraic version of the coordinate transformation matrix between the coupler system $\Sigma(C; x, y)$ and the base $\Sigma_0(A; X, Y)$:

$$\mathcal{T} = \begin{pmatrix} x_0^2 + x_3^2 & 0 & 0 \\ -2x_0y_1 + 2x_3y_2 & x_0^2 - x_3^2 & -2x_0x_3 \\ -2x_0y_2 - 2x_3y_1 & 2x_0x_3 & x_0^2 - x_3^2 \end{pmatrix} \rightarrow \begin{pmatrix} 1 \\ X \\ Y \end{pmatrix} = \mathcal{T} \begin{pmatrix} 1 \\ x \\ y \end{pmatrix}. \qquad (2)$$

Using the fact that points C and D move on circles $c_1 : X = a\cos(t), Y = a\sin(t)$, $c_2 : X = b\cos(s) + d$, $Y = b\sin(s)$ and replacing the coordinates X, Y with the coordinates of C and D in the base frame ($\mathcal{T} \cdot (1,0,0)^T$ and $\mathcal{T} \cdot (1,c,0)^T$, respectively) one can obtain the following four equations:

$$\begin{aligned} a\cos(t)(x_0^2 + x_3^2) + 2(x_0y_1 - x_3y_2) &= 0, \\ a\sin(t)(x_0^2 + x_3^2) + 2(x_0y_2 + x_3y_1) &= 0, \\ (b\cos(s) + d)(x_0^2 + x_3^2) - c(x_0^2 - x_3^2) + 2(x_0y_1 - x_3y_2) &= 0, \\ b\sin(s)(x_0^2 + x_3^2) - 2x_0x_3c + 2(x_0y_2 + x_3y_1) &= 0 \end{aligned} \tag{3}$$

Using the tangent of the half-angle substitutions (Weierstraß substitution),

$$\cos(t) = \frac{1-u^2}{1+u^2},\ \sin(t) = \frac{2u}{1+u^2},\ \cos(s) = \frac{1-v^2}{1+v^2},\ \sin(s) = \frac{2v}{1+v^2}$$

yields:

$$\begin{aligned} a(1-u^2)(x_0^2 + x_3^2) + 2(1+u^2)(x_0y_1 - x_3y_2) &= 0, \\ au(x_0^2 + x_3^2) + (1+u^2)(x_0y_2 + x_3y_1) &= 0, \\ b(1-v^2)(x_0^2 + x_3^2) + (1+v^2)((d-c)x_0^2 + (d+c)x_3^2 + 2(x_0y_1 - x_3y_2)) &= 0 \\ bv(x_0^2 + x_3^2) - c(1+v^2)x_0x_3 + (y_2x_0 + y_1x_3)(1+v^2) &= 0 \end{aligned} \tag{4}$$

Eqs. (4) describe the four-bar completely and they have a nice symmetry: if the input-output parameters u and v are eliminated, then two equations in the four homogeneous image space coordinates x_0, x_3, y_1 and y_2 remain.

$$\begin{aligned} H_1 :&(x_0^2 + x_3^2)a^2 - 4y_1^2 - 4y_2^2 = 0 \\ H_2 :&(b^2 - c^2 + 2cd - d^2)x_0^2 + 4(cy_1 - dy_1)x_0 + (b^2 - c^2 - 2cd - d^2)x_3^2 + \\ &4(cy_2 + dy_2)x_3 - 4y_1^2 - 4y_2^2 = 0 \end{aligned}$$

They determine the coupler motion in the three dimensional image space $\mathbb{P}^3$. Geometrically these equations describe two hyperboloids. The intersection curve of both hyperboloids represents the kinematic image of the four-bar motion. This interpretation is reported e.g. in Bottema-Roth [1] and it was successfully used in the analysis of planar parallel manipulators (see e.g. [5]).

If, on the other hand, the image space coordinates x_i, y_j are eliminated from Eqs. (4) then a single equation remains which describes the IO-relation of the four-bar. Using the normalizing condition $x_0 = 1$ yields:

$$k : Au^2v^2 + Bu^2 - 8\,abuv + Cv^2 + D = 0, \qquad \text{where} \tag{5}$$

$$\begin{aligned} A &= (a-b+c+d)\,(a-b-c+d)\,, \quad B = (a+b-c+d)\,(a+b+c+d) \\ C &= (a+b-c-d)\,(a+b+c-d)\,, \quad D = (a-b+c-d)\,(a-b-c-d) \end{aligned}$$

It is of interest to note that all eight $\pm$ combinations of b, c, d, while a remaining positive, appear as binary products in these coefficients. By using the normalizing

condition $x_0 = 1$ π-turns of the coupler frame with respect to the base frame are excluded. This case is treated by using $x_0 = 0$ as a normalizing condition in a second computation, but here only complex or discrete solutions are obtained, which are of no interest at this point. Some elementary properties of the *IO*-equation (5), which are independent of the design parameters of the four-bar are:

1. k is a quartic curve,
2. k has two double points, the points at infinity of the u and v axes of the parameter plane,
3. k is of class 8 and has 12 inflection points and 8 double tangents,
4. k has genus 1, is therefore an elliptic curve.

These properties will be proven in the following paragraphs. Item one of this list is obvious from Eq. (5). The second item can be shown as follows: at first Eq. (5) is homogenized with homogenizing coordinate w.

$$\begin{aligned} k_h : {} & (-d+a+c-b)(-d+a-c-b)w^4 + (d+a-c+b)(d+a+c+b)u^2w^2 - \\ & 8abuvw^2 + (-d+a-c+b)(-d+a+c+b)v^2w^2 + \\ & (d+a+c-b)(d+a-c-b)u^2v^2 = 0 \end{aligned} \tag{6}$$

Differentiation with respect to the three variables u, v, w yields:

$$\begin{aligned} \frac{\partial k_h}{\partial u} = {} & 2(d+a-c+b)(d+a+c+b)uw^2 - \\ & 8abw^2v + 2(d+a+c-b)(d+a-c-b)uv^2 = 0 \end{aligned} \tag{7}$$

$$\begin{aligned} \frac{\partial k_h}{\partial v} = {} & -8abuw^2 + 2(-d+a-c+b)(-d+a+c+b)vw^2 + \\ & 2(d+a+c-b)(d+a-c-b)u^2v = 0 \end{aligned} \tag{8}$$

$$\begin{aligned} \frac{\partial k_h}{\partial w} = {} & 4(-d+a+c-b)(-d+a-c-b)w^3 + \\ & 2(d+a-c+b)(d+a+c+b)u^2w - \\ & 16abuvw + 2(-d+a-c+b)(-d+a+c+b)v^2w = 0 \end{aligned} \tag{9}$$

A simple computation shows that the four Eqns. (6), (7), (8) and (9) in the three unknowns u, v, w have two common solutions which are independent of the design parameters a, b, c, d:

$$D_1 := \{w = 0, u = 1, v = 0\}, \qquad D_2 := \{w = 0, u = 0, v = 1\} \tag{10}$$

The corresponding points are the points at infinity of the u- and v-axis. Both points can have real or complex tangents depending on the values of the design parameters. Possible combinations of these cases have different meanings for the corresponding mechanisms which will be discussed separately.

The third item of the properties list follows directly from the Plücker formula which links the class ν, the degree n, the number of double points d and the number of cusps r:

$$\nu = n(n-1) - 2d - 3r, \tag{11}$$

As the degree of the IO equation is four, the number of double points is two and the number of cusps is zero, the class is eight. The genus one of the curve, independent of the design parameters, also follows from classical formulas and can be found already in the textbook of Fladt [2].

From these properties and a theorem on algebraic curves proven by A. Harnack in [4], which relates the branches of an algebraic curve to its genus, one can immediately conclude that a four-bar can never have more than two assembly modes. Harnack proofs that an algebraic curve of genus p can have at most $p+1$ branches. The input-output equation k is a quartic curve of genus 1, therefore, following Harnack, it can have at most two branches. Each branch corresponds to one assembly mode. This concludes the proof of the above mentionend properties.

The coefficients A, B, C, D in Eq. (5) are closely related to the well known Grashof conditions and determine the topology of the four-bar. The reality of the tangents of the double points D_1 and D_2 decides the topology of the mechanism. There are three possibilities:

1. The tangents of both double points are real, that means that both arms can completely turn around; the mechanism is a double crank (Fig. 2).

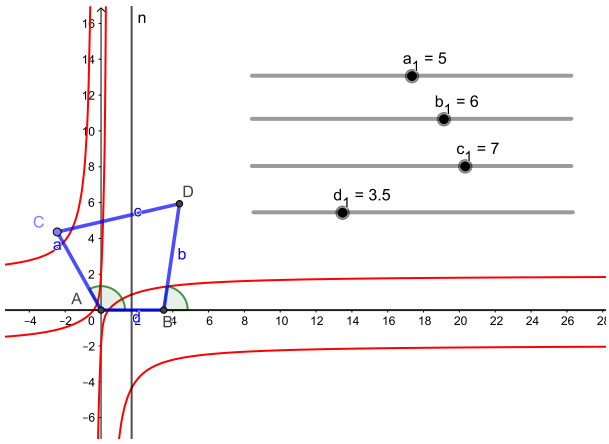

Fig. 2. Four-bars and IO-curves: double crank, two assembly modes

2. One pair of double point tangents is real and the other is complex conjugate (the double point is an acknode or hermit point). The mechanism is a crank-rocker. Which arm makes the rocker depends on the double point which is the acknode (Fig. 3). In the figure one can also see that the curve consists of two different branches and this means that the mechanism has two assembly modes. An easy computation yields the maximum and minimum of the rocker angle in both assemblies. The corresponding points on the IO curve are shown in Fig. 3 as M, U on one branch and N, V on the other branch. The

interval between the the maximum and the minimum of the v-values (distance of the horizontal tangents) yields the swing angle of the rocker.

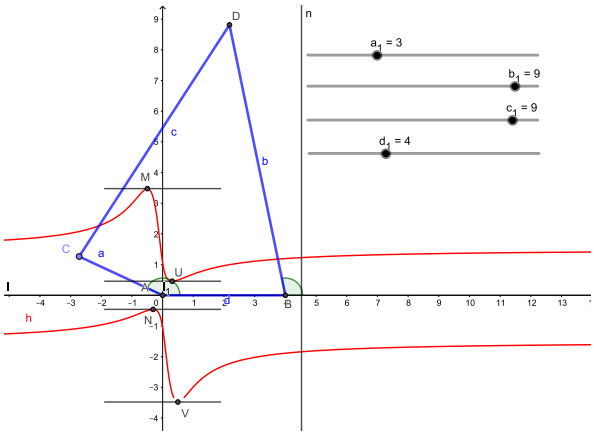

Fig. 3. Four-bars and IO-curves: crank-rocker, two assembly modes

3. Both pairs of double point tangents are complex (both double points are acknodes): The mechanism is a double rocker. The IO curve is finitely closed (Fig. 4). The enclosing rectangle with sides parallel to the u- and v- axes determines the maximum and minimum rocker angles. The dashed curves in Fig. 4 are the curves given by the partial derivatives.

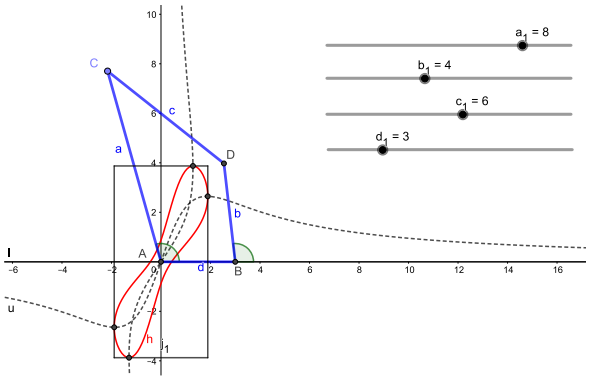

Fig. 4. Four-bars and IO-curves: double rocker,

2.1 Special Cases

Several special cases can occur in a four-bar mechanism. All of them also show up in special IO curves. In the following some of these designs are discussed and linked to special types of the IO curves.

Degree reduction of the IO curve: The degree of the IO curve drops when the coefficient $A = (d + a + c - b)\,(d + a - c - b)$ of x^2y^2 in Eq. (6) vanishes. There are several possibilities:

1. $(d + a - c - b) = 0$, then k_h reduces to

   $$w^2(a^2w^2+a^2v^2-2abw^2-2abuv-acw^2-acv^2+b^2w^2+b^2u^2+bcw^2+bcv^2) = 0.$$

   k_h splits into a hyperbola and the line at infinity. The mechanism is a folding four-bar (Fig. 5).

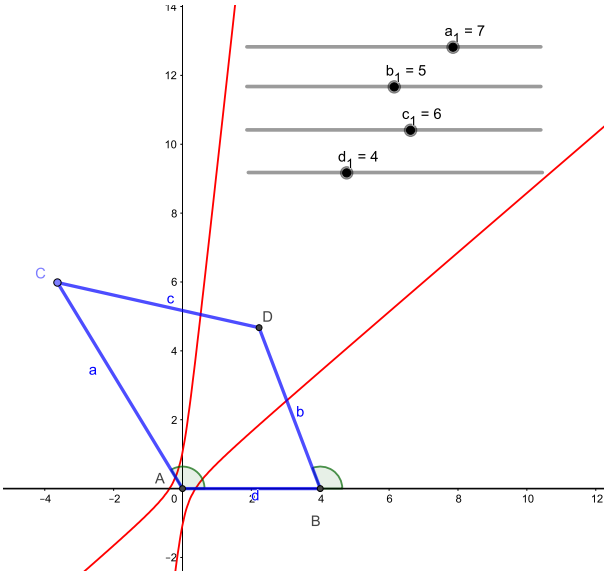

Fig. 5. Folding four-bar $a + d = b + c$.

2. $(d + a + c - b) = 0$. then k_h reduces to

   $$w^2(a^2w^2+a^2v^2-2abw^2-2abuv+acw^2+acv^2+b^2w^2+b^2u^2-bcw^2-bcu^2) = 0.$$

   This case has only one folding assembly, but generates no mechanism, because the hyperbola is complex.

3. Further degree reduction occurs when $a = b$ and $c = d$. This yields the parallel-bar mechanism. Then k_h reduces to three linear terms:

$$w^2(-y + x)(bu - bv + du + dv) = 0 \tag{12}$$

The first term in Eq. (12) corresponds to the line at infinity. The second term is the IO equation for the parallel bar, which is obviously a 1:1 transmission and the third term is the constant ratio transmission equation for the anti-parallelogram mechanism.

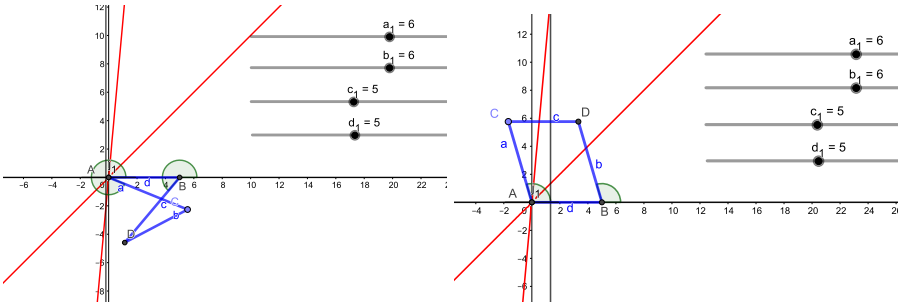

Fig. 6. Parallel-bar mechanism, both assembly modes

Folding four-bar mechanisms: Folding of the four-bar can only occur when the input angle is either 0° or 180°. The design conditions for folding are that the sum of two sides is equal to the sum of the other two. Hence three possibilities exist: 1. $a + b = c + d$, 2. $a + c = b + d$ and 3. a+d=b+c. The last case had been treated already in the last paragraph. The two other cases remain.

1. $a + b = c + d$. Substitution into Eq. (6) yields:

$$a(a - c)u^2v^2 + w^2(a + b)(a - c + b)u^2 - 2abuvw^2 + bw^4(b - c) = 0$$

Fig. 7 shows the general situation on the left. The folding happens at $u = 0$ and $v = \infty$. When additionally $c = b$ holds, then k_h splits into the line $u = 0$ and a cubic curve.

$$u(aw^2u + auv^2 + bw^2ux - 2bw^2v - buv^2) = 0$$

The line $u = 0$ belongs to a full rotation capability of the mechanism about the point B in the folded position. The corresponding mechanism is a kite four-bar (Fig. 7 right).

2. $a + c = b + d$ Substitution into Eq. (6) yields:

$$a(a + c)u^2w^2 - 2abuvw^2 + (b - c)v^2w^2 + (a + c - b)(a - b)u^2v^2 = 0$$

The coefficient of w^4 vanishes and the folding happens at $u = v = 0$ (Fig. 8).

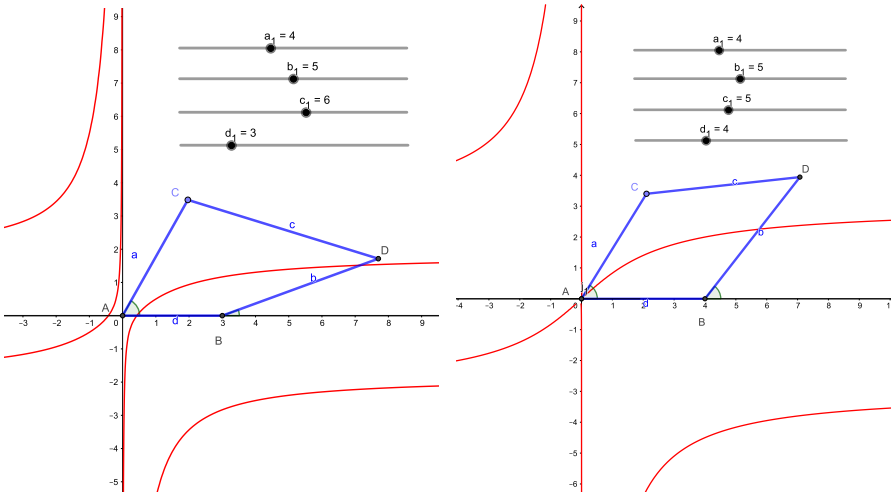

Fig. 7. Left: Folding four-bar mechanism $a + b = c + d$ right: Kite-mechanism

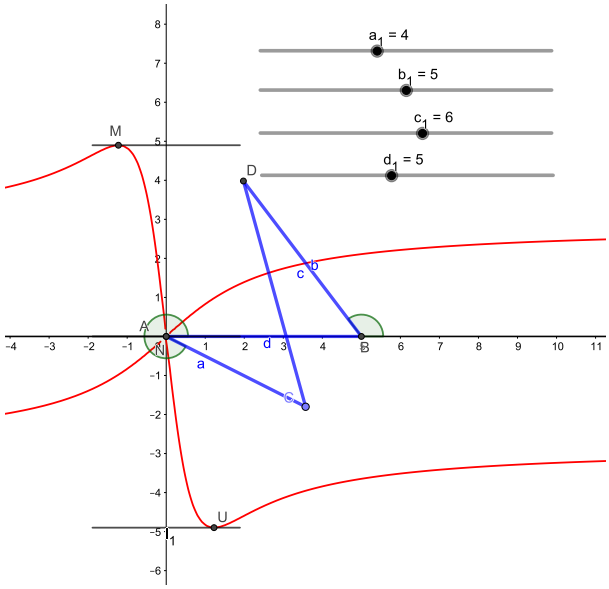

Fig. 8. Folding four-bar mechanism $a + c = b + d$

3 Design Parameter Space

The nice structure of the coefficients A, B, C, D gives reason for an interpretation in a three dimensional projective space. As d can never become zero it is chosen as homogenizing coordinate and set to $d = 1$. It turns out that the eight linear factors in Eq. (5) can be interpreted as eight planes determined by the faces of a

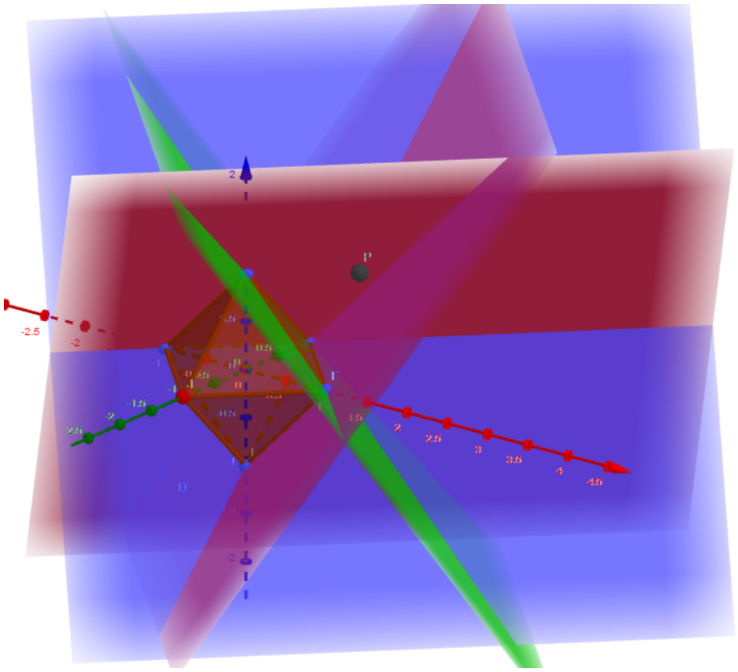

Fig. 9. Geometric interpretation of the linear factors of Eq. (5).

regular octahedron with vertices $V_1 = (1,0,0), V_2 = (-1,0,0), V_3 = (0,1,0), V_4 = (0,-1,0), V_5 = (0,0,1), V_6 = (0,0,-1)$. The eight planes cluster the design space into several different sectors that give answers to the question if the double points are knots or hermits. The reality of the double point tangents yield necessary conditions for the decision if an arm of the four-bar is a crank or a rocker. Fig. 9 shows four out of the eight planes and a point P in a sector bounded by three planes. It can be shown that this region corresponds to the case of the crank-rocker mechanism.

More important is the fact that the IO-equation can easily be used for approximate function generation (see [6]).

4 Conclusions

In the paper an algebraic version of the input-output equation of planar four-bar mechanisms was derived. It turned out that the curve is in general of degree four and several algebraic and differential geometric properties of this curve were derived and linked to the topology of the corresponding mechanisms. It was shown that special topologies of the mechanism correspond to special designs of the IO curve. In the special cases this curve has either a finite double point or the degree drops. It is believed that this work can be a starting point for a new type of IO synthesis for four-bar mechanisms.

References

1. O. Bottema and B. Roth. *Theoretical Kinematics*. North-Holland Publishing Company, 1979.
2. K. Fladt. *Analytische Geometrie ebener Kurven*. Akademische Verlagsgesellschaft, 1962.
3. F. Freudenstein. *Design of Four-Link Mechanisms*. Ph. D. thesis, Columbia University, New York, 1954.
4. A. Harnack. Über die Vielteiligkeit der ebenen algebraischen Curven. *Mathematische Annalen*, 10:189–198, 1876.
5. M.J.D. Hayes. *Kinematics of General Planar Stewart-Gough Platforms,*. PhD thesis, McGill University, Montreal, Que., Canada, 1999.
6. M.J.D. Hayes, M. Husty, and M. Pfurner. Input-output equation for planar four-bar linkages. In Lenarčič and Parenti-Castelli, editors, *Advances in Robot Kinematics*. Springer, 2018. ARK 2018, accepted for presentation and publication.
7. H. Kerle, B. Corves, and M. Hüsing. *Getriebetechnik*. Springer Vieweg, 2015.
8. K. Luck and K.-H. Modler. *Getriebetechnik*. Springer, 1995.
9. J.M. McCarthy. *Geometric Design of Linkages*, volume 11 of *Interdiciplnary Applied Mathematics*. Springer, 2000.
10. K.-H. Siecker. Neue Erkenntnisse in der Maßanalyse ebener Koppelgetriebe durch Verwendung der algebraischen Methode. *VDI-Berichte*, 12:157–163, 1956.

AN ALGEBRAIC INPUT-OUTPUT EQUATION FOR PLANAR RRRP AND PRRP LINKAGES

Mirja Rotzoll[1], M. John D. Hayes[1], Manfred L. Husty[2]

[1] Department of Mechanical and Aerospace Engineering,
Carleton University,
Ottawa, ON K1S 5B6, Canada

[2] Unit Geometry and CAD,
University of Innsbruck,
6020 Innsbruck, Austria

Corresponding Author:
Professor M. John D. Hayes
Department of Mechanical and Aerospace Engineering,
Carleton University,
1125 Colonel By Dr.,
Ottawa, ON K1S 5B6, Canada

Tel: 613-520-2600 Ext. 5661

email: john.hayes@carleton.ca

Abstract

In this paper the algebraic input-output (IO) equations for planar RRRP and PRRP linkages are derived by mapping the linkage displacement constraints into Study's soma coordinates and then using tangent-half angle substitutions to transform the trigonometric into algebraic expressions. Both equations are found to be equivalent to the one that has already been derived for RRRR linkages, giving exciting new insight into kinematic analysis and synthesis of planar four-bar linkages. The algebraic properties of the IO curve equations yield information regarding the topology of the linkage, such as the sliding position limits of the prismatic joints and/or the angle limits of the rotational joints. Additionally, the utility of the equations is successfully demonstrated with two approximate synthesis examples.

Keywords: function generator; four-bar linkages; Study soma coordinates.

1 Introduction

In 1954 F. Freudenstein developed an elegant trigonometric equation for planar four-bar linkages connected by four rotational (R) joints (Freudenstein, 1954). The equation, nowadays known as the *Freudenstein equation*, is widely used in function-generator analysis and synthesis theory. It gives designers a tool to identify the link lengths of mechanisms that optimally transform, typically in a least-squares sense, a specific input angle into a desired output angle governed by a specified functional relation, $f(\psi) = \varphi$. Let d be the distance between the centres of the R-joints connected to the relatively non-moving base; a the driver or input link length which is moving with an angle ψ; b the follower or output link length which is moving with an angle φ; and c the coupler length of a planar RRRR linkage, see Fig. 1. Then, the displacement of the mechanism in terms of the link lengths a, b, c, d, the input angle ψ, and the output angle φ is governed by the following input-output (IO) equation

$$k_1 + k_2 \cos(\varphi_i) - k_3 \cos(\psi_i) \quad = \quad \cos(\psi_i - \varphi_i). \tag{1}$$

Eq. (1) is linear in the k_i Freudenstein parameters, which are defined in terms of the link length ratios as:

$$k_1 \equiv \frac{(a^2 + b^2 + d^2 - c^2)}{2ab}; \quad k_2 \equiv \frac{d}{a}; \quad k_3 \equiv \frac{d}{b}.$$

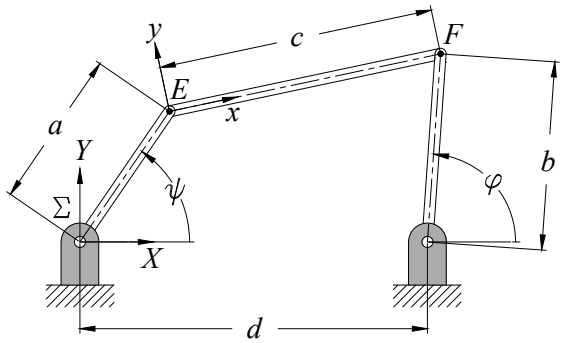

Figure 1: Planar 4R function generator.

In (Hayes et al., 2018) the authors Hayes, Husty, and Pfurner provided an alternative derivation of a general algebraic IO equation for the same type of mechanism:

$$Au^2v^2 + Bu^2 + Cv^2 - 8abuv + D = 0 \tag{2}$$

where

$$\begin{aligned} A &= (a-b-c+d)(a-b+c+d) = A_1A_2; \\ B &= (a+b-c+d)(a+b+c+d) = B_1B_2; \\ C &= (a+b-c-d)(a+b+c-d) = C_1C_2; \\ D &= (a-b+c-d)(a-b-c-d) = D_1D_2; \\ u &= \tan\frac{\psi}{2}; \\ v &= \tan\frac{\varphi}{2}. \end{aligned}$$

Eq. (2) is an algebraic quartic equation in terms of input and output joint angle parameters u and v. It was obtained by mapping the linkage constraint equations of the input and output links, *i.e.*, circular motion for the distal R-joints, into Study's soma coordinates (Study, 1903; Bottema and Roth, 1990), converting the trigonometric expressions into algebraic ones by applying the tangent of the half-angle, or Weierstraß, substitutions (Bradley and Smith, 1995), and finally eliminating the Study coordinates to obtain the quartic IO curve (Hayes et al., 2018; Husty and Pfurner, 2018). The soma coordinates are used to represent distinct spatial rigid body displacements in three dimensional Euclidean space as distinct points in a higher dimensional projective space. Eight projective soma coordinates result from mapping a displacement to the seven dimensional projective kinematic mapping image space. A displacement can be represented in Euclidean space as a change in position and orientation of a moving coordinate system expressed with respect to a non-moving one. The first four soma coordinates are typically established as the four Euler rotation parameters (Bottema and Roth, 1990; Husty et al., 1997) to quantify the new orientation, while the remaining four represent the translation component of the displacement and are obtained as distinct linear combinations of the Cartesian coordinates of the new location of the origin of the moving coordinate system and the Euler parameters. For planar displacements two of the Euler parameters and two of the translation parameters are identically zero.

We believe that this new method for determining the IO equation can be further expanded to four-bar mechanisms of any topology for planar, spherical, and spatial mechanisms. Ultimately, this would provide designers with a versatile tool for optimal synthesis of function generating mechanisms. While others have examined the possibilities of a unified approach to four-bar mechanism analysis and synthesis, see (Bai and Angeles, 2008) for example, proposed methods failed to identify a single algebraic and constraint-based IO equation that is truly generalised to four-bars containing two, one, or no prismatic (P) joints. Planar four-bar mechanisms containing more than two P-joints result in linear IO relations and can only generate translations. Hence, they are not considered herein.

In this paper we will derive the algebraic IO equations for RRRP, and PRRP linkages using the same technique developed in (Hayes et al., 2018). The main goal is to demonstrate that the method of deriving the algebraic forms of the IO equations using Study's soma and elimination theory (Salmon, 1885; Cox et al., 1997) lead to precisely the same equation, namely Eq. (2), with only the roles of constant and variable changing for certain design

parameters. We will then interpret some important characteristics of the resulting algebraic IO curves in the coordinate plane of the input and output variables employing the theory of planar algebraic curves (Husty et al., 1997; Salmon, 1879a,b; Primrose, 1955; Hilton, 1920; Harnack, 1876). Finally, we will illustrate these characteristics with two function generator approximate synthesis examples using the algebraic form of the associated IO equation.

2 Algebraic IO Equation for RRRP Function Generators

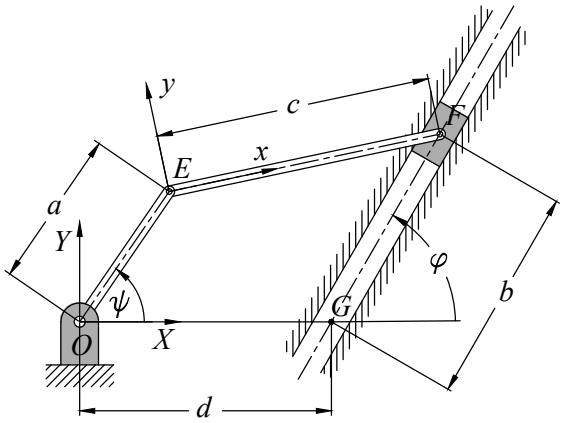

Figure 2: Planar RRRP function generator.

The planar RRRP linkage, also called a crank-slider, is a widely used mechanism found in a variety of applications, such as piston-cylinder engines or reciprocating pumps (Wunderlich, 1970; Uicker et al., 2017). This linkage transforms a rotational input motion into a reciprocating translational output motion. A schematic of the linkage type is shown in Fig. 2. In the first step, as in the derivation of Eq. (2), the displacement constraints of the driver and follower have to be defined (Hayes et al., 2018; Husty and Pfurner, 2018). For that purpose, let Σ_1 be a fixed Cartesian coordinate system whose origin is at the centre of the ground-fixed driver R-joint, E the intersection point of the driver and coupler link centre lines, and F the intersection point of the coupler and the follower link centre lines. While point E is moving on a circle with a radius of length a around the origin O of Σ_1, F is moving on a line which intersects the baseline at point G making a fixed angle φ at a distance d from the origin of Σ_1. Hence, the positions of E and F can be described as points in Σ_1 by the following array element constraint equations

$$\begin{array}{rcl} X_E - a\cos\psi & = & 0, \\ Y_E - a\sin\psi & = & 0, \end{array} \tag{3}$$

$$\begin{array}{rcl} X_F - d - b\cos\varphi & = & 0, \\ Y_F - b\sin\varphi & = & 0. \end{array} \tag{4}$$

Note that these constraint equations are identical to those formulated for the 4R linkage in (Hayes et al., 2018), but where the roles of b and φ are reversed: b here is a variable distance and φ is a fixed angle. This allows us to proceed in determining the IO equation in the same manner. Let Σ_2 be a coordinate frame, which moves with the coupler, whose origin is centred at E with x-axis pointing towards F. Then the homogeneous transformation matrix, expressed in soma coordinates $(x_0 : x_3 : y_1 : y_2)$, between the two coordinate frames is given by (Hayes et al., 2018)

$$\mathbf{T} = \frac{1}{x_0^2 + x_3^2} \begin{bmatrix} x_0^2 + x_3^2 & 0 & 0 \\ 2(-x_0 y_1 + x_3 y_2) & x_0^2 - x_3^2 & -2x_0 x_3 \\ -2(x_0 y_2 + x_3 y_1) & 2x_0 x_3 & x_0^2 - x_3^2 \end{bmatrix}. \tag{5}$$

For example, a point (x, y) in Σ_2 can be expressed as a point (X, Y) in Σ_1 using the coordinate transformation

$$\begin{bmatrix} 1 \\ X \\ Y \end{bmatrix} = \mathbf{T} \begin{bmatrix} 1 \\ x \\ y \end{bmatrix} \tag{6}$$

Now, in the coordinate frame Σ_2 the two end points of the coupler E and F have coordinates $(x, y) = (0, 0)$ and $(c, 0)$, respectively. These are transformed using Eq. (6) to their representations in Σ_1, and the results are equated to the coordinates for points E and F in Eqs. (3) and (4), which, when simplified, reveal the following four array element position constraint equations in terms of the link lengths, input and output angles ψ and φ, as well as the four soma coordinates x_0, x_3, y_1, and y_2:

$$\left.\begin{aligned} -a\cos\psi(x_0^2 + x_3^2) + 2(-x_0 y_1 + x_3 y_2) &= 0; \\ -a\sin\psi(x_0^2 + x_3^2) - 2(x_0 y_1 + x_3 y_2) &= 0; \\ -(b\cos\varphi + d)(x_0^2 + x_3^2) + c(x_0^2 - x_3^2) + 2(-x_0 y_1 + x_3 y_2) &= 0; \\ -b\sin\varphi(x_0^2 + x_3^2) + 2c(x_0 x_3) - 2(x_0 y_2 + x_3 y_1) &= 0. \end{aligned}\right\} \tag{7}$$

The tangent of the half angle substitutions

$$u = \tan\frac{\psi}{2}, \quad v = \tan\frac{\varphi}{2}, \tag{8}$$

$$\cos\psi = \frac{1 - u^2}{1 + u^2}, \quad \sin\psi = \frac{2u}{1 + u^2}, \tag{9}$$

$$\cos\varphi = \frac{1 - v^2}{1 + v^2}, \quad \sin\varphi = \frac{2v}{1 + v^2}, \tag{10}$$

are used to transform the trigonometric constraint-based relations in Eq. (7) to algebraic equations. After eliminating the image space coordinates x_i and y_i using resultants and

elimination theory, then collecting the results for the variables u and b, the following algebraic IO equation emerges

$$k := \; Au^2b^2 + Bb^2 + Cu^2b - 8abuv + Db + Eu^2 + F \; = \; 0, \tag{11}$$

where

$$\begin{aligned} A &= v^2 + 1, \\ B &= v^2 + 1, \\ C &= -2\,(v-1)\,(v+1)\,(a+d)\,, \\ D &= 2\,(v-1)\,(v+1)\,(a-d)\,, \\ E &= \left(v^2+1\right)(a+c+d)\,(a-c+d)\,, \\ F &= \left(v^2+1\right)(a+c-d)\,(a-c-d)\,. \end{aligned}$$

By rearranging Eq. (11) it can easily be shown that it is identical to Eq. (2) when the terms multiplying u and v are collected and factored instead of u and b. The difference from a designers' perspective is only that the variables of the 4R linkage are the IO angle parameters u and v, while those for the RRRP linkage are the input angle parameter u and output slider distance b.

2.1 Interpretation of the RRRP IO Equation

Analysing Eq. (11) using the theory of planar algebraic curves (Husty et al., 1997; Primrose, 1955) one can see that it has the following characteristics which are independent of the constant design parameter lengths a, c, d, and constant angle parameter v.

1. Eq. (11) is of degree $n = 4$ in variables u and b.
2. It contains two double points, $DP = 2$, each located at the intersections with the line at infinity of the u- and b-axis in the u-b variable design parameter plane.
3. It has genus $p = 1$, hence, it is an elliptic curve and the maximum number of assembly modes of the linkage becomes $m = p + 1 = 2$ (Husty and Pfurner, 2018; Harnack, 1876).

These three characteristics are now proved to be true for all non-degenerate planar RRRP linkages. The first item is obvious by inspection. The proof of the second item requires that Eq. (11) be homogenised. If we use the arbitrary homogenising coordinate w we obtain

$$k_h := \; Au^2b^2 + Bb^2w^2 + Cu^2bw - 8avubw^2 + Dbw^3 + Eu^2w^2 + Fw^4 \; = \; 0, \tag{12}$$

which now contains seven terms all homogeneously of degree 4 in terms of u, b, and w. The three partial derivatives of k_h with respect to the three variable coordinates u, b, and w are

all homogeneously of degree 3:

$$\left.\begin{array}{rcl} \dfrac{\partial k_h}{\partial u} &=& 2Aub^2 + 2Cubw - 8avbw^2 + 2Euw^2 \quad = \quad 0; \\ \dfrac{\partial k_h}{\partial b} &=& 2Au^2b + 2Bbw^2 + Cu^2w - 8avuw^2 + Dw^3 \quad = \quad 0; \\ \dfrac{\partial k_h}{\partial w} &=& 2Bb^2w + Cu^2b - 16avubw + 3Dbw^2 + 2Eu^2w + 4Fw^3 \quad = \quad 0. \end{array}\right\} \tag{13}$$

Equations (12) and (13) have two common solutions which are independent of the link lengths a, c, and d, as well as angle parameter v, which are embedded in the coefficients A, B, C, D, E, and F:

$$S_1 := \{u = 1, b = 0, w = 0\}, \quad S_2 := \{u = 0, b = 1, w = 0\}. \tag{14}$$

These two points, called *double points*, common to all algebraic IO curves for every planar RRRP four-bar mechanism are the points on the line at infinity $w = 0$ of the u- and b-axes, respectively. Each of these double points can have real or complex tangents depending on the values of the three constant link lengths a, c, and d, which in turn determines the nature of the mobility of the linkage. Since these two double points are uniquely defined relative to the regular points on the curve, they are also known as *singular points* (Primrose, 1955; Hilton, 1920).

The discriminant of Eq. (12), evaluated at a double point, reveals whether that double point has a pair of real or complex conjugate tangents (Husty et al., 1997; Hilton, 1920) in turn yielding information about the topology of the mechanism (Husty and Pfurner, 2018; Hilton, 1920). If the tangents are complex conjugates the double point is an acnode: a *hermit* point that satisfies the equation of the curve but is isolated from all other points on the curve. If this is the case then the slider travel, represented by b, is restricted. The discriminant and the meaning of its value are (Husty et al., 1997; Hilton, 1920)

$$\Delta \;=\; \left(\frac{\partial^2 k_h}{\partial u \partial w}\right)^2 - \frac{\partial^2 k_h}{\partial u^2}\frac{\partial^2 k_h}{\partial w^2} \quad \left\{\begin{array}{rcl} > \;0 & \Rightarrow & \text{two real distinct tangents (crunode),} \\ = \;0 & \Rightarrow & \text{two real coincident tangents (cusp),} \\ < \;0 & \Rightarrow & \text{two complex conjugate tangents (acnode).} \end{array}\right.$$

For the homogeneous IO equation of an RRRP linkage, Eq. (12), the discriminant of the point at infinity $(u : b : w) = (0 : 1 : 0)$ on the b-axis is

$$\Delta = -4(v^2 + 1)^2, \tag{15}$$

meaning that the double point associated with the output slider is always an acnode independently of the link lengths and orientation of the slider. It should not surprise that the discriminant of Eq. (12) is always negative, since the slider must always have finite translation limits.

To determine whether the rotational input link is a crank or a rocker, it is sufficient to determine if the numerical value of the coefficient E in Eq. (11) is less than zero when the

coordinates in Σ_1 are transformed by the rotation about O_{Σ_1} required to make $v = 1$, *i.e.*, $\varphi = \pi/2$. Since the two factors $(v^2 + 1)$ and $(a + c + d)$ in E must always be greater than zero, it is a simple matter to show that the condition for input link a to be a crank reduces to

$$a - c + d \;<\; 0. \tag{16}$$

The proof for the third item comes from the definition of genus, which in this case is the difference between the maximum number of double points for a curve of degree 4 and the actual number of double points it possesses. The maximum number of double points, DP_{max} for an arbitrary algebraic curve of degree n is given by (Hunt, 1978)

$$DP_{max} \;=\; \frac{1}{2}(n-1)(n-2).$$

The maximum number of double points for a curve of degree 4 is 3. We see that because the algebraic IO curve has only 2 double points, it is deficient by 1, hence its genus is $p = 1$. Because of this, it cannot be parameterised, and it is defined to be an *elliptic* curve (Primrose, 1955). This definition does not mean that the curve has the form of an ellipse, rather that the curve can be expressed, with a suitable change of variables, as an elliptic curve. In the plane, every elliptic curve with real coefficients can be put in the standard form

$$x_2^2 \;=\; x_1^3 + Ax_1 + B$$

for some real constants A and B. We now consider some illustrative RRRP examples.

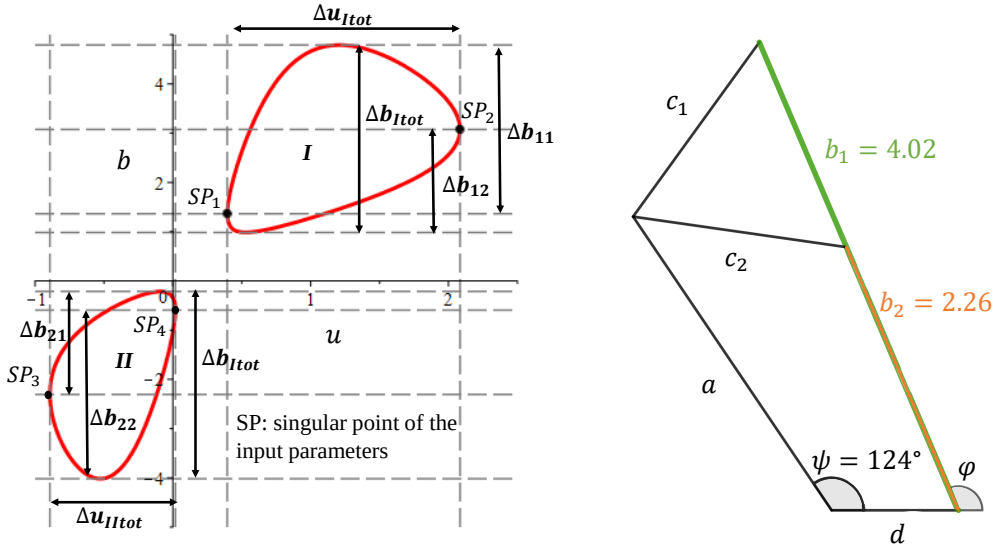

Figure 3: RRRP where $a = 2.8$, $c = 1.7$, $d = 1$, $v = 1.5$.

Example 1. Design parameter selection: $a = 2.8$; $c = 1.7$; $d = 1$; $v = 1.5$.

With the chosen design parameters, the input link a is a rocker because Eq. (16) is > 0 for some $-\pi \leq \psi \leq \pi$. Two different assembly modes I and II can be identified examining Fig. 3. Each assembly mode has two locations where the mechanism is positioned at an input singular configuration where the tangents of the IO equation are vertical, separating each assembly mode into two working modes. If the link is assembled according to the upper right part of the curve (assembly mode I), Δu_{Itot} and Δb_{Itot} correspond to the maximum swing angle and maximum sliding position, respectively. Considering each working mode separately, Δb_{11} and Δb_{12} correspond to the maximum sliding position in assembly mode I. Similarly, if the link is assembled according to the lower left part of the curve (assembly mode II), Δu_{IItot} and Δb_{IItot} correspond to the maximum swing angle and maximum sliding position. The maximum sliding positions for each working mode are Δb_{21} and Δb_{22}.

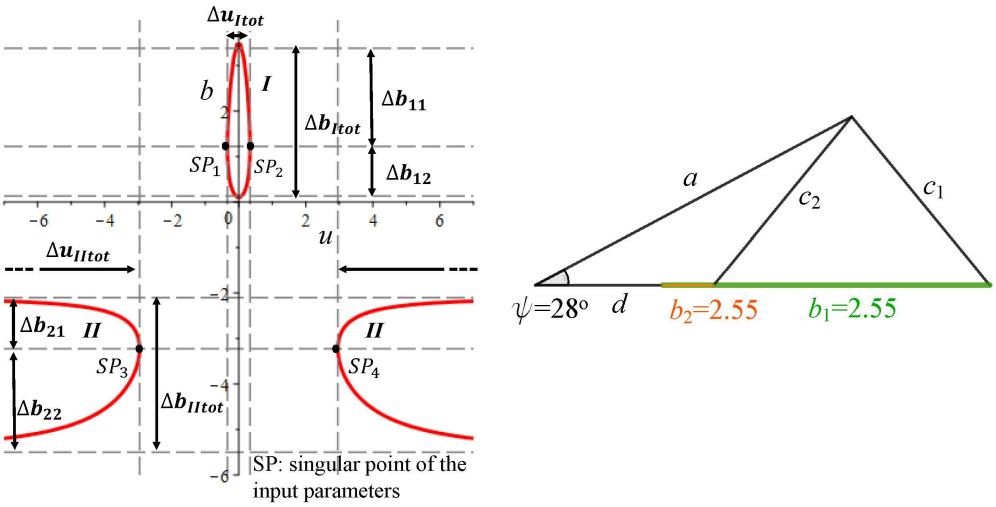

Figure 4: RRRP where $a = 2.8$, $c = 1.7$, $d = 1$, $v = 0$.

Example 2. Design parameter selection: $a = 2.8$; $c = 1.7$; $d = 1$; $v = 0$.

Taking the same design parameters, but changing the orientation of the slider to $v = 0$ reveals a representation of the IO equation as shown in Fig. 4. Again, examining Eq. (16) shows that the expression is not < 0 for every $-\pi \leq \psi \leq \pi$, hence, the input link is a rocker. The linkage is once again split into two assembly modes, I and II. Due to the chosen parametrisation according to Eq. (8) and as $\psi = \pi$ is included in assembly mode I, the graph contains the point at $u = \pm\infty$, explaining the asymptotes of the IO equation. The maximum swing angle as well as the maximum sliding position can be evaluated analogous to the previous example.

Example 3. Design parameter selection: $a = 2$; $c = 2.5$; $d = 1$; $v = 0.2$.

These design parameters yield an IO equation illustrated in Fig. 5. In contrast to the previous examples, Eq. (16) is < 0 meaning that the input link a can fully rotate. This linkage also possesses two assembly modes I and II, resulting in identical maximum sliding position, $\Delta b_{Itot} = \Delta b_{IItot}$. In this example, points where the mechanism is located at an

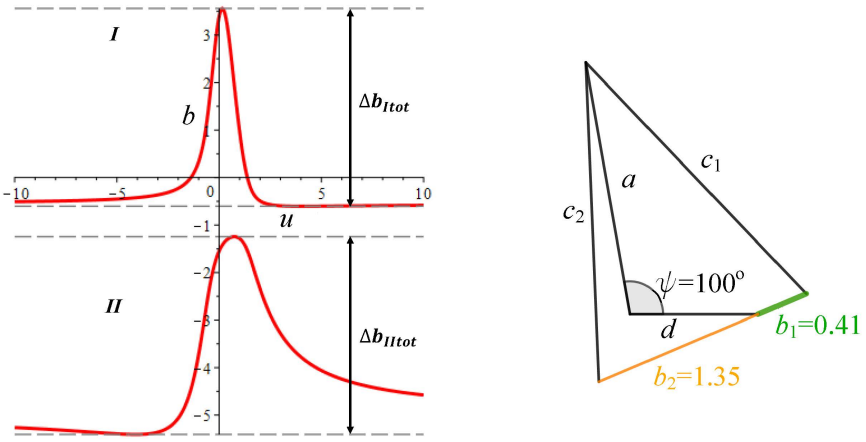

Figure 5: RRRP where $a = 2$, $c = 2.5$, $d = 1$, $v = 0.2$.

input singular configuration do not exist. The output linkage movement is unambiguously defined via the linkage assembly.

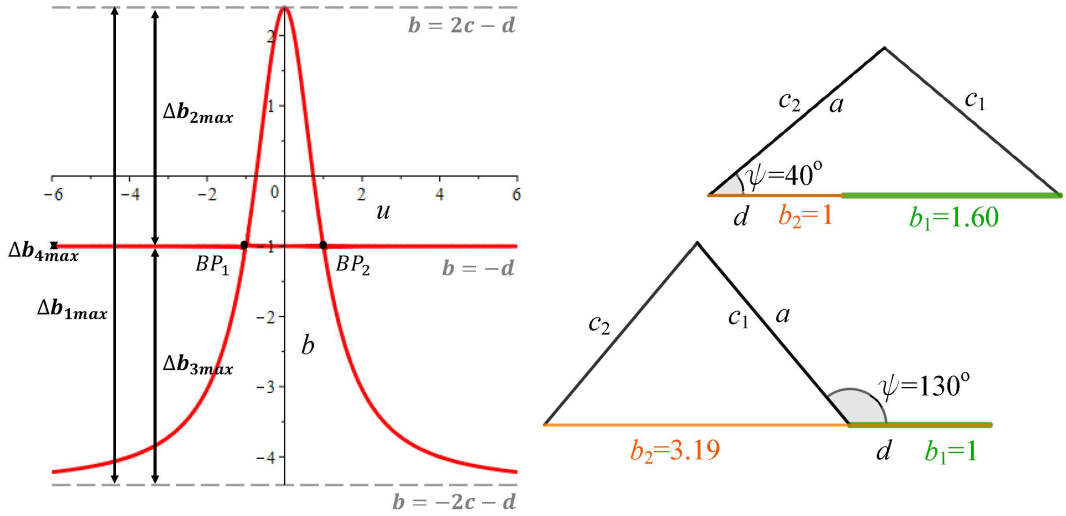

Figure 6: RRRP where $a = c = 1.7$, $d = 1$, $v = 0$.

Example 4. A very special RRRP linkage arises when $a = c$ and $v = 0$.

With these conditions, the factors of Eq. (11) simplify to

$$(b + d)(bu^2 + 2cu^2 + du^2 + b - 2c + d) = 0. \tag{17}$$

As a result, this special IO equation is decomposed into two operation modes. Moreover, two additional double points can be observed. These double points, the bifurcation points, BP_1 and BP_2, are always located at

$$BP_1(+1,-d), \qquad\qquad BP_2(-1,-d).$$

This IO equation has four different working modes, the input link a is able to rotate completely, and the mechanism has the ability to fold. From Eq. (17), the global maximum is found at $b_{max} = 2c - d$ and the global minimum is the asymptote at $b_{max} = -2c - d$ which leads to the following four maximum sliding positions $\Delta b_{i_{max}}$

$$\Delta b_{1_{max}}, = 4a = 4c \qquad \Delta b_{2_{max}}, = 2c \qquad \Delta b_{3_{max}}, = 2c \qquad \Delta b_{4_{max}}, = 0. \tag{18}$$

An example of the IO equation (where $a = c = 1.7$ and $d = 1$) is illustrated in Fig. 6.

2.2 RRRP Approximate Synthesis

To show that Eq. (11) can be used to generate arbitrary functions of the form $f(\psi) = b$, an example approximating the curve

$$b = cos(\psi) \tag{19}$$

is considered. For this example, 50 sample points were evenly distributed within the interval $-3 \leq u \leq 3$.

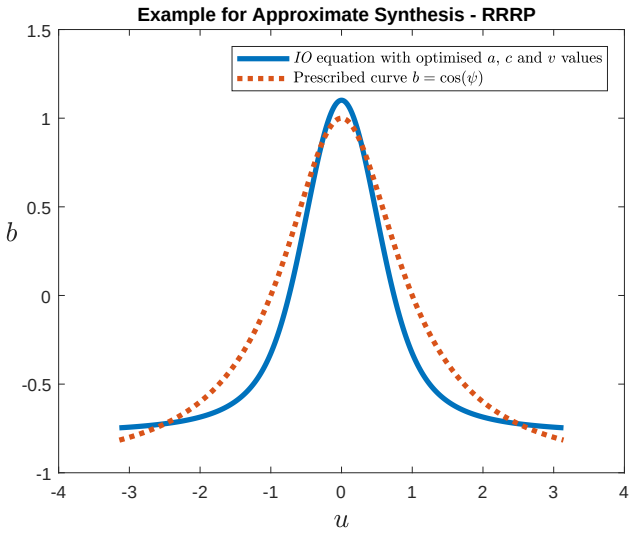

Figure 7: $a = 0.9426$, $c = 1.1587$, $d = 1$, $v = 1.5 \times 10^{-5}$.

The Newton-Gauss algorithm was used to iteratively minimise the structural error, the error residual found between the prescribed curve and the curve generated by the linkage (Tinubu and Gupta, 1984). The optimised function approximation with an RRRP linkage is obtained with the identified design parameters $a = 0.9426$, $c = \pm 1.1587$, $d = 1$,

and $v = \pm 1.5 \times 10^{-5}$. Fig.7 illustrates the structural error of the identified linkage. This example underscores the applicability of the general algebraic IO equation for RRRP in addition to RRRR linkages.

3 Algebraic Equation for PRRP Function Generators

As it was demonstrated that the general algebraic IO equation is useful for RRRP mechanism synthesis, it is reasonable to expect that the equation is equally valid for PRRP mechanisms. We won't consider mechanisms with greater than two P-joints since such linkages can only generate translations. The PRRP mechanism consists of one prismatic, two rotational, and another prismatic joint. In addition to a translational output motion b, the input motion a of the function generator is also a translation governed by a functional relation expressed by $f(a) = b$. The most common configuration is the elliptical trammel whose prismatic joint directions are perpendicular to each other, but for a general PRRP mechanism the P-joint axes may have any non-zero angle between them, as illustrated in Fig. 8.

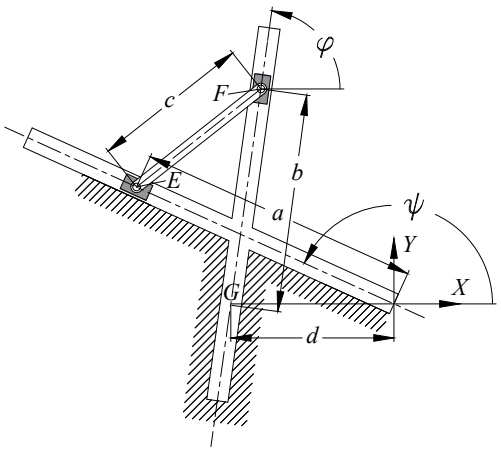

Figure 8: A PRRP linkage.

Since the two prismatic joints are both moving on a line, the initial constraint equations for the PRRP can again be set up according to Eqs. (3) and Eqs. (4). Note that in this particular case, the variables of the IO equation become a and b, while u, v, c, and d represent the design parameters. According to the same derivation for the RRRP and the RRRR function generators, but instead treating both a and b as variables, the IO equation of the function generator becomes

$$Aa^2 + Bb^2 + Cab + Da + Eb + F = 0, \tag{20}$$

where the coefficients are factors of constants u, c, d, and v:

$$\begin{aligned}
A &= \left(v^2+1\right)\left(u^2+1\right); \\
B &= \left(v^2+1\right)\left(u^2+1\right); \\
C &= -2\left(uv-u+v+1\right)\left(uv+u-v+1\right); \\
D &= 2\,d\left(v^2+1\right)\left(u-1\right)\left(u+1\right); \\
E &= -2\,d\left(v-1\right)\left(v+1\right)\left(u^2+1\right); \\
F &= -\left(v^2+1\right)\left(u^2+1\right)\left(c-d\right)\left(c+d\right).
\end{aligned}$$

Again, by collecting the variables in a different way it can easily be shown that Eq. (20) is identical to Eqs. (2) and (11).

3.1 Interpretation of the PRRP IO Equation

Eq. (20) has the following characteristics.

1. It is of degree $n = 2$.
2. It is a quadratic equation in two variables, thus, the IO equation is a conic section.
3. It's IO curve possesses genus $p = 0$, hence the maximum number of assembly modes of the linkage is $m = p + 1 = 1$ (Husty and Pfurner, 2018; Harnack, 1876).

From the discriminant, Δ_q, of the quadratic form associated with the conic section implied by Eq. (20)

$$\Delta_q = \begin{vmatrix} A & C/2 \\ C/2 & B \end{vmatrix}, \tag{21}$$

we can, according to Tab. 1, determine whether the conic is an ellipse, parabola or hyperbola (Glaeser et al., 2016). For Eq. (20) the discriminant reduces to

$$\begin{vmatrix} \left(v^2+1\right)\left(u^2+1\right) & -\left(uv-u+v+1\right)\left(uv+u-v+1\right) \\ -\left(uv-u+v+1\right)\left(uv+u-v+1\right) & \left(v^2+1\right)\left(u^2+1\right) \end{vmatrix} =$$

$$4\left(uv+1\right)^2\left(u-v\right)^2 \tag{22}$$

Discriminant of a non-degenerated conic	Shape
$\Delta_q > 0$	ellipse
$\Delta_q = 0$	parabola
$\Delta_q < 0$	hyperbola

Table 1: Impact of the discriminant value on the shape of function the PRRP can generate.

Since Eq. (22) is independent of link lengths then $\Delta_q \geq 0$ for all PRRP linkages and the conic represented by Eq. (20) can never be an hyperbola. The graph of the IO equation is always an ellipse with but one exception: if $u = -1/v$ or $u = v$, the conic becomes a special parabola, *i.e.*, two parallel lines. A distinguished ellipse, the circle, arises when $A = B$ and $C = 0$ which are the cases for

$$u = \pm 1, \;\; v = 0 \qquad\qquad u = 0, \;\; v = \pm 1, \tag{23}$$

i.e., when the axes are perpendicular to each other. These findings align with the literature (Sangwin, 2009) proving that this type of mechanism generates an ellipse, confirming the validity of the derived PRRP IO equation.

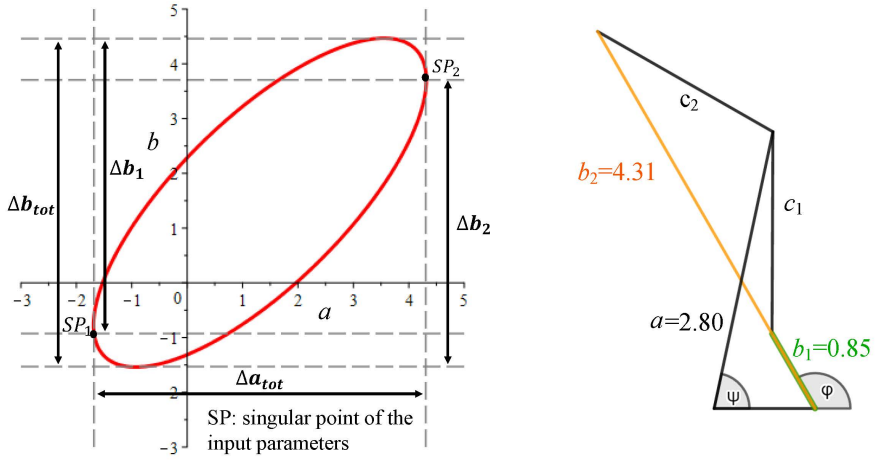

Figure 9: PRRP where $v = 1.7$, $u = 0.8$, $c = 2$, $d = 1$.

Example 5. Design parameter selection: $v = 1.7$; $u = 0.8$; $c = 2$; $d = 1$.

Fig. (9) illustrates the maximum sliding positions a_{tot} and b_{tot}. Considering a to be the input slider, two singular points separate the curve into two working modes. Hence, the output slider can have two different maximum sliding positions Δb_1 and Δb_2.

3.2 PRRP Approximation Synthesis

To show that Eq. (20) can also be used to generate a general function $f(a) = b$, we now consider an example where the desired function is

$$b = cos(a). \tag{24}$$

For this example 50 sample points are selected to be evenly distributed within the interval $0 \leq a \leq 2$. Again, the Newton-Gauss algorithm is used to minimise the structural error. As a result, the best approximation with a PRRP linkage is obtained with the identified

constants $c = 2.0313$, $d = 1$, $u = -1.1868$, and $v = 0.1353$, or $c = 2.0313$, $u = 1.1868$ and $v = -0.1353$. The designer may chose between these two different assembly modes. The structural error is illustrated in Fig. 10. The desired curve is illustrated in red, and the blue curve represents the approximation obtained by the PRRP linkage. For this example, the approximation obtained by the PRRP function generator is notably close to the prescribed curve. Hence, this example confirms the applicability of Eq. (20) for approximate synthesis problems.

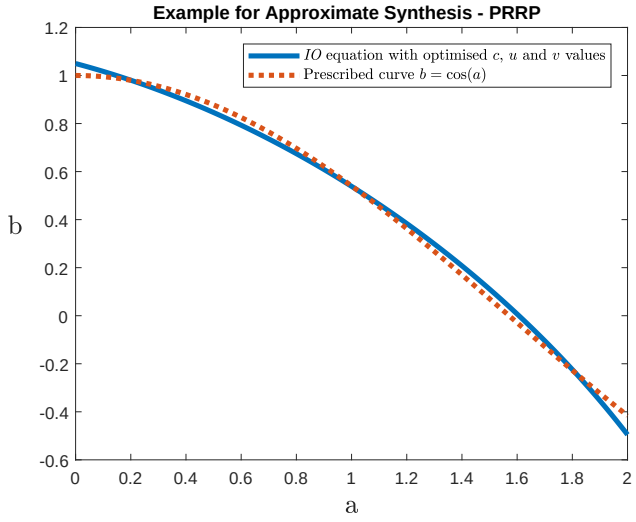

Figure 10: PRRP: $v = 0.1353$, $u = -1.1868$, $c = .03132$, $d = 1$.

4 Conclusions

In this paper two algebraic *IO* equations for RRRP and PRRP linkages were derived. It was shown that these equations are identical to the algebraic equation for RRRR linkages derived in (Hayes et al., 2018). We believe this to be a remarkable result having never been reported in the vast body of archival literature collected since antiquity! Analysing the equations revealed that the RRRP linkage can have a maximum of two assembly modes which can be divided into two working modes. A folding mechanism occurs if $a = c$ and $v = 0$. The PRRP linkage has only one assembly mode. It was demonstrated that its *IO* curve is either an ellipse or if $u = -1/v$ or $u = v$ two parallel lines. Furthermore, both equations were verified by a synthesis example that approximated the respective design parameters. Being able to expand the algebraic *IO* equation to two additional linkages, RRRP and PRRP, helps designers to choose the optimal linkage with the optimal design parameters with reduced time and effort. The generalisation of this paper is an important step towards the main goal of synthesising the optimal linkage of planar, spherical, or spatial function generators.

Acknowledgements

The authors gratefully acknowledge the partial financial support of this research by Mitacs Canada through a Globalink Research Grant awarded to the first author.

References

S. Bai and J. Angeles. A Unified Input-output Analysis of Four-bar Linkages. *Mechanism and Machine Theory*, 43(2):240–251, 2008.

O. Bottema and B. Roth. *Theoretical Kinematics.* Dover Publications, Inc., New York, NY, U.S.A., 1990.

Gerald L. Bradley and Karl J. Smith. *Calculus.* Prentice Hall, Englewood Cliffs, NJ, U.S.A., 1995.

D. Cox, J. Little, and D. O'Shea. *Ideals, Varieties, and Algorithms: an Introduction to Computational Algebraic Geometry and Commutative Algebra,* second edition. Springer-Verlag, Berlin, Germany, 1997.

F. Freudenstein. *Design of Four-link Mechanisms.* PhD thesis, Columbia University, New York, N.Y., USA, 1954.

G. Glaeser, H. Stachel, and B. Odehnal. *The Universe of Conics: From the Ancient Greeks to* 21^{st} *Century Developments.* Springer, 2016.

A. Harnack. Über die Vielteiligkeit der ebenen algebraischen Kurven. In *Mathematische Annalen*, pages 189–198, 1876.

M.J.D. Hayes, M.L. Husty, and M. Pfurner. Input-output Equation for Planar Four-bar Linkages. In *International Symposium on Advances in Robot Kinematics*, pages 12–19. Springer, 2018.

H. Hilton. *Plane Algebraic Curves.* Clarendon Press, Oxford, England, 1920.

K.H. Hunt. *Kinematic Geometry of Mechanisms.* Clarendon Press, Oxford, England, 1978.

M. Husty, A. Karger, H. Sachs, and W. Steinhilper. *Kinematik und Robotik.* Springer-Verlag Berlin Heidelberg New York, 1997.

M.L. Husty and M. Pfurner. An Algebraic Version of the Input-output Equation of Planar Four-bar Mechanisms. pages 746–757. *International Conference on Geometry and Graphics*, Milan, Italy, 2018.

E.J.F Primrose. *Plane Algebraic Curves.* MacMillan, 1955.

G. Salmon. *A Treatise on Conic Sections,* 6^{th} edition. Longmans, Green, and Co., London, England, 1879a.

G. Salmon. *A Treatise on the Higher Plane Curves,* 3^{rd} edition. Hodges, Foster, and Figgis, Dublin, Rep. of Ireland, 1879b.

G. Salmon. *Lessons Introductory to the Modern Higher Algebra,* 4^{th} edition. Hodges, Foster, and Figgis, Dublin, Rep. of Ireland, 1885.

C. Sangwin. The Wonky Trammel of Archimedes. *Teaching Mathematics and Its Applications: International Journal of the IMA*, 28(1):48–52, 2009.

E. Study. *Geometrie der Dynamen.* Teubner Verlag, Leipzig, Germany, 1903.

S.O. Tinubu and K.C. Gupta. Optimal Synthesis of Function Generators Without the Branch Defect. *Journal of Mechanisms, Transmissions, and Automation in Design*, 106 (3):348–354, 1984.

J.J. Uicker, G.R. Pennock, and J.E. Shigley. *Theory of Machines and Mechanisms,* 5^{th} edition. Oxford University Press, New York, N.Y., 2017.

W. Wunderlich. *Ebene Kinematik.* Hochschultaschenbücher-Verlag, Mannheim, Wien, Zürich, 1970.

A General Method for Determining Algebraic Input-output Equations for Planar and Spherical 4R Linkages

Mirja Rotzoll[1], M. John D. Hayes[1], Manfred L. Husty[2], and Martin Pfurner[2]

Abstract A new and completely general method for determining the algebraic input-output (*IO*) equations for planar and spherical 4R linkages is presented in this paper. First, the forward kinematics transformation matrix of an arbitrary planar or spherical open 4R kinematic chain is computed in terms of its Denavit-Hartenberg parameters, where the link twist and joint angles are converted to their tangent half-angle parameters. This transformation matrix is mapped to its corresponding eight Study coordinates. The serial kinematic chain is conceptually closed by equating the forward kinematics transformation to the identity matrix. Equating the two corresponding Study arrays yields four equations in terms of the four revolute joint angle parameters. Gröbner bases are then used to eliminate the two intermediate joint angle parameters leaving an algebraic polynomial in terms of the input and output joint angle parameters and the four twist angle or link length parameters. In the limit, as the sphere radius becomes infinite and the link twist angle parameters are expressed as ratios of arc length and sphere radius in the general spherical algebraic *IO* equation, the only terms that remain are those in the planar 4R *IO* equation.

Key words: Algebraic input-output equation, planar and spherical four-bar linkage, Study coordinates, kinematic mapping.

1 Introduction

Four-bar linkages, consisting of four rigid bodies connected by revolute (R) joints have fascinated mathematicians and engineers for centuries. One of the greatest successes was the establishment of an input-output (*IO*) equation by F. Freudenstein, which correlates the driver input angle ψ to the follower output angle φ according

[1] Carleton University, Department of Mechanical and Aerospace Engineering, Ottawa, ON, Canada.
[2] University of Innsbruck, Unit Geometry and Surveying, Innsbruck, Austria.

to a function $\varphi = f(\psi)$ [5]. The *IO* equation developed in [5] is trigonometric, whereas in [6] an algebraic version is derived by mapping the constraint equations of the driver and follower into Study's kinematic image space [1, 11]. Let a, b, c, d be the link lengths of the four-bar mechanism, and ψ and φ the respective input and output angles, then the movement of the mechanism is governed by the following *IO* equation

$$Au^2v^2 + Bu^2 + Cv^2 - 8abuv + D = 0 \quad (1)$$

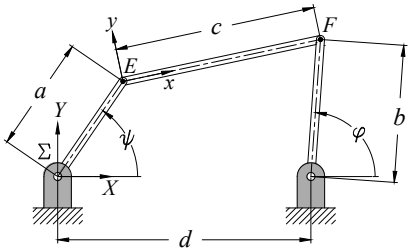

Fig. 1 Planar 4R function generator.

where

$$\begin{aligned}
A &= (a-b-c+d)(a-b+c+d),\\
B &= (a+b-c+d)(a+b+c+d),\\
C &= (a+b-c-d)(a+b+c-d),\\
D &= (a-b+c-d)(a-b-c-d),\\
u &= \tan\frac{\psi}{2},\\
v &= \tan\frac{\varphi}{2}.
\end{aligned}$$

In addition, it was shown in [10] that Equation (1) is not only valid for planar four-bar linkages containing revolute joints, but also for planar four-bar linkages containing up to two prismatic joints. In this paper we will describe a method that can be applied to both planar and spherical four-bar linkages to derive the respective *IO* equations. Moreover, we will show that planar linkages can be interpreted as special cases of spherical linkages, thus, expanding the generality of the *IO* equation obtained in [6].

2 Study's kinematic mapping

Consider a coordinate system Σ_2 that moves with a rigid body relative to a stationary reference frame Σ_1. The Euclidean displacement group $\mathscr{D} \in SO(3)$ can be represented by

$$\mathbf{p}' = \mathbf{A}\mathbf{p} + \mathbf{t} \quad (2)$$

where $\mathbf{p}$ is a 3×1 position vector in Σ_2, $\mathbf{A}$ is a proper orthogonal 3×3 rotation matrix, $\mathbf{t}$ is a 3×1 position vector of the origin of Σ_2 expressed in Σ_1, and $\mathbf{p}'$ is the 3×1 position vector of $\mathbf{p}$ expressed in Σ_1 [7, 9].

Displacements of kinematic chains are often parametrised using the Denavit-Hartenberg (DH) convention [3]. The four associated DH parameters are the link lengths a_i, link twist angles τ_i, joint angles θ_i, and link offsets d_i. According to this convention the coordinate transformation from the coordinate system for joint i relative to the coordinate system of the previous joint $i-1$ is given by

$$ {}^{i-1}_{i}\mathbf{T} = \left[\begin{array}{ccc|c} \cos\theta_i & -\sin\theta_i\cos\tau_i & \sin\theta_i\sin\tau_i & a_i\cos\theta_i \\ \sin\theta_i & \cos\theta_i\cos\tau_i & -\cos\theta_i\sin\tau_i & a_i\sin\theta_i \\ 0 & \sin\tau_i & \cos\tau_i & d_i \\ \hline 0 & 0 & 0 & 1 \end{array}\right] = \left[\begin{array}{c|c} \mathbf{A} & \mathbf{t} \\ \hline 0\ 0\ 0 & 1 \end{array}\right]. \tag{3} $$

With Study's kinematic mapping distinct Euclidean displacements can be represented as distinct points $x = [x_0 : x_1 : x_2 : x_3 : y_0 : y_1 : y_2 : y_3]^{\mathsf{T}} \in P^7$ where the first four entries are obtained using the matrix elements a_{ij} of $\mathbf{A}$

$$ x_0 : x_1 : x_2 : x_3 = \begin{cases} 1 + a_{11} + a_{22} + a_{33} : a_{32} - a_{23} : a_{13} - a_{31} : a_{21} - a_{12}, \\ a_{32} - a_{23} : 1 + a_{11} - a_{22} - a_{33} : a_{12} + a_{21} : a_{31} + a_{13}, \\ a_{13} - a_{31} : a_{12} + a_{21} : 1 - a_{11} + a_{22} - a_{33} : a_{23} + a_{32}, \\ a_{21} - a_{12} : a_{31} + a_{13} : a_{23} + a_{32} : 1 - a_{11} - a_{22} + a_{33}. \end{cases} \tag{4} $$

Four different combinations of the rotation matrix elements are needed since certain displacements make one or more of the relations lead to $(0:0:0:0)$, the exceptional generator in P^7. Once the x_i have been determined, the remaining four entries are computed as linear combinations of the vector elements of the translation $\mathbf{t}$ and the x_i determined above, giving

$$ \begin{aligned} y_0 &= \tfrac{1}{2}(t_3x_3 + t_2x_2 + t_1x_1), \quad & y_1 &= \tfrac{1}{2}(t_3x_2 - t_2x_3 - t_1x_0), \\ y_2 &= \tfrac{1}{2}(-t_3x_1 + t_1x_3 - t_2x_0), \quad & y_3 &= \tfrac{1}{2}(-t_3x_0 + t_2x_1 - t_1x_2). \end{aligned} \tag{5} $$

These eight Study parameters must fulfill the Study condition in order to represent a Euclidean displacement, meaning the eight ratios represent a point on Study's seven dimensional quadric $\mathscr{S}$

$$ x_0y_0 + x_1y_1 + x_2y_2 + x_3y_3 = 0 \tag{6} $$

excluding the exceptional generator $\mathscr{E}$

$$ (x_0 : x_1 : x_2 : x_3) = (0:0:0:0). \tag{7} $$

3 Planar four-bar linkage

To derive the algebraic *IO* equation for planar four-bar mechanisms using the DH convention [3] and Study's kinematic mapping [11], we first consider the four-bar mechanism to be an open kinematic chain connected by four rotational joints as shown in Fig. 2. The respective DH parameters are listed in Table 1. Note that for planar mechanisms all link twists and all link offsets are identically zero. This simplifies the overall transformation matrix ${}^{0}_{4}\mathbf{T}$, which maps the coordinates of points described in the end-link coordinate frame to those of the base frame:

$$ {}^{0}_{4}\mathbf{T} = {}^{0}_{1}\mathbf{T}\,{}^{1}_{2}\mathbf{T}\,{}^{2}_{3}\mathbf{T}\,{}^{3}_{4}\mathbf{T}, \tag{8} $$

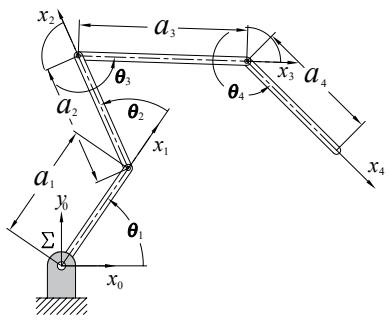

Fig. 2 Open 4R chain.

Table 1 DH parameters for open 4R chain.

joint axis i	link length a_i	link angle θ_i	link offset d_i	link twist τ_i
1	a_1	θ_1	0	0
2	a_2	θ_2	0	0
3	a_3	θ_3	0	0
4	a_4	θ_4	0	0

where the transformation matrices ${}^0_1\mathbf{T}$, ${}^1_2\mathbf{T}$, ${}^2_3\mathbf{T}$ and ${}^3_4\mathbf{T}$ are evaluated according to Equation (3). The computed transformation matrix can be mapped onto Study's quadric using Equations (4, 5) resulting in a Study array with zero entries for x_1, x_2, y_0 and y_3. After normalizing, the remaining four Study parameters become

$$x_0 = (2v_2v_3v_4 - 2v_2 - 2v_3 - 2v_4)v_1 + (-2v_3 - 2v_4)v_2 - 2v_3v_4 + 2, \tag{9}$$

$$x_3 = ((-2v_3 - 2v_4)v_2 - 2v_3v_4 + 2)v_1 - 2v_2v_3v_4 + 2v_2 + 2v_3 + 2v_4, \tag{10}$$

$$\begin{aligned} y_1 = {} & ((v_4(a_1 - a_2 + a_3 - a_4)v_3 - a_1 + a_2 + a_3 + a_4)v_2 + (-a_1 - a_2 + a_3 + a_4)v_3 \\ & - v_4(a_1 + a_2 + a_3 - a_4))v_1 + ((a_1 - a_2 + a_3 + a_4)v_3 + v_4(a_1 - a_2 - a_3 + a_4))v_2 \\ & + v_4(a_1 + a_2 - a_3 + a_4)v_3 - a_1 - a_2 - a_3 - a_4, \end{aligned} \tag{11}$$

$$\begin{aligned} y_2 = {} & (((a_1 - a_2 + a_3 + a_4)v_3 + v_4(a_1 - a_2 - a_3 + a_4))v_2 + v_4(a_1 + a_2 - a_3 + a_4)v_3 \\ & - a_1 - a_2 - a_3 - a_4)v_1 + (-v_4(a_1 - a_2 + a_3 - a_4)v_3 + a_1 - a_2 - a_3 - a_4)v_2 \\ & + (a_1 + a_2 - a_3 - a_4)v_3 + v_4(a_1 + a_2 + a_3 - a_4), \end{aligned} \tag{12}$$

where $v_i = \tan(\theta_i/2)$.

To close the four-bar mechanism, ${}^0_4\mathbf{T}$ is equated to the identity matrix which we also map using Equations (4, 5) onto Study's quadric, resulting in the following Study parameters after normalising:

$$I \mapsto [1:0:0:0:0:0:0:0]^{\mathsf{T}} \in P^7 \tag{13}$$

Equating the Study array of the overall transformation ${}^0_4\mathbf{T}$ to the Study array of the identity matrix, i.e. setting Equations (10-12) equal to zero, forces the coordinate frame of the end-effector to align with that of the base; but to satisfy the DH

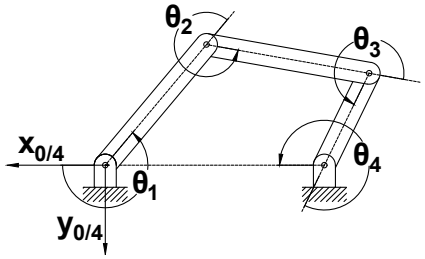

Fig. 3 Closed 4R kinematic chain.

convention they are both rotated by π. Thus, the joint angles, θ_i, are measured as illustrated in Fig. 3. We select the three Equations that are equal to zero, (10-12), and manipulate them with Gröbner bases to eliminate the intermediate joint angle parameters, v_2 and v_3. After collecting the input and output angle parameters v_1 and v_4, the following algebraic *IO* equation emerges

$$Av_1^2v_4^2 + Bv_1^2 + Cv_4^2 - 8a_1a_3v_1v_4 + D = 0, \tag{14}$$

where

$$\begin{aligned} A &= (a_1 - a_2 + a_3 - a_4)(a_1 + a_2 + a_3 - a_4) &&= A_1A_2, \\ B &= (a_1 + a_2 - a_3 - a_4)(a_1 - a_2 - a_3 - a_4) &&= B_1B_2, \\ C &= (a_1 - a_2 - a_3 + a_4)(a_1 + a_2 - a_3 + a_4) &&= C_1C_2, \\ D &= (a_1 + a_2 + a_3 + a_4)(a_1 - a_2 + a_3 + a_4) &&= D_1D_2. \end{aligned}$$

It can be shown that Equation (14) is identical to Equation (1) if the phase shift of the input and output angle as well as the different notation are considered.

4 Spherical four-bar linkage

It will now be demonstrated that the same procedure can be applied to determine the *IO* equation for spherical linkages. The DH parameters for a spherical open 4R kinematic chain are listed in Table 2. Note that in the spherical case all link lengths, a_i, and offsets, d_i, are zero with strict adherence to the DH conventions for assigning parameters [3]. After evaluating the overall transformation matrix in terms of DH parameters by applying Equation (3), the result can be mapped with Equations (4, 5) onto Study's quadric. Then setting $v_i = \tan(\theta_i/2)$ and $\alpha_i = \tan(\tau_i/2)$ into the result

Table 2 Open spherical 4R kinematic chain DH parameters.

joint axis i	link length a_i	link angle θ_i	link offset d_i	link twist τ_i
1	0	θ_1	0	τ_1
2	0	θ_2	0	τ_2
3	0	θ_3	0	τ_3
4	0	θ_4	0	τ_4

gives a Study array with non-zero entries for x_0, x_1, x_2 and x_3, while the y_i are all identically zero, as expected:

$$
\begin{aligned}
x_0 = {} & ((2\alpha_4((v_2v_3v_4+v_2-v_3+v_4)v_1+(v_3-v_4)v_2+v_3v_4+1)\alpha_3 \\
& +(2v_2v_3v_4-2v_2+2v_3+2v_4)v_1+(-2v_3-2v_4)v_2+2v_3v_4-2)\alpha_2 \\
& +((-2v_2v_3v_4-2v_2-2v_3+2v_4)v_1+(2v_3-2v_4)v_2-2v_3v_4-2)\alpha_3 \\
& +(2((v_2v_3v_4-v_2-v_3-v_4)v_1+(v_3+v_4)v_2+v_3v_4-1))\alpha_4)\alpha_1 \\
& +(((2v_2v_3v_4+2v_2-2v_3+2v_4)v_1+(-2v_3+2v_4)v_2-2v_3v_4-2)\alpha_3 \\
& -(2((v_2v_3v_4-v_2+v_3+v_4)v_1+(v_3+v_4)v_2-v_3v_4+1))\alpha_4)\alpha_2 \\
& +(2((v_2v_3v_4+v_2+v_3-v_4)v_1+(v_3-v_4)v_2-v_3v_4-1))\alpha_4\alpha_3 \\
& +(2v_2v_3v_4-2v_2-2v_3-2v_4)v_1+(-2v_3-2v_4)v_2-2v_3v_4+2; \qquad (15) \\
x_1 = {} & ((((-2v_2v_3v_4-2v_2+2v_3-2v_4)v_1+(-2v_3+2v_4)v_2-2v_3v_4-2)\alpha_3 \\
& +(2((v_2v_3v_4-v_2+v_3+v_4)v_1+(-v_3-v_4)v_2+v_3v_4-1))\alpha_4)\alpha_2 \\
& -2\alpha_4((v_2v_3v_4+v_2+v_3-v_4)v_1+(-v_3+v_4)v_2+v_3v_4+1)\alpha_3 \\
& +(-2v_2v_3v_4+2v_2+2v_3+2v_4)v_1+(-2v_3-2v_4)v_2-2v_3v_4+2)\alpha_1 \\
& +((2((v_2v_3v_4+v_2-v_3+v_4)v_1+(-v_3+v_4)v_2-v_3v_4-1))\alpha_4\alpha_3 \\
& +(2v_2v_3v_4-2v_2+2v_3+2v_4)v_1+(2v_3+2v_4)v_2-2v_3v_4+2)\alpha_2 \\
& +((-2v_2v_3v_4-2v_2-2v_3+2v_4)v_1+(-2v_3+2v_4)v_2+2v_3v_4+2)\alpha_3 \\
& +(2((v_2v_3v_4-v_2-v_3-v_4)v_1+(-v_3-v_4)v_2-v_3v_4+1))\alpha_4; \qquad (16) \\
x_2 = {} & (((((-2v_3+2v_4)v_2-2v_3v_4-2)v_1+2v_2v_3v_4+2v_2-2v_3+2v_4)\alpha_3 \\
& -(2(((v_3+v_4)v_2-v_3v_4+1)v_1+v_2v_3v_4-v_2+v_3+v_4))\alpha_4)\alpha_2 \\
& +(2(((v_3-v_4)v_2-v_3v_4-1)v_1+v_2v_3v_4+v_2+v_3-v_4))\alpha_4\alpha_3 \\
& +((-2v_3-2v_4)v_2-2v_3v_4+2)v_1+2v_2v_3v_4-2v_2-2v_3-2v_4)\alpha_1 \\
& +(-(2(((v_3-v_4)v_2+v_3v_4+1)v_1+v_2v_3v_4+v_2-v_3+v_4))\alpha_4\alpha_3 \\
& +((2v_3+2v_4)v_2-2v_3v_4+2)v_1-2v_2v_3v_4+2v_2-2v_3-2v_4)\alpha_2 \\
& +(((-2v_3+2v_4)v_2+2v_3v_4+2)v_1+2v_2v_3v_4+2v_2+2v_3-2v_4)\alpha_3 \\
& -(2(((v_3+v_4)v_2+v_3v_4-1)v_1+v_2v_3v_4-v_2-v_3-v_4))\alpha_4; \qquad (17) \\
x_3 = {} & (((2(((v_3-v_4)v_2+v_3v_4+1)v_1-v_2v_3v_4-v_2+v_3-v_4))\alpha_4\alpha_3 \\
& +((-2v_3-2v_4)v_2+2v_3v_4-2)v_1-2v_2v_3v_4+2v_2-2v_3-2v_4)\alpha_2 \\
& +(((2v_3-2v_4)v_2-2v_3v_4-2)v_1+2v_2v_3v_4+2v_2+2v_3-2v_4)\alpha_3 \\
& +2\alpha_4(((v_3+v_4)v_2+v_3v_4-1)v_1-v_2v_3v_4+v_2+v_3+v_4))\alpha_1 \\
& +((((-2v_3+2v_4)v_2-2v_3v_4-2)v_1-2v_2v_3v_4-2v_2+2v_3-2v_4)\alpha_3 \\
& -(2(((v_3+v_4)v_2-v_3v_4+1)v_1-v_2v_3v_4+v_2-v_3-v_4))\alpha_4)\alpha_2 \\
& +2\alpha_4(((v_3-v_4)v_2-v_3v_4-1)v_1-v_2v_3v_4-v_2-v_3+v_4)\alpha_3 \\
& +((-2v_3-2v_4)v_2-2v_3v_4+2)v_1-2v_2v_3v_4+2v_2+2v_3+2v_4. \qquad (18)
\end{aligned}
$$

Again, the open kinematic chain is closed by equating the Study array to the corresponding identity array in Study coordinates, i.e. setting Equations (16-18) equal

to zero. Subsequently, we use Gröbner bases to eliminate the intermediate angle parameters v_2 and v_3 from Equations (16-18), and obtain the desired *IO* equation

$$Av_1^2v_4^2 + Bv_1^2 + Cv_4^2 + 8\alpha_1\alpha_3\left(\alpha_4^2+1\right)\left(\alpha_2^2+1\right)v_1v_4 + D = 0, \tag{19}$$

where

$$\begin{aligned}
A &= (\alpha_1\alpha_2\alpha_3 - \alpha_1\alpha_2\alpha_4 + \alpha_1\alpha_3\alpha_4 - \alpha_2\alpha_3\alpha_4 + \alpha_1 - \alpha_2 + \alpha_3 - \alpha_4)\\
&\quad (\alpha_1\alpha_2\alpha_3 - \alpha_1\alpha_2\alpha_4 - \alpha_1\alpha_3\alpha_4 - \alpha_2\alpha_3\alpha_4 - \alpha_1 - \alpha_2 - \alpha_3 + \alpha_4),\\
B &= (\alpha_1\alpha_2\alpha_3 + \alpha_1\alpha_2\alpha_4 - \alpha_1\alpha_3\alpha_4 - \alpha_2\alpha_3\alpha_4 + \alpha_1 + \alpha_2 - \alpha_3 - \alpha_4)\\
&\quad (\alpha_1\alpha_2\alpha_3 + \alpha_1\alpha_2\alpha_4 + \alpha_1\alpha_3\alpha_4 - \alpha_2\alpha_3\alpha_4 - \alpha_1 + \alpha_2 + \alpha_3 + \alpha_4),\\
C &= (\alpha_1\alpha_2\alpha_3 - \alpha_1\alpha_2\alpha_4 - \alpha_1\alpha_3\alpha_4 + \alpha_2\alpha_3\alpha_4 - \alpha_1 + \alpha_2 + \alpha_3 - \alpha_4)\\
&\quad (\alpha_1\alpha_2\alpha_3 - \alpha_1\alpha_2\alpha_4 + \alpha_1\alpha_3\alpha_4 + \alpha_2\alpha_3\alpha_4 + \alpha_1 + \alpha_2 - \alpha_3 + \alpha_4),\\
D &= (\alpha_1\alpha_2\alpha_3 + \alpha_1\alpha_2\alpha_4 + \alpha_1\alpha_3\alpha_4 + \alpha_2\alpha_3\alpha_4 - \alpha_1 - \alpha_2 - \alpha_3 - \alpha_4)\\
&\quad (\alpha_1\alpha_2\alpha_3 + \alpha_1\alpha_2\alpha_4 - \alpha_1\alpha_3\alpha_4 + \alpha_2\alpha_3\alpha_4 + \alpha_1 - \alpha_2 + \alpha_3 + \alpha_4).
\end{aligned}$$

It can be shown that Equation (19) is identical to the corresponding trigonometric *IO* equation for spherical four-bar linkages found in [9].

5 Planar 4R linkages as a special case of the spherical 4R linkage

The two algebraic *IO* equations for planar and spherical 4R linkages already suggest some similarities. As demonstrated in [8], the motion of the planar 4R linkage represents a special case of the spherical 4R linkage. To show that the same relationship is true for the *IO* equations, we consider the directions of the joint axes. While the joint axes of the spherical 4R linkage intersect in the centre of the sphere, the joint axes of the planar 4R linkage are all parallel. In Euclidean space E^3 parallel lines never intersect, however, they do meet in a point at infinity in any projective extension of E^3 [2, 4]. This suggests that if the radius of a spherical linkage approaches infinity, the linkage becomes a planar mechanism in the limit [8]. As the link twist parameters α_i of the spherical *IO* equation are proportional to the ratios of the arc lengths to the sphere radius [12], we can make the following substitution in Equation (19)

$$\alpha_i \propto \frac{a_i}{r}. \tag{20}$$

In the resulting equation the first two cubic factors simplify to

$$\begin{aligned}
\lim_{r\to\infty} &-\frac{1}{r}\left(\frac{a_1a_2a_3}{r^2} - \frac{a_1a_2a_4}{r^2} + \frac{a_1a_3a_4}{r^2} - \frac{a_2a_3a_4}{r^2} + a_1 - a_2 + a_3 - a_4\right)\\
&\left(-\frac{a_1a_2a_3}{r^2} + \frac{a_1a_2a_4}{r^2} + \frac{a_1a_3a_4}{r^2} + \frac{a_2a_3a_4}{r^2} + a_1 + a_2 + a_3 - a_4\right).
\end{aligned} \tag{21}$$

In the limit the only terms remaining inside the parentheses in Equation (21) are

$$(a_1 - a_2 + a_3 - a_4)(a_1 + a_2 + a_3 - a_4) = A_1A_2. \tag{22}$$

Proceeding with the other cubic factors in the same manner the algebraic *IO* equation for a spherical 4R mechanism leads directly to that of a planar 4R, Equation (14), in the limit. As mentioned, this aligns with the results from [8], and further confirms the validity of the derived *IO* equations as well as the observation in [9] that there exists a connection between the planar and the spherical 4R *IO* equations via the RSSR linkage.

6 Conclusions

We have successfully demonstrated a general method to derive the algebraic *IO* equations for spherical and planar 4R linkages. It requires defining the DH parameters for an open 4R kinematic chain, mapping its coordinate transformation matrix onto Study's quadric, conceptually closing the 4R chain by equating the corresponding Study coordinates to the identity array and eliminating the intermediate joint angles using Gröbner bases. Moreover, we have shown that the planar 4R *IO* equation represents a special case of the spherical 4R by evaluating the limit at infinity of the equation.

References

1. Bottema, O., Roth, B.: Theoretical Kinematics. Dover Publications, Inc., New York, NY, U.S.A. (1990)
2. Coxeter, H.S.M.: Non-Euclidean Geometry, *5th edition*. University of Toronto Press, Toronto, On., Canada (1965)
3. Denavit, J., Hartenberg, R.S.: A kinematic notation for lower-pair mechanisms based on matrices. Trans ASME J. Appl. Mech. **23**, 215–221 (1955)
4. Fishback, W.T.: Projective and Euclidean Geometry, *2nd edition*. John Wiley & Sons, Inc., New York, N.Y., U.S.A. (1969)
5. Freudenstein, F.: Design of four-link mechanisms. Ph.D. thesis, Columbia University, New York, N.Y., USA (1954)
6. Hayes, M.J.D., Husty, M.L., Pfurner, M.: Input-output equation for planar four-bar linkages. In: International Symposium on Advances in Robot Kinematics, pp. 12–19. Springer (2018)
7. Husty, M.L., Karger, A., Sachs, H., Steinhilper, W.: Kinematik und Robotik. Springer-Verlag Berlin Heidelberg New York (1997)
8. McCarthy, J.M.: "Planar and Spatial Rigid Motion as Special Cases of Spherical and 3-Spherical Motion". Journal of Mechanisms, Transmissions, and Automation in Design **105**(3), 569–575 (1983)
9. McCarthy, J.M., Soh, G.S.: Geometric Design of Linkages, 2nd Edition *Interdiciplinaty Applied Mathematics*. Springer, New York, N.Y. (2011)
10. Rotzoll, M., Hayes, M.J.D., Husty, M.L.: An algebraic input-output equation for planar RRRP and PRRP linkages. *Canadian Committee for the Theory of Machines and Mechanisms*, Montreal, Canada (2019)
11. Study, E.: Geometrie der Dynamen. Teubner Verlag, Leipzig, Germany (1903)
12. Uicker, J.J., Pennock, G.R., Shigley, J.E.: Theory of Machines and Mechanisms, *5th edition*. Oxford University Press, New York, N.Y., U.S.A. (2017)

Design Parameter Space of Planar Four-bar Linkages

M. John D, Hayes[1], Mirja Rotzoll[1], and Manfred L. Husty[2]

[1] Carleton University, Department of Mechanical and Aerospace Engineering, Ottawa, ON, Canada
[2] University of Innsbruck, Unit Geometry and CAD, Innsbruck, Austria

Abstract. A new algebraic input-output relation for planar four-bar mechanisms is a quartic curve in the input-output joint angle parameter plane. This equation contains four terms with quadratic coefficients of link lengths which all factor into the product of two linear terms. The structure of these eight linear factors suggests that they are the eight faces of an octahedron in a design parameter space of the link lengths. In this paper we show that the design parameter octahedron space implies a complete classification scheme for all 27 possible planar $4R$ mechanisms, in addition to linkages containing one, or two prismatic joints.

Keywords: Algebraic input-output relation; planar four-bar linkage; design parameter octahedron.

1 Introduction

In the firmament of mechanical design the four-bar linkage burns as its brightest star. This is seen to be true when one considers the tremendous volume of literature investigating analysis and design of four-bar mechanisms, ranging from antiquity to present [1]. In this paper we investigate the geometry of the design parameter space of planar four-bar mechanisms. Since we will be concerned with the input-output (IO) relation, we will use the standard description of a planar $4R$ function generator for reference. Such a function generator correlates driver and follower angles such that the mechanism generates the function $\varphi = f(\psi)$, or vice versa, see Fig. 1.

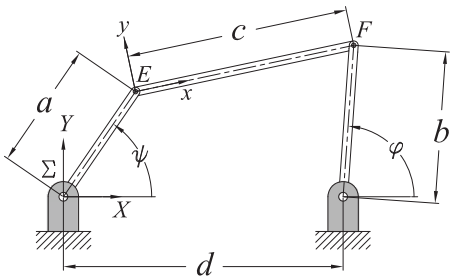

Fig. 1. Planar $4R$ linkage.

Surprisingly, design methods have not focused on algebraic IO equations, rather they generally use the transcendental Freudenstein synthesis equations [3], or variants thereof. The Freudenstein equation relating the input to the

T. Uhl (ed.), *Advances in Mechanism and Machine Science*,
Mechanisms and Machine Science 73,
https://doi.org/10.1007/978-3-030-20131-9_23

output angles of a planar $4R$ four-bar mechanism, with link lengths as in Fig. 1, was first put forward in [4]. In the equation the angle ψ is traditionally selected to be the input while φ is the output angle:

$$k_1 + k_2 \cos(\varphi_i) - k_3 \cos(\psi_i) = \cos(\psi_i - \varphi_i). \tag{1}$$

Eq. (1) is linear in the k_i Freudenstein parameters, which are defined in terms of the link length ratios as:

$$k_1 \equiv \frac{(a^2 + b^2 + d^2 - c^2)}{2ab}; \quad k_2 \equiv \frac{d}{a}; \quad k_3 \equiv \frac{d}{b}.$$

In this paper we use instead the algebraic IO relation derived in [7] and the geometric analysis of the quartic algebraic IO curve in [8] to show that it implies a classification scheme for all 27 possible planar $4R$ mechanisms [11]. The classification scheme characterises all Grashof and non-Grashof ranges of motion of the input and output links. Moreover, the structure of the algebraic IO equation suggests a design parameter space [8] that will be examined more fully in this paper.

Study's kinematic mapping image space coordinates and resultants were employed in [7] to derive the IO equation. Then Weierstraß (tangent of the half-angle) substitutions

$$u = \tan\left(\frac{\psi}{2}\right), \; v = \tan\left(\frac{\varphi}{2}\right)$$

were applied to convert the trigonometric equation to an algebraic one, which has the following form:

$$Au^2v^2 + Bu^2 + Cv^2 - 8abuv + D = 0 \tag{2}$$

where;

$$\begin{aligned} A = (a-b-c+d)(a-b+c+d) &= A_1A_2; \\ B = (a+b-c+d)(a+b+c+d) &= B_1B_2; \\ C = (a+b-c-d)(a+b+c-d) &= C_1C_2; \\ D = (a-b+c-d)(a-b-c-d) &= D_1D_2. \end{aligned}$$

Eq. (2) is quartic in the coordinate plane of u and v. Since the distance d between the ground fixed links can be viewed as a scaling factor for function generators, without loss in generality we can normalise a, b, and c by d and consider the design parameter sub-space comprised of three mutually orthogonal bases distances with $d = 1$. Another way of looking at the design parameter sub-space is as the projection of the four dimensional space onto the hyperplane $d = 1$.

Regardless, it is shown in [8] that the quartic curve represented by Eq. (2) has two double points, and therefore possesses genus 1. The double points are the points at infinity of the u and v axes in the u-v plane. Each of these double points can have real or complex tangents depending on the values of the link lengths, which in turn determines the nature of the mobility of the linkage, as well as the number of assembly modes (the maximum is two), and the number of folding assemblies (the maximum is three).

2 Design Parameter Octahedron

In the design parameter space, the eight linear factors in Eq. (2) can be interpreted as the eight faces of a regular octahedron determined by the six vertices $V = (a, b, c)$: $V_1 = (1, 0, 0)$; $V_2 = (-1, 0, 0)$; $V_3 = (0, 1, 0)$; $V_4 = (0, -1, 0)$; $V_5 = (0, 0, 1)$; $V_6 = (0, 0, -1)$, see Fig. 2.

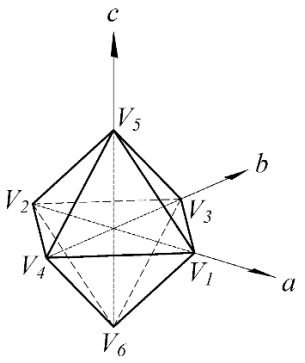

Fig. 2. Design parameter octahedron.

Each face of the octahedron lies entirely in one of the eight quadrants in the parameter space. Given the octahedron, four questions that naturally arise.

1. What do the six vertices imply?
2. What is the significance of points on the octahedron edges?
3. What is the significance of points on the octahedron faces?
4. What is the significance of the location of a general point in the parameter space?

2.1 The Six Octahedron Vertices

With reference to Fig. 2, each of the six octahedron vertices lie at the terminal ends of the design parameter space basis unit vectors, **a**, **b**, and **c**. They comprise the six points $V_{1,2} = (\pm 1, 0, 0)$, $V_{3,4} = (0, \pm 1, 0)$, $V_{5,6} = (0, 0, \pm 1)$. Each vertex is the point common to the planes of four faces and represents a degenerate planar four-bar mechanism with no mobility because it contains two links of zero length and two links of unit length.

2.2 The Twelve Octahedron Edges

Again, referring to Fig. 2, each of the twelve octahedron edges, excluding the vertices, is the line in common with two octahedron faces. Each edge lies entirely in one of eight design parameter sub-space coordinate planes. For example, the edge that lies in the coordinate plane spanned by the positive basis vectors **a** and **b** is the intersection of the face planes defined by the vertices $\{V_1, V_3, V_5\}$ and $\{V_1, V_6, V_3\}$. Each edge represents a degenerate four-bar mechanism with no mobility because it contains one link of zero length.

2.3 Points on the Eight Octahedron Faces

Because of the beautiful structure of the eight linear factors in Eq. (2), it may be shown in a straightforward way that each of the linear factors defines one of eight planes containing one of the octahedron faces. In Euclidean space, E_3,

a necessary and sufficient condition that four points, whose homogeneous point coordinates are $(x_0 : x_1 : x_2 : x_3)$, $(y_0 : y_1 : y_2 : y_3)$, $(z_0 : z_1 : z_2 : z_3)$ and $(w_0 : w_1 : w_2 : w_3)$, be coplanar is that [2, 5]

$$\begin{vmatrix} x_0 & x_1 & x_2 & x_3 \\ y_0 & y_1 & y_2 & y_3 \\ z_0 & z_1 & z_2 & z_3 \\ w_0 & w_1 & w_2 & w_3 \end{vmatrix} = 0. \tag{3}$$

It follows that the plane determined by three distinct points has the equation

$$X_0x_0 + X_1x_1 + X_2x_2 + X_3x_3 = 0, \tag{4}$$

where the *plane coordinates* $[X_0 : X_1 : X_2 : X_3]$ are obtained by Grassmannian expansion [10] of the matrix in Eq. (3), giving

$$\begin{vmatrix} y_1 & y_2 & y_3 \\ z_1 & z_2 & z_3 \\ w_1 & w_2 & w_3 \end{vmatrix} x_0 + \begin{vmatrix} y_0 & y_3 & y_2 \\ z_0 & z_3 & z_2 \\ w_0 & w_3 & w_2 \end{vmatrix} x_1 + \begin{vmatrix} y_0 & y_1 & y_3 \\ z_0 & z_1 & z_3 \\ w_0 & w_1 & w_3 \end{vmatrix} x_2 + \begin{vmatrix} y_0 & y_2 & y_1 \\ z_0 & z_2 & z_1 \\ w_0 & w_2 & w_1 \end{vmatrix} x_3 = 0. \tag{5}$$

Employing the Grassmannian expansion we obtain the equation of the plane containing the octahedron face defined by the vertices $\{V_1, V_6, V_3\}$ using their homogeneous coordinates: $V = (1 : a : b : c) \Rightarrow V_1 = (1 : 1 : 0 : 0)$, $V_6 = (1 : 0 : 0 : -1)$, $V_3 = (1 : 0 : 1 : 0)$. Using the determinants in Eq. (5) and the three vertices reveals the corresponding plane coordinates as

$$[X_0 : X_1 : X_2 : X_3] \;=\; \left[\begin{vmatrix} 1 & 0 & 0 \\ 0 & 0 & -1 \\ 0 & 1 & 0 \end{vmatrix} : \begin{vmatrix} 1 & 0 & 0 \\ 1 & -1 & 0 \\ 1 & 0 & 1 \end{vmatrix} : \begin{vmatrix} 1 & 1 & 0 \\ 1 & 0 & -1 \\ 1 & 0 & 0 \end{vmatrix} : \begin{vmatrix} 1 & 0 & 1 \\ 1 & 0 & 0 \\ 1 & 1 & 0 \end{vmatrix} \right] \;=\; [1 : -1 : -1 : 1]. \tag{6}$$

Hence, the plane equation containing face $\{V_1, V_6, V_3\}$ can be expressed as

$$1 - a - b + c = 0. \tag{7}$$

When the coordinates in Eq. (7) are homogenised, the relation can be expressed as

$$a + b - c - d = 0. \tag{8}$$

Thus, the plane equation determined by the three vertices $\{V_1, V_6, V_3\}$ is precisely the linear factor C_1 in Eq. (2). The remaining seven linear factors in Eq. (2) are, similarly, the plane equations for the seven other octahedron faces. If a point in the design parameter space satisfies Eq. (8), then it lies in the plane of the face spanned by the three vertices $\{V_1, V_6, V_3\}$, and the corresponding mechanism has link lengths constrained by the relation $a + b = c + d$. Depending on the lengths of the individual links satisfying this relation the resulting mechanism can be

a double crank, double rocker, or crank rocker, and can have as many as three folding configurations and assembly modes [8, 11].

Similarly, points in the planes of the faces spanned by vertices $\{V_2, V_5, V_3\}$ and by vertices $\{V_1, V_5, V_4\}$ lead to the plane equations

$$1 + a - b - c = 0 \text{ and } 1 - a + b - c = 0,$$

which correspond to the linear factors A_1 and D_1 respectively, when the coordinates are homogenised giving

$$a - b - c + d = 0 \text{ and } a - b + c - d = 0.$$

Points laying in the planes of these two faces correspond to linkages with link lengths constrained by the relations $a + d = b + c$ and $a + c = b + d$. Again, depending on the lengths, the resulting mechanisms can be a double-crank, double-rocker, or crank-rocker, and can have as many as three folding configurations and assembly modes. However, points in the planes spanned by the remaining five faces, corresponding to linear factors A_2, B_1, B_2, C_2, and D_2 represent linkages with zero finite mobility because either the sum of the magnitudes of all the link lengths is identically zero, or one link length is equal to the sum of the lengths of the remaining three links.

2.4 A General Point in the Design Parameter Space

The location of a single point in the design parameter space is a specific planar $4R$ whose link lengths satisfy Eq. (2). The values of the link lengths are directed distances, and hence can be positive or negative. Clearly, if one of the lengths is identically zero, then the resulting $3R$ linkage is a structure. The absolute values of the link lengths identified with Eq. (2) lead to an alternate form of the classification scheme for planar $4R$ linkages first presented in [11] and later refined in [9], and hence to an expression for the Grashof condition. Recall that the Grashof condition states that a planar $4R$ will contain one link that can fully rotate if

$$l + s < p + q, \tag{9}$$

where l and s refer to the lengths of the longest and shortest links, while p and q are the lengths of the two intermediate links.

Input Link, *a*. The limits of angular displacement for the input link, a, if they exist, can be determined using the law of cosines and the two triangles formed by the lengths a and d when the coupler and output link align, giving lengths $c - b$ and $c + b$, respectively, see Fig. 3. In order for $\psi_{\min}$ and $\psi_{\max}$ to exist, then

$$-1 \leq \cos(\psi) \leq 1. \tag{10}$$

It can be shown using the methods in [9, 11] that the conditions leading to

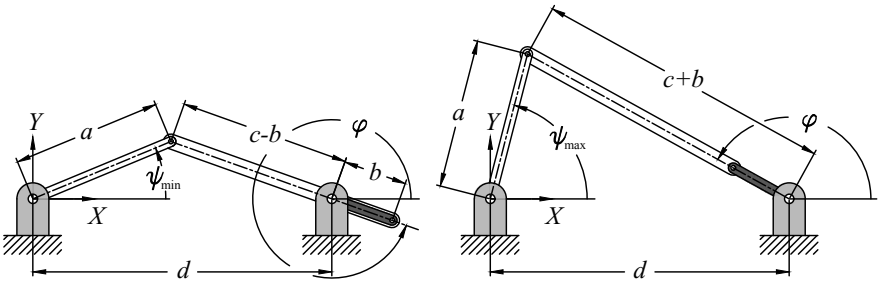

Fig. 3. The angular limits of the output link, if they exist, are $\psi_{\min}$ and $\psi_{\min}$.

$-1 < \cos(\psi) > 1$ can be expressed as the product of two linear factors from Eq. (2). The fist product concerns the existence of $\psi_{\min}$:

$$(a+b-c-d)(a-b+c-d) > 0 \quad (\text{i.e. } C_1 D_1 > 0). \tag{11}$$

If this condition is satisfied, then both factors must be either positive or negative, and the input link has no $\psi_{\min}$. This implies that the input link can rotate through $\psi = 0$ reaching angles below the line joining the centres of the two ground fixed R-pairs. If this condition is not satisfied then one of either C_1 or D_1 is negative and $\psi_{\min}$ may be computed, using the upper sign $(c-b)^2$, as[1]

$$\psi_{\substack{\min \\ \max}} = \cos^{-1}\left(\frac{a^2+d^2-(c\mp b)^2}{2ad}\right). \tag{12}$$

Referring again to Fig. 3, the second product concerns the existence of $\psi_{\max}$, and can be expressed as:

$$(a-b-c+d)(a+b+c+d) < 0 \quad (\text{i.e. } A_1 B_2 < 0). \tag{13}$$

If this condition is satisfied then $\psi_{\max}$ does not exist, and the input link can rotate through π. Since B_2 must always be positive, this condition simplifies to

$$a + d < b + c. \tag{14}$$

If the condition in Eq. (13) is not satisfied, then it must be that $a + d \geq b + c$, and $\psi_{\max}$ may be computed using the lower sign $(c+b)^2$ in Eq. (12).

The classification, as in [11], uses the observation that if $C_1 D_1 > 0$ and $A_1 < 0$ then neither $\psi_{\min}$ nor $\psi_{\max}$ exist, and the input link is a fully rotatable crank and therefore the link lengths must satisfy the Grashof condition. If $C_1 D_1 > 0$ while $A_1 \geq 0$ then $\psi_{\max}$ exists, but not $\psi_{\min}$, and the input link is a 0-rocker because it rocks through 0 between the $\pm\psi_{\max}$ limits. If $C_1 D_1 \leq 0$ while $A_1 < 0$

[1] Note that $\cos(\psi)$ returns the same value for $\pm\psi$. Hence, the $\cos^{-1}$ function leads to two limiting values of $\pm\psi_{\min}$ and $\pm\psi_{\max}$, one for each of the *elbow up* and *elbow down* configurations of the linkage.

then $\psi_{\min}$ exists, but not $\psi_{\max}$, and the input link is a π-rocker because it rocks through π between the $\pm\psi_{\min}$ limits. Alternately, if $C_1 D_1 \leq 0$ and $A_1 \geq 0$ then both $\psi_{\min}$ and $\psi_{\max}$ exist and the input link is a rocker which can pass through neither 0 nor π and rocks in one of two sperate ranges: $\psi_{\min} \leq \psi_{\max}$; or $-\psi_{\max} \leq -\psi_{\min}$.

Output Link, *b*. The limits of angular displacement for the output link, b, if they exist, can be determined using the law of cosines and the two triangles formed by the lengths b and d when the coupler and input link align, giving lengths $c + a$ and $c - a$, respectively, see Fig. 4. Note that φ in this case is an exterior angle, and the corresponding angle used in the law of cosines is $\pi - \varphi$ necessitating a sign change: $-\cos(\pi - \varphi) = \cos(\varphi)$. In order for $\varphi_{\min}$ and $\varphi_{\max}$ to exist, then

$$-1 \leq \cos(\varphi) \leq 1. \tag{15}$$

The conditions leading to $-1 > \cos(\varphi) > 1$ can be expressed as the products of

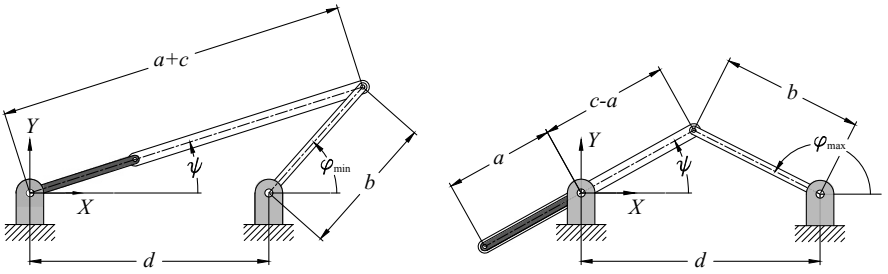

Fig. 4. The angular limits of the output link, if they exist, are $\varphi_{\min}$ and $\varphi_{\min}$.

two linear factors from Eq. (2). If $\varphi_{\min}$ does not exist then a and c can't align and:

$$(a - b + c - d)(a + b + c + d) > 0 \quad \text{(i.e. } D_1 B_2 > 0\text{)}. \tag{16}$$

Since B_2 is always positive, then in order to satisfy Eq. (16) D_1 must also be positive. This leads to the simpler expression for the condition in Eq. (16):

$$a + c > b + d. \tag{17}$$

If this condition is satisfied, then $\varphi_{\min}$ does not exist and the output link can rotate through $\varphi = 0$ reaching angles below the line joining the centres of the two ground fixed R-pairs. When this condition is not satisfied then D_1 is either identically zero or negative meaning that $\varphi_{\min}$ exists and may be computed using the upper sign $(a + c)^2$ in Eq. (18) as

$$\varphi_{\substack{\min \\ \max}} = \cos^{-1}\left(\frac{(a \pm c)^2 - (b^2 + d^2)}{2bd}\right). \tag{18}$$

Referring again to Fig. 4, the second product concerns the existence of $\varphi_{\max}$, and can be expressed as:

$$(a-b-c+d)(a+b-c-d) < 0 \quad \text{(i.e. } A_1C_1 < 0\text{)}. \tag{19}$$

If this condition is satisfied then $\varphi_{\max}$ does not exist, and the output link can rotate through π. Satisfying this condition requires that one factor is positive while the other is negative. If the condition in Eq. (19) is not satisfied, then it must be that A_1 and C_1 are either both positive or negative. In this case $\varphi_{\max}$ may be computed using the lower sign $(a-c)^2$ in Eq. (18).

Again, following [11], the Grashof condition for this case is $A_1C_1 < 0$ and $D_1 > 0$. Using these conditions as indicators, the output link can also be a crank, a 0-rocker, a π-rocker, or a rocker restricted to one of the two separate ranges $\varphi_{\min} \leq \varphi_{\max}$; or $-\varphi_{\max} \leq -\varphi_{\min}$.

Implications of Vanishing Linear Factors. The remaining conditions to consider are if any one, or more, of the three factors are identically zero. Consider the following zeros:

$$\begin{aligned} A_1 = 0 \;&\Rightarrow\; a-b-c+d = 0 \;\Rightarrow\; a+d = b+c; \\ C_1 = 0 \;&\Rightarrow\; a+b-c-d = 0 \;\Rightarrow\; a+b = c+d; \\ D_1 = 0 \;&\Rightarrow\; a-b+c-d = 0 \;\Rightarrow\; a+c = b+d. \end{aligned}$$

If only one of $A_1 = 0$, $C_1 = 0$, or $D_1 = 0$, then the mechanism is a point on one of the planes containing the faces of the octahedron spanned by either vertices $\{V_2, V_5, V_3\}$, $\{V_1, V_6, V_3\}$, or $\{V_4, V_1, V_5\}$, respectively. In each case, the linkage has a single folding configuration. If two of the factors are identically zero, then the mechanism is represented by a point that lies on the line of intersection of the two corresponding faces, which is never an octahedron edge for pairs of these three faces. In this case, the linkage has two folding configurations because of the equality in length of two different sums of pairs of link lengths. Finally, if all three factors are simultaneously identical to zero, the corresponding mechanism is represented by the point common to the planes of all three associated octahedron faces. It is a simple matter to show this leads to a third order equation with only one solution: $a = b = c = d$. In the design parameter space normalised with $d = 1$, this means the point $(1, 1, 1)$, a rhombus linkage possessing three folding configurations.

2.5 Classification

Any planar $4R$ linkage can be classified according to the values of the three linear factors A_1, C_1, and D_1 which can each either be positive, identically zero, or negative. Using the criteria from above the linkage type can be classified according to it's link lengths. All 27 possible mechanisms are listed in Table 1.

#	A_1	C_1	D_1	Input a	Output b	#	A_1	C_1	D_1	Input a	Output b
1	+	+	+	0-rocker	0-rocker	15	0	0	-	crank	π-rocker
2	+	+	0	0-rocker	0-rocker	16	0	-	+	π-rocker	crank
3	+	+	-	rocker	rocker	17	0	-	0	crank	crank
4	+	0	+	0-rocker	crank	18	0	-	-	crank	π-rocker
5	+	0	0	0-rocker	crank	19	-	+	+	crank	crank
6	+	0	-	0-rocker	π-rocker	20	-	+	0	crank	crank
7	+	-	+	rocker	crank	21	-	+	-	π-rocker	π-rocker
8	+	-	0	0-rocker	crank	22	-	0	+	crank	crank
9	+	-	-	0-rocker	π-rocker	23	-	0	0	crank	crank
10	0	+	+	crank	crank	24	-	0	-	crank	π-rocker
11	0	+	0	crank	crank	25	-	-	+	π-rocker	0-rocker
12	0	+	-	π-rocker	π-rocker	26	-	-	0	crank	0-rocker
13	0	0	+	crank	crank	27	-	-	-	crank	rocker
14	0	0	0	crank	crank						

Table 1. Classification of all possible planar $4R$ linkages. Shaded cells satisfy the Grashof condition.

2.6 Continuous Sets of Points in the Design Parameter Space

Planar four-bar linkages however are not exclusively jointed with R-pairs, they often contain P-pairs. However, four-bar mechanisms containing more than two P-pairs cannot move the coupler in general plane motion, rather they can only generate translations and hence are not considered here. A kinematic inversion of an $RRRP$ linkage will possess one variable link length and one variable joint angle, typically called a *slider-crank*. Hence the roles of fixed constant and variable in Eq. 2 can be reassigned to generate a function of the form $b = f(u)$, for example. The important thing to note is that the same IO equation can be used for kinematic synthesis! The resulting mechanism however, will not be represented by a single point in the design parameter space. Rather, it will be represented by a line parallel to the basis vector direction representing the variable link length. The length of the line will be determined by the extremities of the slider translation. This will be interesting to investigate in function generation optimisation problems, but will be left for future work.

The kinematic inversions of the *elliptic-trammel* $PRRP$ linkage are the $RPPR$ and $RRPP$ linkages known as Oldham's coupling and the Scotch yoke, respectively. These linkages possess two variable link lengths. It turns out that Eq. 2 can also be used for function generation synthesis. We believe this to be remarkable! Again, the roles of fixed constant and variable are reassigned. In this case the function generation synthesis problem can be modelled with Eq. 2 to generate functions of the form $b = f(a)$, while the angles represented by u and v are now constants that are identified in the synthesis. In the design parameter space the resulting mechanism will be represented by a curve that is the approximated functional relationship between lengths a and b over the desired maximum input-output range. Again, algorithm development for approximate

function generation problems for $PRRP$ type linkages will be left for future work.

3 Conclusions

In this paper we have considered the design and analysis of planar four-bar linkages that can move the coupler in general plane motion in a fundamentally new way. Using the algebraic IO curve from [7, 8] we have shown that the eight linear factors of link lengths can be interpreted as the eight faces of a regular octahedron in the function generator design parameter space of link lengths projected into the hyperplane $d = 1$. We have shown that a point in the design parameter space represents a planar $4R$ linkage, while it's location implies the IO limits of the input and output links yielding the classification from [11]. We believe that this work, together with [8], will lead to a new approach to approximate synthesis optimisation using continuous approximate synthesis as introduced in [6].

References

1. Ceccarelli, M., Editor: Distinguished Figures in Mechanism and Machine Science, Their Contributions and Legacies Part 1. Springer, New York, U.S.A. (2007)
2. Coxeter, H.S.M.: Projective Geometry, *second edition*. University of Toronto Press, Toronto, On., Canada (1974)
3. Freudenstein, F.: "An Analytical Approach to the Design of Four-link Mechanisms.". Trans. ASME **vol 77**, pages 483–492 (1954)
4. Freudenstein, F.: Design of four-link mechanisms. Ph.D. thesis, Columbia University, New York, N.Y., USA (1954)
5. Gans, D.: Transformations and Geometries. Appelton-Century-Crofts, New York, N.Y., U.S.A. (1969)
6. Guigue, A., Hayes, M.J.D.: "Continuous Approximate Synthesis of Planar Function-generators Minimising the Design Error". Mechanism and Machine Theory **vol 101**, pages 158–167, DOI: 10.1016/j.mechmachtheory.2016.03.012 (2016)
7. Hayes, M.J.D., Husty, M.L., Pfurner., M.: "Input-output Equation for Planar Four-bar Linkages". pp. 12–19. *16th Advances in Robotic Kinematics*, eds. Lenarčič, J. and Parenti-Castelli, V., Springer, New York (2018)
8. Husty, M.L., Pfurner, M.: "An Algebraic Version of the Input-Output Equation of Planar Four-Bar Mechanisms". pp. 746–757. *International Conference on Geometry and Graphics*, Milan, Italy (2018)
9. McCarthy, J.M., Soh, G.S.: Geometric Design of Linkages, 2nd Edition *Interdiciplinary Applied Mathematics*. Springer, New York, N.Y. (2011)
10. Klein, F.: Elementary Mathematics from an Advanced Standpoint: Geometry. Dover Publications, Inc., New York, N.Y., U.S.A. (1939)
11. Murray, A.P., Larochelle, P.M.: "A Classification Scheme for Planar $4R$, Spherical $4R$, and Spatial $RCCR$ Linkages to Facilitate Computer Animation". *Proceedings of 1998 ASME Design Engineering Technical Conferences (DETC'98)*, Atlanta, Georgia, U.S.A. (September 13-16, 1998)

Design Parameter Space of Spherical Four-bar Linkages

M.J.D. Hayes[1], M. Rotzoll[2], C. Ingalls[3], and M. Pfurner[4]

Abstract. Four link twist angles are the design parameters for spherical 4R linkages: changing the magnitudes of the twist angles changes the motion characteristics of the linkage. A new quartic algebraic input-output equation for spherical four-bar linkages, obtained in another paper, contains four terms which each factor into pairs of distinct cubics in the link twists. These eight cubic factors possess a symmetry that suggest they combine to form a shape that, at least locally, bears a remarkable resemblance to a pair of dual tetrahedra in the design parameter space of the link twists. In this paper we show that the location of points relative to the eight distinct cubic surfaces implies a complete classification scheme for all possible spherical 4R linkages. Moreover, we show that the design parameter spaces of both the spherical and planar 4R linkages, with suitable scaling, intersect in 12 lines which form the 12 edges of a pair of dual tetrahedra.

Key words: Spherical four-bar linkages; design parameter space; uniform polyhedral compound.

1 Introduction

Over the millennia, four-bar linkages have become ubiquitous with applications ranging from aircraft landing gear deployment systems to beer bottle cap clamps. One might, however naïvely, be led to the conclusion that all is known. Nonetheless, through continued investigation, commencing with the ground breaking work of Ferdinand Freudenstein in the 1950s [5, 6], new discoveries and new insight continue to be obtained, often with surprising results. See [10], for example, for a comprehensive collection of results offered by a vast array of investigators over the last 175 years.

The algebraic input-output (IO) equation for any planar four-bar linkage is a polynomial equation in the variable input (driver) link and output (follower) link angle parameters expressed in terms of the link lengths. Because the link lengths

[1]Mech. and Aero. Engineering, Carleton University, Canada, e-mail: john.hayes@carleton.ca
[2]Mech. and Aero. Engineering, Carleton University, Canada, e-mail: mirja.rotzoll@carleton.ca
[3]School of Math. and Stats., Carleton University, Canada, e-mail: colin.ingalls@carleton.ca
[4]Unit Geometry and Surveying, University of Innsbruck, e-mail: martin.pfurner@uibk.ac.at

Table 1 Denavit-Hartenberg parameters for a planar 4R chain.

joint axis i	link length a_i	link angle θ_i	link offset d_i	link twist τ_i
1	a_1	θ_1	0	0
2	a_2	θ_2	0	0
3	a_3	θ_3	0	0
4	a_4	θ_4	0	0

impose mobility constraints on the input and output links, they are considered design parameters. Since the coupler motion is embedded in the polynomial, the IO equation is well suited to function generation synthesis. Moreover, it is an algebraic equation so the theory of algebraic geometry [2] can be applied to reveal characteristics of the IO relationship that may otherwise be occluded by trigonometry.

Individual link coordinate systems are assigned according to the original Denavit-Hartenberg convention [4]. Link parameters of length, a_i, joint angle, θ_i, link offset, d_i, and link twist angle, τ_i are all defined relative to these coordinate systems. For a planar 4R linkage the design parameters are the four link lengths, a_1, a_2, a_3, and a_4, see Fig. 1(a), as the relative lengths determine the mobility capability of the linkage, while the relative angles between the links θ_1, θ_2, θ_3, and θ_4, are variables in the IO equation. The link offsets and twist angles are all identically zero, see Table 1. Note that the base coordinate system illustrated in Fig. 1(a) is an artifact of the method used to derive the algebraic IO equation, see [13] for the details. Regardless, only the origin and direction of the $z_{0/4}$-axis are fixed by the convention while the direction of the $x_{0/4}$-axis is rotated by π radians compared to the usual representation, while the $y_{0/4}$-axis completes the right-handed coordinate system.

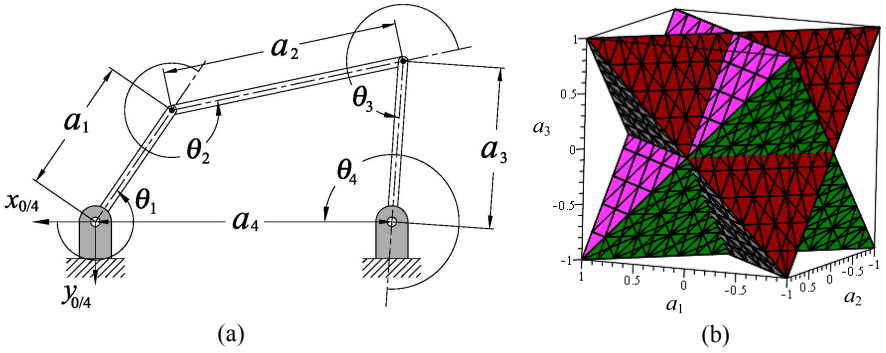

Fig. 1 Planar 4R chain and associated design parameter tetrahedra.

The algebraic IO equation for a planar 4R linkage is a planar quartic curve in the IO angle parameters $v_1 = \tan\theta_1/2$ and $v_4 = \tan\theta_4/2$ [7]. The link length coefficients are embedded in four quadratic terms that are each comprised of two factors that are linear sums of link lengths. The algebraic IO equation, as derived in [13], is

$$Av_1^2v_4^2 + Bv_1^2 + Cv_4^2 - 8a_1a_3v_1v_4 + D = 0, \tag{1}$$

where

$$\begin{aligned} A &= (a_1 - a_2 + a_3 - a_4)(a_1 + a_2 + a_3 - a_4) &&= A_1A_2, \\ B &= (a_1 + a_2 - a_3 - a_4)(a_1 - a_2 - a_3 - a_4) &&= B_1B_2, \\ C &= (a_1 - a_2 - a_3 + a_4)(a_1 + a_2 - a_3 + a_4) &&= C_1C_2, \\ D &= (a_1 + a_2 + a_3 + a_4)(a_1 - a_2 + a_3 + a_4) &&= D_1D_2. \end{aligned}$$

Since we are dealing with function generators, the scale of the linkage is irrelevant. Without loss in generality, we can normalise the four link lengths by a_4, the distance between the centres two ground fixed R-pairs, thereby setting $a_4 = 1$. Projected into this hyperplane, the remaining three lengths can be used to establish three mutually orthogonal basis vectors. The eight symmetric linear factors, having the form $(a_1 \pm a_2 \pm a_3 \pm 1)$, can be represented as eight planes in the a_i for the eight permutations in sign. These eight planes intersect in the 12 edges of a pair of dual regular tetrahedra [8] while the plane segments bounded by the 12 edges are the tetrahedra faces, see Fig. 1(b).

These two tetrahedra belong to the only uniform polyhedral compound, called the stellated octahedron, which has order 48 octahedral symmetry [3]. This double tetrahedron has a regular octahedron at its core and shares its eight vertices with the cube [3]. Distinct points in this design parameter space represent distinct function generators and the locations of the points relative to the eight planes containing the faces of the double tetrahedron completely determines the mobility of the input and output links. There are 27 types of mobility conditions, determined using the techniques found in [8, 11], which depend on the signs of the sums of lengths in the three terms A_1, B_1, and C_1 from Eq. (1).

The focus of this paper is the design parameter space corresponding to spherical 4R linkages. Thus, the quartic algebraic IO equation for spherical 4R mechanisms, as derived in [13], is manipulated to examine the design parameter space implied by the magnitudes of the link twist angle parameters defined as $\alpha_i = \tan(\tau_i/2)$, where τ_i specifies the twist angles according to the original Denavit-Hartenberg convention [4]. For a spherical 4R the design parameters are the four link twist angles, τ_i, while the relative link angles are the four variable θ_i. The link lengths and offsets are identically zero, see Table 2. In comparison with the design parameter space of planar 4R mechanisms [8] we see some startling similarities. But first, the spherical 4R IO equation needs some discussion.

Table 2 DH parameters a spherical 4R chain.

joint axis i	link length a_i	link angle θ_i	link offset d_i	link twist τ_i
1	0	θ_1	0	τ_1
2	0	θ_2	0	τ_2
3	0	θ_3	0	τ_3
4	0	θ_4	0	τ_4

2 The Spherical 4R Algebraic IO Equation

The R-pair axes of a spherical 4R mechanism all intersect at the centre of the sphere, while those of a planar 4R mechanism are all parallel meaning that they can be thought of as intersecting in the same point at infinity of the projective extension of the planar 4R Euclidean plane. As shown in [13], this means that the planar 4R mechanism is a special case of the spherical 4R. In the limit, as the radius of the sphere tends towards infinity, the algebraic IO equations of the spherical and planar 4R mechanisms are projectively equivalent. This suggests that there should be some similarities between the respective design parameter spaces.

A new and general method for deriving an algebraic form of the spherical 4R mechanism IO equation is presented in [13]. This method, using Study's kinematic mapping [1, 15], can also be used to derive the algebraic IO equation for planar 4R mechanisms, and we are working towards applying it to spatial 4R's. Regardless, the algebraic IO equation for spherical 4R's has the form

$$Av_1^2v_4^2 + Bv_1^2 + Cv_4^2 + 8\alpha_1\alpha_3\left(\alpha_4^2+1\right)\left(\alpha_2^2+1\right)v_1v_4 + D = 0, \tag{2}$$

where

$$\begin{aligned}
A &= (\alpha_1\alpha_2\alpha_3 - \alpha_1\alpha_2\alpha_4 + \alpha_1\alpha_3\alpha_4 - \alpha_2\alpha_3\alpha_4 + \alpha_1 - \alpha_2 + \alpha_3 - \alpha_4)\\
&\quad (\alpha_1\alpha_2\alpha_3 - \alpha_1\alpha_2\alpha_4 - \alpha_1\alpha_3\alpha_4 - \alpha_2\alpha_3\alpha_4 - \alpha_1 - \alpha_2 - \alpha_3 + \alpha_4),\\
B &= (\alpha_1\alpha_2\alpha_3 + \alpha_1\alpha_2\alpha_4 - \alpha_1\alpha_3\alpha_4 - \alpha_2\alpha_3\alpha_4 + \alpha_1 + \alpha_2 - \alpha_3 - \alpha_4)\\
&\quad (\alpha_1\alpha_2\alpha_3 + \alpha_1\alpha_2\alpha_4 + \alpha_1\alpha_3\alpha_4 - \alpha_2\alpha_3\alpha_4 - \alpha_1 + \alpha_2 + \alpha_3 + \alpha_4),\\
C &= (\alpha_1\alpha_2\alpha_3 - \alpha_1\alpha_2\alpha_4 - \alpha_1\alpha_3\alpha_4 + \alpha_2\alpha_3\alpha_4 - \alpha_1 + \alpha_2 + \alpha_3 - \alpha_4)\\
&\quad (\alpha_1\alpha_2\alpha_3 - \alpha_1\alpha_2\alpha_4 + \alpha_1\alpha_3\alpha_4 + \alpha_2\alpha_3\alpha_4 + \alpha_1 + \alpha_2 - \alpha_3 + \alpha_4),\\
D &= (\alpha_1\alpha_2\alpha_3 + \alpha_1\alpha_2\alpha_4 + \alpha_1\alpha_3\alpha_4 + \alpha_2\alpha_3\alpha_4 - \alpha_1 - \alpha_2 - \alpha_3 - \alpha_4)\\
&\quad (\alpha_1\alpha_2\alpha_3 + \alpha_1\alpha_2\alpha_4 - \alpha_1\alpha_3\alpha_4 + \alpha_2\alpha_3\alpha_4 + \alpha_1 - \alpha_2 + \alpha_3 + \alpha_4).
\end{aligned}$$

In this equation the joint angle parameters are $v_i = \tan\theta_i/2$, where the IO angle parameter pair are v_1 and v_4, while the four link twist angle parameters are $\alpha_i = \tan\tau_i/2$. The link twist angles, τ_i, are defined using the original Denavit-Hartenberg assignment convention [4]. It can be shown that Eq. (2) is identical to the corresponding trigonometric IO equation for spherical four-bar linkages found in [11].

2.1 Interpretation of the Spherical 4R IO Equation

Analysing Eq. (2) using the theory of planar algebraic curves [12] one can see that it has characteristics which are independent of the constant design parameters α_i.

Clearly, Eq. (2) is of degree $n = 4$ in variables v_1 and v_4. It is also of interest to determine the planar curve's double, or singular, points. To identify these double points Eq. (2) must first be homogenised. We arbitrarily select w to be the homogenising coordinate, which gives

$$k_h : \; Av_1^2v_4^2 + Bv_1^2w^2 + Cv_4^2w^2 + 8\alpha_1\alpha_3(\alpha_4^2+1)(\alpha_2^2+1)v_1v_4w^2 + Dw^4 = 0. \quad (3)$$

The double points are revealed by the locations of where the Jacobian ideal vanishes [12]. This ideal is generated by

$$\left(\frac{\partial k_h}{\partial v_1}, \; \frac{\partial k_h}{\partial v_4}, \; \frac{\partial k_h}{\partial w}.\right) \quad (4)$$

Solving the system of equations implied by Eq. (4) for v_1, v_4, and w reveals two double points located at infinity along the v_1- and v_4-axes, which exactly mirrors the results reported in [9] for planar 4R mechanisms:

$$(v_1 : v_4 : w) \; = \; (1:0:0); \; (0:1:0). \quad (5)$$

These two double points are common to all algebraic IO curves for every spherical 4R four-bar mechanism. Each of these double points can have real or complex tangents depending on the values of the four constant link twist parameters α_i, which in turn determines the nature of the mobility of the linkage.

The discriminant of Eq. (3), evaluated at a double point, reveals whether that double point has a pair of real or complex conjugate tangents [2] in turn yielding information about the topology of the mechanism [9]. The discriminant and the meaning of its value are [2]

$$\Delta = \left(\frac{\partial^2 k_h}{\partial v_i \partial w}\right)^2 - \frac{\partial^2 k_h}{\partial v_i^2}\frac{\partial^2 k_h}{\partial w^2} \begin{cases} > 0 \Rightarrow \text{two real distinct tangents (crunode)}, \\ = 0 \Rightarrow \text{two real coincident tangents (cusp)}, \\ < 0 \Rightarrow \text{two complex conjugate tangents (acnode)}. \end{cases}$$

For the homogeneous IO equation of a spherical 4R linkage, Eq. (3), the discriminant of the point at infinity $(v_1 : v_4 : w) = (1:0:0)$ on the v_1-axis is obtained by setting $i = 4$ in the discriminant equation, i.e. ∂v_4, while the discriminant of the other point at infinity on the v_4-axis is obtained by setting $i = 1$ in the discriminant equation, i.e. ∂v_1, giving

$$\Delta_{v_1} = -4AB, \quad \Delta_{v_4} = -4AC. \quad (6)$$

Since the values of Eq.s (6) depend on the products and sums of link twist angle parameters their values may be either greater than, less than, or identically equal to zero. Certainly, the classification of the mobility of the input and output links is determined by these values.

Finally, because an equation of degree $n = 4$ can have a maximum of three double points, the algebraic IO equation possesses genus 1 since it has only two. Because of this, it cannot be parameterised by rational functions, and is defined to be an *elliptic*

curve [12]. Moreover, since the curve has genus 1 for every spherical 4R linkage, there are, at most, two assembly modes roughly corresponding to "elbow-up" and "elbow-down" [9].

3 Spherical 4R Design Parameter Space

The eight factors in the four coefficients A, B, C, and D in Eq. 2 are cubics in the α_i design constant twist angle parameters and have an intoxicating symmetric structure. When α_1, α_2, and α_3 are projected into the hyperplane $\alpha_4 = 1$ for a spherical 4R function generator, we can treat the three twist angle parameters α_1, α_2, and α_3 as mutually orthogonal basis vector directions. Fig.s 2(a) and (b) illustrate the eight factors in each of the planar and spherical 4R IO equations where the surfaces are plotted in the ranges $a_i = \pm 1$ and $\alpha_i = \pm 1$. The planar 4R surface is a regular double tetrahedron with the special property of being the only uniform polyhedral compound [3]. The spherical 4R surfaces have the appearance of being a double tetrahedron, but they are cubic surfaces and therefore are not.

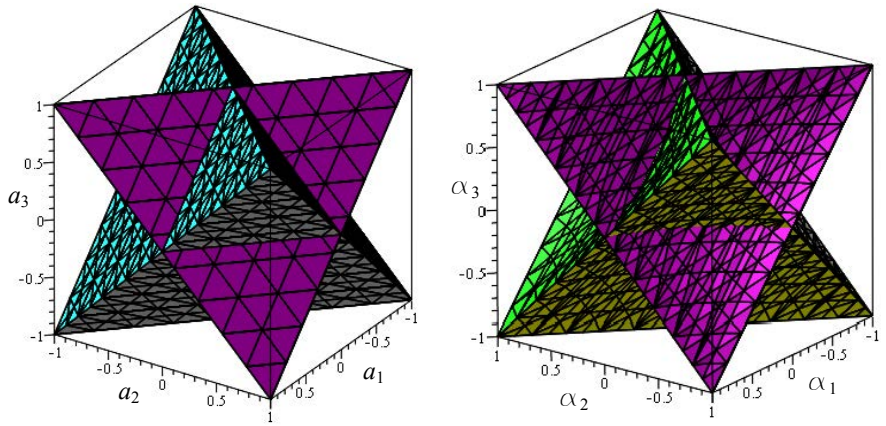

Fig. 2 Design parameter space surfaces: (a) planar 4R; (b) spherical 4R.

Cubic surfaces have fascinated mathematicians for several centuries. Clearly, the eight cubic factors in Eq. (2) possess some special properties. The first cubic factor in coefficient A from Eq. (2), which we will name A_1, after α_4 has been set to 1, can be homogenised with coordinate w to reveal

$$A_{1,h}: \ \alpha_1\alpha_2\alpha_3 - \alpha_1\alpha_2 w + \alpha_1\alpha_3 w - \alpha_2\alpha_3 w + \alpha_1 w^2 - \alpha_2 w^2 + \alpha_3 w^2 - w^3. \qquad (7)$$

The double points for this cubic are revealed by the locations of where the Jacobian ideal generated by

$$\left(\frac{\partial A_{1,h}}{\partial \alpha_1}, \frac{\partial A_{1,h}}{\partial \alpha_2}, \frac{\partial A_{1,h}}{\partial \alpha_3}, \frac{\partial A_{1,h}}{\partial w}\right) \tag{8}$$

vanishes. It turns out that all eight cubics share the same three double points, namely

$$(\alpha_1 : \alpha_2 : \alpha_3 : w) \;=\; (1:0:0:0);\; (0:1:0:0);\; (0:0:1:0). \tag{9}$$

The discriminant evaluated at each of the three double points, common to all eight cubics, is $\Delta = 4$ for each double point. Since this discriminant is always greater than zero, the double points are all ordinary [2] because there are two distinct, real tangents at each double point. Alternately, we observe that each cubic surface meets the plane at infinity in the three lines $\alpha_1 = \alpha_2 = \alpha_3 = 0$. The singular double points are the vertices of this triangle. It can be shown that the two lines through each vertex are in the tangent singular cone at the vertex and because the Hessian of $A_{1,h}$ is non-zero at each vertex then each one is an ordinary double point.

It is well known that cubic surfaces can contain as many as 27 lines [14]. It is also shown in [14] that a cubic surface possessing three ordinary double points can have, at most, 12 lines. While the procedure for determining the lines is not particularly germane to this paper, nonetheless it can be shown that of these 12 lines six are complex and six are real. Of the six real lines three are at infinity. The remaining three lines on each surface intersect each other in an equilateral triangle. Moreover, different pairs of the cubics share a line, meaning that there are 12 distinct lines among the eight cubics. The set of twelve distinct lines on each of the eight surfaces intersect to form the edges of a double tetrahedron! This double tetrahedron can be regarded, philosophically, as the intersection of planar and spherical 4R design parameter spaces. Treating the α_i as directed distances the location of a point in this space determines the linkage mobility, as for planar 4R linkages [8].

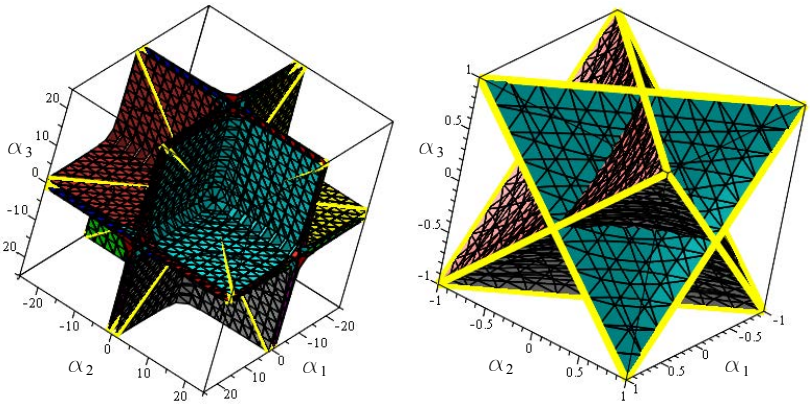

Fig. 3 12 distinct lines, three on each of eight cubics: (a) zoomed out; (b) zoomed in.

4 Conclusions

In this paper we have shown that there is a profound relationship between the design parameter spaces of planar and spherical 4R linkages. Indeed, if we ignore the difference between units of length for the a_i and measures of angle for the α_i and simply consider the magnitudes, we see that the design parameter spaces of planar and spherical 4R linkages intersect in the edges of the only uniform polyhedral compound, called the stellated octahedron, which has order 48 octahedral symmetry: a regular double tetrahedron that intersects itself in a regular octahedron. We believe that there is something remarkable in the fact that the design parameter spaces of these two classes of mechanism intersect in the only uniform polyhedral compound in the universe of polyhedra!

References

1. Bottema, O., Roth, B.: Theoretical Kinematics. Dover Publications, Inc., New York, N.Y. (1990)
2. Cipolla, R., Giblin, P.: Visual Motion of Curves and Surfaces. Cambridge University Press, Cambridge, U.K. (2000)
3. Coxeter, H.S.M.: Regular Polytopes, 3^{rd} Edition. Dover Publications, Inc., New York, N.Y., U.S.A. (1973)
4. Denavit, J., Hartenberg, R.S.: A Kinematic Notation for Lower-pair Mechanisms Based on Matrices. Trans ASME J. Appl. Mech. **23**, 215221 (1955)
5. Freudenstein, F.: "An Analytical Approach to the Design of Four-link Mechanisms". Trans. ASME **vol 77**, pages 483–492 (1954)
6. Freudenstein, F.: "Approximate Synthesis of Four-Bar Linkages". Trans. ASME **vol 77**, pages 853–861 (1955)
7. Hayes, M.J.D., Husty, M.L., Pfurner, M.: "Input-output Equation for Planar Four-bar Linkages". pp. 12–19. *16^{th} Advances in Robotic Kinematics*, eds. Lenarčič, J. and Parenti-Castelli, V., Springer, New York (2018)
8. Hayes, M.J.D., Rotzoll, M., Husty, M.L., Pfurner, M.: "Design Parameter Space of Planar Four-bar Linkages". Proceedings of the 15^{th} IFToMM World Congress (June 30-July 4, 2019)
9. Husty, M.L., Pfurner, M.: "An Algebraic Version of the Input-Output Equation of Planar Four-Bar Mechanisms". pp. 746–757. *International Conference on Geometry and Graphics*, Milan, Italy (2018)
10. McCarthy, J.M., Soh, G.S.: Geometric Design of Linkages, 2nd Edition *Interdiciplinaty Applied Mathematics*. Springer, New York, N.Y. (2011)
11. Murray, A.P., Larochelle, P.M.: "A Classification Scheme for Planar 4*R*, Spherical 4*R*, and Spatial *RCCR* Linkages to Facilitate Computer Animation". *Proceedings of 1998 ASME Design Engineering Technical Conferences (DETC'98)*, Atlanta, Georgia, U.S.A. (September 13-16, 1998)
12. Primrose, E.: Plane Algebraic Curves. MacMillan (1955)
13. Rotzoll, M., Hayes, M.J.D., Husty, M.L., Pfurner, M.: "A General Method for Determining Algebraic Input-output Equations for Planar and Spherical 4R Linkages". Submitted to *17^{th} International Symposium: Advances in Robotic Kinematics*, Ljubljana, Slovenia (June 28-July 2, 2020)
14. Segre, B.: The Non-singular Cubic Surfaces; a New Method of Investigation with Special Reference to Questions of Reality. Oxford, The Clarendon Press (1942)
15. Study, E.: Geometrie der Dynamen. Teubner Verlag, Leipzig, Germany (1903)

Mobility Classification in the Design Parameter Space of Spherical 4R Linkages

M. John D. Hayes and Mirja Rotzoll

Carleton University, Ottawa, Ontario, Canada
john.hayes@carleton.ca
mirja.rotzoll@carleton.ca

Abstract. The four arc length angles of the links in a spherical 4R linkage completely determines the mobility of the driver and follower (input and output) links. Its design parameter space therefore consists of the four arc length angle tangent half-angle parameters $\alpha_i,\ i \in \{1, 2, 3, 4\}$. Treating these parameters as homogeneous coordinates one can, without affecting the mobility characteristics, project the four-space into the hyperplane of one of the parameters which represents a three-space in the remaining parameters. When the three α_i are treated as basis directions then the location of a point in the space determines the mobility characteristics of the chain. The algebraic input-output equation of the spherical 4R, an algebraic polynomial in terms of the four α_i and the input and output angle tangent half-angle parameters v_1 and v_4, is a planar quartic curve in v_1 and v_4. Four of the coefficients each factor into the product of two cubic surfaces in the four α_i. Each of the eight cubic factors contain linear terms where the four linear α_i possess eight distinct variations in sign. In this paper the spherical cosine law is used to identify conditions enabling the input and output links to be fully rotatable cranks or to have angular displacement limits in several ways. The occurrence or absence of angular displacement limits for the input and output links is completely determined by the signs of products of four of the linear portions of the cubic coefficients, and therefore by the location of a point in the design parameter space spanned by the α_i.

Keywords: Spherical 4R · Design parameter space · Mobility limits.

1 Introduction

Spherical 4R linkages have been the focus of research for centuries [2]. Arguably the most successful mechanical system built on spherical 4R closed complex kinematic chains is the Agile Eye [7], introduced in 1994 and used as a camera pointing system. Four years later the mobility conditions on the input and output links in spherical function generators were classified using the trigonometric input-output (IO) equation [12], but 24 years earlier type and mobility considerations were examined [6]. This type of mechanical system still excites the imagination, see [11] for a recent example. Hence, we believe there is sufficient justification to revisit the mobility conditions on the input and output

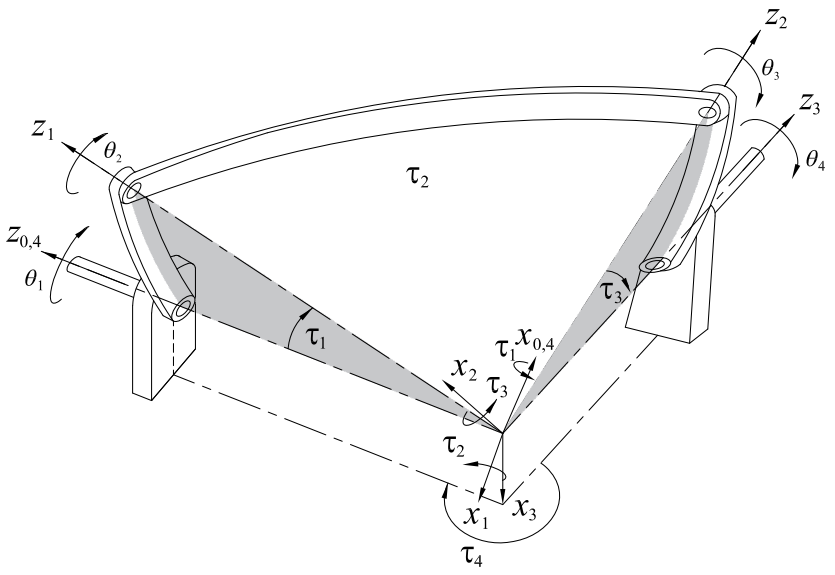

Fig. 1. Spherical 4R DH reference frames and parameters.

links of spherical 4R mechanisms imposed by the fixed distances between the R-pair centres in light of a novel algebraic IO equation [13].

Consider the arbitrary spherical 4R linkage illustrated in Fig. 1. The IO equation expresses the functional relationship between the input and output angles, $\theta_1 = f(\theta_4)$ in terms of the constant angular distances between the four R-pair centres, τ_i. The derivation of the algebraic form of the spherical IO equation makes use of the original Denavit-Hartenberg (DH) parametrisation of the kinematic geometry [3]. It also requires that all measures of angle be converted to algebraic parameters using the so called *Weierstrass*[1] tangent half-angle substitutions:

$$\begin{aligned} v_i = \tan\frac{\theta_i}{2}, \qquad \alpha_i &= \tan\frac{\tau_i}{2}; \\ \cos\theta_i = \frac{1-v_i^2}{1+v_i^2}, \quad \cos\tau_i &= \frac{1-\alpha_i^2}{1+\alpha_i^2}; \\ \sin\theta_i = \frac{2v_i}{1+v_i^2}, \quad \sin\tau_i &= \frac{2\alpha_i}{1+\alpha_i^2}. \end{aligned}$$

[1] Named after mathematician Karl Weierstrass (1815 - 1897), without any claim of the substitution in Weierstrass' own writings. Indeed, these substitutions are first used in a recognisable way [1] by Leonhard Euler in [5], but come from the much older rational parameterisation of the unit circle which uses the t-line construction and the formula $x = (1-t^2)/(1+t^2)$, $y = 2t/(1+t^2)$. This substitution goes back in some form to Euclid, at least, who used it to generate Pythagorean triples [4].

Making these substitutions the algebraic form of the IO equation is derived as [13]

$$Av_1^2v_4^2 + Bv_1^2 + Cv_4^2 + 8\alpha_1\alpha_3\left(\alpha_4^2+1\right)\left(\alpha_2^2+1\right)v_1v_4 + D = 0, \tag{1}$$

where

$$\begin{aligned}
A \;=\; A_1A_2 = {} & (\alpha_1\alpha_2\alpha_3 - \alpha_1\alpha_2\alpha_4 + \alpha_1\alpha_3\alpha_4 - \alpha_2\alpha_3\alpha_4 + \alpha_1 - \alpha_2 + \alpha_3 - \alpha_4) \\
& (\alpha_1\alpha_2\alpha_3 - \alpha_1\alpha_2\alpha_4 - \alpha_1\alpha_3\alpha_4 - \alpha_2\alpha_3\alpha_4 - \alpha_1 - \alpha_2 - \alpha_3 + \alpha_4)\,, \\
B \;=\; B_1B_2 = {} & (\alpha_1\alpha_2\alpha_3 + \alpha_1\alpha_2\alpha_4 - \alpha_1\alpha_3\alpha_4 - \alpha_2\alpha_3\alpha_4 + \alpha_1 + \alpha_2 - \alpha_3 - \alpha_4) \\
& (\alpha_1\alpha_2\alpha_3 + \alpha_1\alpha_2\alpha_4 + \alpha_1\alpha_3\alpha_4 - \alpha_2\alpha_3\alpha_4 - \alpha_1 + \alpha_2 + \alpha_3 + \alpha_4)\,, \\
C \;=\; C_1C_2 = {} & (\alpha_1\alpha_2\alpha_3 - \alpha_1\alpha_2\alpha_4 - \alpha_1\alpha_3\alpha_4 + \alpha_2\alpha_3\alpha_4 - \alpha_1 + \alpha_2 + \alpha_3 - \alpha_4) \\
& (\alpha_1\alpha_2\alpha_3 - \alpha_1\alpha_2\alpha_4 + \alpha_1\alpha_3\alpha_4 + \alpha_2\alpha_3\alpha_4 + \alpha_1 + \alpha_2 - \alpha_3 + \alpha_4)\,, \\
D \;=\; D_1D_2 = {} & (\alpha_1\alpha_2\alpha_3 + \alpha_1\alpha_2\alpha_4 + \alpha_1\alpha_3\alpha_4 + \alpha_2\alpha_3\alpha_4 - \alpha_1 - \alpha_2 - \alpha_3 - \alpha_4) \\
& (\alpha_1\alpha_2\alpha_3 + \alpha_1\alpha_2\alpha_4 - \alpha_1\alpha_3\alpha_4 + \alpha_2\alpha_3\alpha_4 + \alpha_1 - \alpha_2 + \alpha_3 + \alpha_4)\,.
\end{aligned}$$

The eight cubic factors in the four coefficients A, B, C, and D are symmetric singular cubics which each possess three finite lines and three common lines at infinity [9]. Different pairs of the eight surfaces have one finite line in common, meaning there are 12 distinct finite lines among the eight surfaces. The finite lines contain the twelve edges of a regular double tetrahedron. Without loss in generality, the surfaces are projected into the hyperplane $\alpha_4 = 1$ for visualisation, see Fig. 2. If the α_i are interpreted as directed distances, each distinct point in this space represents a different spherical 4R linkage, while it's location implies the mobility of the input and output links, hence the space is called the design parameter space of spherical 4R linkages.

2 Mobility Conditions

The magnitudes of the linear components of four of the eight coefficient factors in Eq. (1) determine the mobility of the input and output links leading to results remarkably similar to [8]. Hence, the location of a point in the projection of the design parameter space illustrated in Fig. 2 defines the mobility of a linkage assembled with the links possessing the distances between the R-pairs implied by the values of α_1, α_2, and α_3 with $\alpha_4 = 1$. The effect of normalising α_1, α_2, and α_3 with α_4 is to place the associated function-generator on the surface of a unit sphere and merely scales the angular distances between the R-pairs. The linear components of interest are contained in the factors A_1, B_1, C_1, and D_1 in Eq. (1), and are correspondingly labelled as

$$\left.\begin{array}{ll} A_{l1} = \alpha_1 - \alpha_2 + \alpha_3 - \alpha_4, & B_{l1} \;= \alpha_1 + \alpha_2 - \alpha_3 - \alpha_4, \\ C_{l1} = -\alpha_1 + \alpha_2 + \alpha_3 - \alpha_4, & D_{l1} = -\alpha_1 - \alpha_2 - \alpha_3 - \alpha_4. \end{array}\right\} \tag{2}$$

The following classification requires that α_4 correspond to the relatively non-moving link.

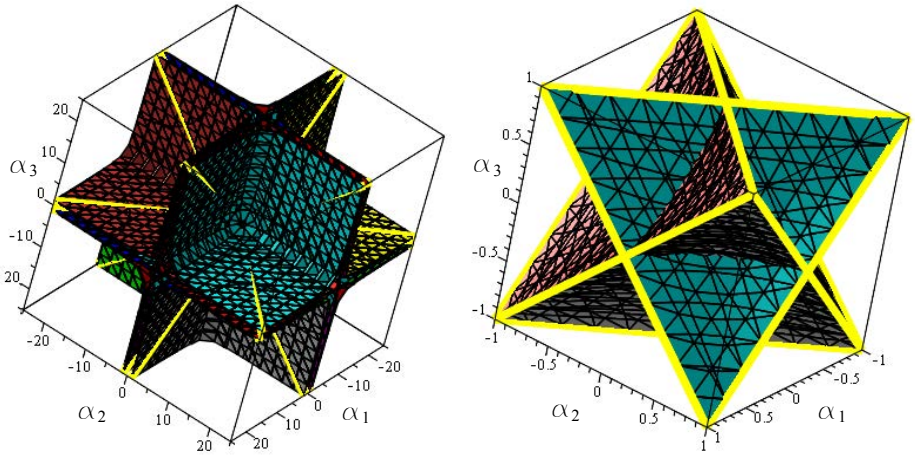

Fig. 2. Eight cubic surfaces in the spherical 4R design parameter space: (a) zoomed out; (b) zoomed in.

Existence Condition for $\boldsymbol{\theta_{1_{min}}}$. Examining the spherical 4R illustrated in Fig. 1 the input link can correspond to either τ_1 or τ_3. We arbitrarily assign the input link to be τ_1 and θ_1 its input angle. If the relative lengths of the links permit, the links corresponding to τ_2 and τ_3 can align on the same great circle. In this configuration θ_1 will be either at its minimum or maximum value. If the arc length of the great circle segment is determined by the angle $\tau_2 - \tau_3$ then θ_1 will be at its minimum value, denoted $\theta_{1_{min}}$. In order to be able to attain this configuration then it must be that $\cos\theta_{1_{min}} \leq 1$. If, on the other hand, $\cos\theta_{1_{min}} > 1$ then the alignment of τ_2 and τ_3 on the same great circle is not mechanically possible and τ_1 will be able to traverse the positive x_0-axis passing through $\theta_1 = 0$. This condition can be modelled using the law of cosines for spherical triangles [14]

$$\cos\theta_{1_{min}} = \frac{\cos(\tau_2 - \tau_3) - \cos\tau_1 \cos\tau_4}{\sin\tau_1 \sin\tau_4} \; > \; 1. \tag{3}$$

Rearranging Eq (3) and using the addition/subtraction identity

$$\cos\phi_1 \cos\phi_2 + \sin\phi_1 \sin\phi_2 = \cos(\phi_1 - \phi_2)$$

yields the equivalent condition of

$$\cos(\tau_2 - \tau_3) > \cos(\tau_1 - \tau_4). \tag{4}$$

Because the magnitude of the cosine function decreases as the absolute value of its argument increases in the range $0 \leq \Delta\tau \leq \pi$, Eq. (4) can be re-expressed equivalently as

$$(\tau_2 - \tau_3)^2 < (\tau_1 - \tau_4)^2, \; \Rightarrow \; (\tau_2 - \tau_3)^2 - (\tau_1 - \tau_4)^2 \; < \; 0. \tag{5}$$

This difference of squares is factored according to $a^2 - b^2 = (a+b)(a-b)$, giving

$$(\tau_1 + \tau_2 - \tau_3 - \tau_4)(-\tau_1 + \tau_2 - \tau_3 + \tau_4) < 0. \tag{6}$$

Converting these factors of sums and differences of angles to their algebraic equivalents yields sums and differences of the α_i which correspond to $-A_{l1}$ and B_{l1}, two linear components of the factors listed in Eq. (2), giving

$$\underbrace{(\alpha_1 + \alpha_2 - \alpha_3 - \alpha_4)}_{B_{l1}}\underbrace{(-\alpha_1 + \alpha_2 - \alpha_3 + \alpha_4)}_{-A_{l1}} < 0, \tag{7}$$

or

$$A_{l1}B_{l1} > 0. \tag{8}$$

Hence, the condition for $\theta_{1_{min}}$ to exist is $A_{l1}B_{l1} \leq 0$. If, on the other hand, $A_{l1}B_{l1} > 0$ then the link defined by α_1 can cross the positive x_0-axis, passing through 0.

Existence Condition for $\boldsymbol{\theta_{1_{max}}}$. If the relative lengths of the links allow τ_2 and τ_3 to align on the same great circle with arc length determined by $\tau_2 + \tau_3$ then θ_1 will be at its maximum value, denoted $\theta_{1_{max}}$. The condition enabling link α_1 to pass through π on the x_0-axis, meaning that $\theta_{1_{max}}$ does not exist, is again modelled with the law of cosines for spherical triangles as:

$$\cos\theta_{1_{max}} = \frac{\cos(\tau_2 + \tau_3) - \cos\tau_1 \cos\tau_4}{\sin\tau_1 \sin\tau_4} \; < \; -1. \tag{9}$$

Rearranging Eq. (9) and using the addition/subtraction identity gives the condition

$$\cos(\tau_2 + \tau_3) < \cos(\tau_1 + \tau_4)$$

Now, following the same procedure as for $\theta_{1_{min}}$ leads to the inequality condition for the non-existence of $\theta_{1_{max}}$ as the product of the sums and differences of the linear elements listed in Eq. (2)

$$\underbrace{(\alpha_1 + \alpha_2 + \alpha_3 + \alpha_4)}_{-D_{l1}}\underbrace{(-\alpha_1 + \alpha_2 + \alpha_3 - \alpha_4)}_{C_{l1}} > 0, \tag{10}$$

or

$$C_{l1}D_{l1} < 0. \tag{11}$$

Existence Condition for $\boldsymbol{\theta_{4_{min}}}$. The procedure for determining the conditions on the link lengths for the existence of a minimum output angle, $\theta_{4_{min}}$, is similar to that of determining the conditions for θ_1, but uses a different spherical triangle. In order for $\theta_{4_{min}}$ to exist, then links τ_1 and τ_2 must align on the same

great circle with arc length determined by $\tau_2 - \tau_1$. If this configuration cannot be reached by the mechanism then $\theta_{4_{min}}$ does not exist and $\cos\theta_{4_{min}} > 1$, meaning that τ_4, or α_4 depending on how it is represented, can pass through 0 on the x_4-axis. Hence, the condition required for $\theta_{4_{min}}$ to not exist is given by

$$\cos\theta_{4_{min}} = \frac{\cos\left(\tau_2 - \tau_1\right) - \cos\tau_3\cos\tau_4}{\sin\tau_3\sin\tau_4} \;>\; 1. \tag{12}$$

The equivalent condition, in the range $0 \leq \Delta\tau \leq \pi$, is given by factoring the difference of squares and converting the τ_i to α_i is

$$\underbrace{(-\alpha_1 + \alpha_2 + \alpha_3 - \alpha_4)}_{C_{l1}}\underbrace{(-\alpha_1 + \alpha_2 - \alpha_3 + \alpha_4)}_{-A_{l1}} < 0. \tag{13}$$

This means that the condition for $\theta_{4_{min}}$ to not exist thus enabling α_3 to pass though 0 is

$$A_{l1}C_{l1} > 0. \tag{14}$$

Existence Condition for $\boldsymbol{\theta_{4_{max}}}$. The condition for the existence of $\theta_{4_{max}}$ is that links τ_1 and τ_2 must align on the same great circle with arc length determined by $\tau_1 + \tau_2$. For α_4 to have the ability to pass through π on the x_4-axis is given by $\cos\theta_{4_{max}} < -1$, meaning that

$$\cos\theta_{4_{max}} = \frac{\cos\left(\tau_1 + \tau_2\right) - \cos\tau_3\cos\tau_4}{\sin\tau_3\sin\tau_4} \;<\; -1. \tag{15}$$

Following the same procedure detailed as for $\theta_{1_{min}}$ leads to the condition for the non-existence of $\theta_{4_{max}}$ as

$$\underbrace{(\alpha_1 + \alpha_2 + \alpha_3 + \alpha_4)}_{-D_{l1}}\underbrace{(\alpha_1 + \alpha_2 - \alpha_3 - \alpha_4)}_{B_{l1}} > 0. \tag{16}$$

This means that the condition for $\theta_{4_{max}}$ to not exist thereby enabling α_3 to pass though π is

$$B_{l1}D_{l1} < 0. \tag{17}$$

2.1 Mobility Classification for Spherical 4R Linkages

It is to be seen that the magnitude of four of the linear components, A_{l1}, B_{l1}, C_{l1}, and D_{l1} of the eight cubic factors of the coefficients of Eq. (1) completely determines the mobility of the input and output links. The eight distinct mobility types are listed in Table 1. Depending on the twist angle parameters and sphere radius, each of the first three of the four linear components can be positive, negative, or identically zero, while D_{l1} is always less than zero. In the classification scheme first presented in [12] and later refined in [10] trigonometric relations are

Table 1. Classification of non-folding spherical $4R$ linkages. Shaded cells satisfy the Grashof condition.

#	A_{l1}	B_{l1}	C_{l1}	D_{l1}	Input α_1	Output α_4
1	-	-	-	-	0-rocker	0-rocker
2	+	-	-	-	rocker	rocker
3	-	+	-	-	rocker	crank
4	-	-	+	-	crank	rocker
5	+	+	-	-	0-rocker	π-rocker
6	+	-	+	-	π-rocker	0-rocker
7	-	+	+	-	π-rocker	π-rocker
8	+	+	+	-	crank	crank

only considered. Because the sum of any two angles in a spherical triangle can exceed π, but not 2π, while the sum of the three interior angles is greater than π, but less than 3π, it may happen that the argument of the cosine function is not in the range between 0 and π. To address this the trigonometric form of the D_{l1} term is modified to

$$D'_{l1} = 2\pi - \tau_1 - \tau_2 - \tau_3 - \tau_4.$$

Depending on the magnitudes of the angles D'_{l1} may be less than, greater than, or identically equal to 0. If $D'_{l1} < 0$ then the linkage wraps around the sphere [10]. Regardless, for each of the eight possible mechanism types possessing mobility determined by the signs of the other three linear factors is precisely the same as those for the case where $D'_{l1} > 0$. Moreover, when converted to their algebraic parameters we see that $D'_{l1} = D_{l1}$ since $\tan 2\pi/2 = 0$. Therefore we only consider the eight cases where $D_{l1} < 0$ which aligns with results already established in the literature [10, 12].

Moreover the Grashof condition is satisfied when the product $A_{l1}B_{l1}C_{l1}D_{l1} < 0$. The four possible Grashof linkages are the shaded cells in Table 1. If the link lengths permit any one, or any combination of A_{l1}, B_{l1}, or C_{l1} to be identically zero, then the linkage can fold, however, in the interest of brevity, none of these additional 19 folding linkages are tabulated.

3 Conclusions

In this paper, using the algebraic IO equation for spherical 4R linkages from [13], we have shown that the linear elements of the four of the eight cubic factors of link lengths play a role in characterising the mobility characteristics of the input and output links. Any point in the design parameter space of the link length parameters α_1, α_2, and α_3 projected into the hyperplane $\alpha_4 = 1$ establishes the mobility characteristics listed in Table 1. While the results themselves are not new, the method by which they are obtained is. Moreover, since the same approach can be applied to planar 4R linkages as well, it is approaching the

completely general function generator algebraic IO equation we are attempting to develop for any planar, spherical, or spatial four-bar linkage kinematic architecture.

References

1. Bradley, R.E., D'Antonio, L.A., Sandifer, C.E. (eds.): Euler at 300, an Appreciation. Mathematical Association of America (2007)
2. Ceccarelli, M., Editor: Distinguished Figures in Mechanism and Machine Science, Their Contributions and Legacies Part 1. Springer, New York, U.S.A. (2007)
3. Denavit, J., Hartenberg, R.S.: A Kinematic Notation for Lower-pair Mechanisms Based on Matrices. Trans ASME J. Appl. Mech. **23**, 215221 (1955)
4. Euclid: The Thirteen Books of the Elements, *second edition, translation by Sir T. L. Heath, vol's 1,2,3.* Dover Publications, Inc., New York, N.Y., U.S.A. (1956)
5. Euler, L.: Institutionum Calculi Integralis Volumen Primum (E342, Caput V, paragraph 261). Impensis Academiae Imperialis Scientiarum (1768)
6. Gilmartin, M.J., Duffy, J.: Type and Mobility Analysis of Spherical Four-link Mechanisms. Mechanisms 1972, I. Mech. E. (1972)
7. Gosselin, C.M., Hamel, J.F.: The Agile Eye: a High-performance Three-degree-of-freedom Camera-orienting Device. Proceedings of the 1994 IEEE International Conference on Robotics and Automation (1994)
8. Hayes, M.J.D., Rotzoll, M., Husty, M.L., Pfurner, M.: "Design Parameter Space of Planar Four-bar Linkages". Proceedings of the 15^{th} IFToMM World Congress (June 30-July 4, 2019)
9. Hayes, M.J.D., Rotzoll, M., Ingalls, C., Pfurner, M.: "Design Parameter Space of Spherical Four-bar Linkages". Submitted to *EuCoMeS 2020, 8th European Conference on Mechanism Science*
10. McCarthy, J.M., Soh, G.S.: Geometric Design of Linkages, 2nd Edition *Interdiciplinaty Applied Mathematics*. Springer, New York, N.Y. (2011)
11. Moazami, S., Zargarzadeh, H., Palanki, S.: "Kinematics of Spherical Robots Rolling Over 3D Terrains". Complexity **vol 2019**, https://doi.org/10.1155/2019/7543969 (2019)
12. Murray, A.P., Larochelle, P.M.: "A Classification Scheme for Planar $4R$, Spherical $4R$, and Spatial $RCCR$ Linkages to Facilitate Computer Animation". *Proceedings of 1998 ASME Design Engineering Technical Conferences (DETC'98)*, Atlanta, Georgia, U.S.A. (September 13-16, 1998)
13. Rotzoll, M., Hayes, M.J.D., Husty, M.L., Pfurner, M.: "A General Method for Determining Algebraic Input-output Equations for Planar and Spherical 4R Linkages". Submitted to *17^{th} International Symposium: Advances in Robotic Kinematics*, Ljubljana, Slovenia (June 28-July 2, 2020)
14. Todhunter, T., Leathem, J.G.: Spherical Trigonometry for the Use of Colleges and Schools. Macmillan and Co., Ltd. (1911)

Bibliography

[1] M.J.D. Hayes, K. Parsa, and J. Angeles. "The Effect of Data-Set Cardinality on the Design and Structural Errors of Four-Bar Function-Generators". *Proceedings of the Tenth World Congress on the Theory of Machines and Mechanisms,* Oulu, Finland, pages 437–442, 1999.

[2] A. Guigue and M.J.D. Hayes. "Continuous Approximate Synthesis of Planar Function-generators Minimising the Design Error". *Mechanism and Machine Theory*, vol. 101: pages 158–167, DOI: 10.1016/j.mechmachtheory.2016.03.012, 2016.

[3] M.J.D. Hayes and P.J. Zsombor-Murray. "Solving the Burmester Problem Using Kinematic Mapping". *Proc. of the ASME Design Engineering Technical Conferences: Mechanisms Conference,* Montréal, QC, Canada, on CD, Sept. 2002.

[4] J. Grünwald. "Ein Abbildungsprinzip, welches die ebene Geometrie und Kinematik mit der räumlichen Geometrie verknüpft". *Sitzber. Ak. Wiss. Wien*, vol. 120: pages 677–741, 1911.

[5] W. Blaschke. "Euklidische Kinematik und Nichteuklidische Geometrie". *Zeitschr. Math. Phys.*, vol. 60: pages 61–91 and 203–204, 1911.

[6] K. Brunnthaler, M. Pfurner, and M.L. Husty. "Synthesis of Planar Four-bar Mechanisms". *Transactions of the Canadian Society for Mechanical Engineering*, vol. 30, no. 2: pages 297–313, 2006.

[7] M.J.D. Hayes and S. Radacina Rusu. "Quadric Surface Fitting Applications to Approximate Dimensional Synthesis". *Proceedings of the Thirteenth World Congress on the Theory of Machines and Mechanisms,* Guanajuato, Mexico, June 19-23, 2011.

[8] M.J.D. Hayes and P.J. Zsombor-Murray. "Towards Integrated Type and Dimensional Synthesis of Mechanisms for Rigid Body Guidance". *Proceedings of the CSME Forum 2004,* University of Western Ontario, London, ON., Canada, June 1-4, 2004.

[9] T.J. Luu and M.J.D. Hayes. "Integrated Type and Approximate Dimensional Synthesis of Four-Bar Planar Mechanisms for Rigid Body Guidance". *Latest Advances in Robot Kinematics,* eds. J. Lenarčič and M.L Husty, Springer, New York, 2012.

[10] M.J.D. Hayes, M.L. Husty, and M. Pfurner. "Input-output Equation for Planar Four-bar Linkages". *Advances in Robot Kinematics 2018,* eds. J. Lenarčič and V. Parenti-Castelli*, Springer, New York*, pages 12–19, 2018.

[11] M.L. Husty and M. Pfurner. "An Algebraic Version of the Input-output Equation of Planar Four-bar Mechanisms". *ICGG 2018 - Proceedings of the 18th International Conference on Geometry and Graphics,* ed. L. Cocchiarella*, Springer, New York*, pages 775–786, 2018.

[12] M. Rotzoll, M.J.D. Hayes, and M.L. Husty. "An Algebraic Input-Output Equation for Planar RRRP and PRRP Linkages". *Proceedings of the 10^{th} CCToMM Symposium on Mechanisms, Machines, and Mechatronics*, École de technologie supérieure, Montréal, QC, Canada, May 16-17, 2019.

[13] M. Rotzoll, M.J.D. Hayes, M.L. Husty, and M. Pfurner. "A General Method for Determining Algebraic Input-output Equations for Planar and Spherical 4R Linkages". Submitted to *17^{th} International Symposium: Advances in Robotic Kinematics*, Ljubljana, Slovenia, June 28-July 2, 2020.

[14] M.J.D. Hayes, M. Rotzoll, M.L. Husty, and M. Pfurner. "Design Parameter Space of Planar Four-bar Linkages". Proceedings of the 15^{th} IFToMM World Congress, June 30-July 4, 2019.

[15] M.J.D. Hayes, M. Rotzoll, C. Ingalls, and M. Pfurner. "Design Parameter Space of Spherical Four-bar Linkages". Submitted to *EuCoMeS 2020, 8th European Conference on Mechanism Science.*

[16] M.J.D. Hayes and M. Rotzol. "Mobility Classification of Spherical 4R Linkages". Submitted to *TMM 2020, XIII. International Conference on the Theory of Machines and Mechanisms*, Liberec, Czech Republic, September 7-10, 2020.